

**2D MODEL FIELD THEORIES AT FINITE TEMPERATURE
AND DENSITY ***

V. SCHÖN and M. THIES

*Institute for Theoretical Physics III, University of Erlangen-Nürnberg,
Staudtstr. 7, 91058 Erlangen, Germany*

In certain 1+1 dimensional field theoretic toy models, one can go all the way from microscopic quarks via the hadron spectrum to the properties of hot and dense baryonic matter in an essentially analytic way. This “miracle” is illustrated through case studies of two popular large N models, the Gross-Neveu and the 't Hooft model — caricatures of the Nambu–Jona-Lasinio model and real QCD, respectively. The main emphasis will be on aspects related to spontaneous symmetry breaking (discrete or continuous chiral symmetry, translational invariance) and confinement.

Contents

1	Introduction	2
2	Basics about 1+1 dimensions	4
2.1	Kinematics	5
2.2	Dirac fermions	6
2.3	Scalar bosons	8
2.4	Long range order	8
2.5	Gauge fields	10
2.5.1	Abelian gauge fields	10
2.5.2	Non-Abelian gauge fields	11
2.6	Renormalization	14
2.7	Soluble models of interest for QCD	16
3	Two dimensional models at zero temperature and chemical potential	17
3.1	Gross-Neveu models	17
3.1.1	Vacuum, physical fermion	18
3.1.2	Baryons	20
3.1.3	Mesons	25

*Contribution to the Festschrift in honor of Boris Ioffe, edited by M. Shifman.

3.2	't Hooft model	29
3.2.1	Vacuum, confinement	29
3.2.2	Baryons	35
3.2.3	Mesons	36
3.3	Chiral limit and Goldstone modes	38
4	Finite temperature	44
4.1	Finite temperature versus finite extension	44
4.2	GN model on a cylinder	47
4.3	't Hooft model on a cylinder, decompactification	52
4.4	$1/N$ corrections at finite T , role of pions	58
5	Finite density	60
5.1	GN model as a Fermi gas	60
5.2	't Hooft model as a Fermi gas	64
5.3	Breakdown of translational invariance	66
5.3.1	Strict chiral limit	66
5.3.2	Non-vanishing bare quark masses	69
5.3.3	Comparison to other works	72
6	Phase diagram in the (T, μ)-plane	74
6.1	Chiral GN model with translational invariance	75
6.2	Chiral spiral at finite temperature	78
7	Closing remarks	84

1 Introduction

With the shift in emphasis in field theory from perturbative to non-perturbative phenomena during the last decades, exactly soluble models have acquired a quite respectable status. The limited number of analytical tools available at strong coupling, so painfully felt in quantum chromodynamics (QCD), makes it tempting to look for other sources of inspiration. Except for the celebrated case of supersymmetric $N = 2$ Yang-Mills theory¹, “soluble model” in quantum field theory still means “1+1 dimensional model”. This makes it clear at once that we should not expect such toy models to be in any sense realistic; they can teach us only little (if anything) of direct relevance to the real world. Nevertheless, we find it quite appropriate to include them in a book devoted to analytic approaches to QCD. One can perhaps picture the relationship between QCD and the soluble toy models as follows: If QCD is the sun, then the 1+1 dimensional models are like planets which are gravitating around it, shining

in its light. Their distance to the sun may vary and each of them develops a life of its own, although powered by the sun. Only then can one understand why a theory like the Schwinger model² describing massless electrons which only move along a line, have a linear Coulomb potential and form non-interacting, massive bosons can accumulate close to 1000 citations in the hep-archive up to now. This striking success is shared by the Gross-Neveu (GN) model³ (massless fermions with a point interaction) and the 't Hooft model⁴ (QCD₂ in the large N limit). Whether one likes these models or not — they have become an integral part of the intellectual endeavor to understand the strong interactions and their traces pervade the QCD literature.

There is another aspect which we should like to mention. A soluble model in quantum mechanics is typically solved once and for all, then put into the textbooks where it ceases to play any scientific role. By contrast, a soluble field theory is a laboratory which can be used over and over again for new types of questions — this is the reason why it is so much richer. When browsing through the numerous citations of models like the GN model or the 't Hooft model, one finds the whole history of QCD mapped out — ranging from questions of asymptotic freedom, quark-hadron duality, spectroscopy, scattering, over issues of confinement, covariance, vacuum structure, chiral symmetry breaking, up to sum rules, supersymmetric extensions, “stringy” aspects, heavy quarks, and finally hot and dense baryonic matter, our main topic here. Also some technical developments like light-cone quantization would be unthinkable without 2d models as firm testing ground. Whether in the end these models will help to solve the real hard problems in QCD is still an open question; they certainly help to prepare us intellectually and widen our horizon about the fascinating world of non-perturbative physics and non-Abelian gauge theories.

As will be seen later on, one of the main themes of this article is chiral symmetry and its spontaneous breakdown (SSB). We are aware that studying SSB in low dimensions is like dancing on thin ice — there is the constant danger of falling into the trap of some no-go theorem and making a fool of oneself. Without claiming mathematical rigor, we believe that the large N limit provides a reasonable protection against these perils. Thereby, it significantly enlarges the spectrum of questions which can be addressed within lower dimensional soluble models.

In the spirit of what has been said so far, we have attempted to write this article in a rather self-contained and hopefully pedagogical way. The literature about two-dimensional field theory is not always easy to access for the non-expert, mainly because a number of different, highly specialized techniques are employed by different sub-communities (e.g. bosonization, light-cone quantization, functional methods, conformal and topological field theory). We have

refrained from using genuine 2d-technology as much as possible and instead based our presentation upon a simple yet powerful technique familiar to every physicist, the Hartree-Fock (HF) approximation.^{5,6} For the large N models which we will consider here, one can actually go quite far with a relativistic extension of this basic tool from many-body theory. This should also make the article more readable for those who want to learn field theory while working on QCD related problems (e.g. students or researchers with a nuclear physics background like ourselves).

Finally we should apologize for the perhaps not always balanced choice of citations: It is strongly biased towards work which fits into our approach and may not do justice to other important activities in the field. Our article is not intended as a comprehensive review article of the usual type, but rather an attempt to convey some of the intellectual pleasure of working on QCD motivated, analytically soluble problems, using as example of topical interest hot and dense matter in two-dimensional large N models. This is presumably more adequate for a contribution to a Festschrift like the present one in honor of Boris Ioffe.

2 Basics about 1+1 dimensions

The transition from the real world to 1+1 dimensions has drastic consequences. These consequences are responsible for tremendous technical simplifications of quantum field theory, but also for many unrealistic features and even pathologies which have to be kept in mind. In the present section, we have collected the main kinematical and geometrical facts which are independent of the specific dynamics, as well as some characteristic aspects of two-dimensional gauge theories. The selection of topics is guided by the applications which we have in mind in later sections. Therefore, we leave out a large number of important topics which are closely associated with low dimensions but less relevant for us.^{7,8} These include boson-fermion mappings, existence of anyons with arbitrary statistics, conformal invariance, sigma models, integrability questions as well as relations to matrix models, string theories, and gravity. We will also make no use of the technique of light-cone quantization which has become a powerful tool for dealing with two-dimensional model field theories.⁹ It is not clear to us whether it is of any help in the study of field theory at finite temperature and chemical potential.

2.1 Kinematics

We use the metric and antisymmetric tensors

$$g^{\mu\nu} = \begin{pmatrix} 1 & 0 \\ 0 & -1 \end{pmatrix}, \quad \epsilon^{\mu\nu} = \begin{pmatrix} 0 & -1 \\ 1 & 0 \end{pmatrix} \quad (1)$$

in 1+1 dimensions. Clearly, the Lorentz group $SO(1,1)$ consists only of boosts — there are no rotations (and hence there is no spin). The inhomogeneous Lorentz group or Poincaré group $ISO(1,1)$ has three generators (boost K , momentum P , Hamiltonian H) which satisfy the Poincaré algebra

$$[H, P] = 0, \quad [K, P] = iH, \quad [K, H] = iP. \quad (2)$$

States are characterized by the Casimir operator

$$P_\mu P^\mu = m^2, \quad (3)$$

the dispersion relation has the standard form $E = \sqrt{p^2 + m^2}$. A left-over type of helicity can be defined via Lorentz-boosts

$$\begin{pmatrix} x^0 \\ x^1 \end{pmatrix}' = \begin{pmatrix} \cosh \xi & \sinh \xi \\ \sinh \xi & \cosh \xi \end{pmatrix} \begin{pmatrix} x^0 \\ x^1 \end{pmatrix} \quad (4)$$

with rapidity

$$\xi = \text{artanh } v. \quad (5)$$

States are said to have helicity s if they transform according to

$$|s\rangle' = e^{i\xi s} |s\rangle. \quad (6)$$

Lorentz scalars, vectors and tensors can be constructed in the usual way. If V^μ is a two-vector, its light-cone components transform irreducibly according to helicity ± 1 ,

$$(V^0 \pm V^1)' = e^{\pm \xi} (V^0 \pm V^1). \quad (7)$$

The trace of a tensor T^μ_μ is Lorentz scalar, as is an antisymmetric tensor (e.g. the electric field strength). A symmetric, traceless tensor has helicity 2,

$$(T^{00} \pm T^{01})' = e^{\pm 2\xi} (T^{00} \pm T^{01}). \quad (8)$$

One peculiar feature of massless states in two dimensions is the following: Any number of massless non-interacting particles moving in the same direction with momenta p_i behave kinematically like a single massless particle of momentum $\sum_i p_i$. This is partly responsible for the proliferation of massless modes in certain models.

2.2 Dirac fermions

We start our survey of various aspects of two-dimensional field theory with Dirac fermions which will be the main actors in the following. Canonically, fermions are distinguished from bosons by equal-time anticommutation relations,

$$\{\psi_i(x), \psi_j^\dagger(y)\} = \delta_{ij} \delta(x - y) . \quad (9)$$

Since there is no spin, a Dirac fermion has only two components (particle/antiparticle degrees of freedom). The free Dirac equation reads

$$(i\gamma^\mu \partial_\mu - m)\psi = 0 \quad (10)$$

where the γ -matrices are 2×2 matrices satisfying

$$\{\gamma^\mu, \gamma^\nu\} = 2g^{\mu\nu} . \quad (11)$$

Unless stated otherwise, they will be chosen as

$$\gamma^0 = \begin{pmatrix} 0 & 1 \\ 1 & 0 \end{pmatrix} , \quad \gamma^1 = \begin{pmatrix} 0 & -1 \\ 1 & 0 \end{pmatrix} . \quad (12)$$

The free Dirac Hamiltonian (in first quantization) is

$$h = \gamma^5 p + \gamma^0 m \quad (13)$$

with

$$\gamma^5 = \gamma^0 \gamma^1 = \begin{pmatrix} 1 & 0 \\ 0 & -1 \end{pmatrix} . \quad (14)$$

This representation is well suited for the chiral limit $m \rightarrow 0$. Free spinors (eigenvalues $\pm E_p$ with $E_p = \sqrt{m^2 + p^2}$) are

$$\begin{aligned} u(p) &= \begin{pmatrix} \cos \theta_p/2 \\ \sin \theta_p/2 \end{pmatrix} = \frac{1}{\sqrt{2E_p}} \begin{pmatrix} \sqrt{E_p + p} \\ \sqrt{E_p - p} \end{pmatrix} , \\ v(p) &= \begin{pmatrix} -\sin \theta_p/2 \\ \cos \theta_p/2 \end{pmatrix} = \frac{1}{\sqrt{2E_p}} \begin{pmatrix} -\sqrt{E_p - p} \\ \sqrt{E_p + p} \end{pmatrix} . \end{aligned} \quad (15)$$

For later convenience, we have introduced the free Bogoliubov angle as

$$\theta_p = \text{arccot} \left(\frac{p}{m} \right) \in [0, \pi] . \quad (16)$$

It appears if one diagonalizes h of Eq. (13) by a canonical transformation with the unitary operator

$$U_p = \exp \left\{ -\frac{\theta_p}{2} (a_p^\dagger b_p - b_p^\dagger a_p) \right\} \quad (17)$$

for each mode where a_p and b_p are second quantized operators for right- and lefthanded fermions with momentum p . In the massless limit, right- and left-handed fermions are projected out by

$$P_{R,L} = \frac{1 \pm \gamma^5}{2} . \quad (18)$$

Chiral transformations are defined as

$$\psi \rightarrow e^{i\alpha\gamma^5} \psi , \quad (19)$$

and represent a symmetry of the massless theory (note that γ^5 can be defined in an odd number of space dimensions only). To see the meaning of right/left-handedness in 1+1 dimensions, we specialize the above spinors to $m = 0$, where

$$\theta_p = \Theta(-p)\pi \quad (20)$$

and hence

$$u(p) = \begin{pmatrix} \Theta(p) \\ \Theta(-p) \end{pmatrix} \quad (21)$$

($\Theta(p)$ denotes the Heaviside step function). Thus handedness in two dimensions is correlated with the direction of motion (“right- and left movers”). The Lorentz transformation is consistent with the above definition of kinematic helicity $s = \pm 1/2$ for right- and left-handed fermions, respectively,

$$\psi(x) \rightarrow e^{i\xi\gamma^5/2} \psi(x') , \quad (22)$$

with x' as given in Eq. (4). Another important peculiarity of fermions in two dimensions concerns the vector and axial currents,

$$j_V^\mu = \bar{\psi}\gamma^\mu\psi , \quad j_A^\mu = \bar{\psi}\gamma^\mu\gamma^5\psi \quad (23)$$

and their (partial) conservation laws,

$$\partial_\mu j_V^\mu = 0 , \quad \partial_\mu j_A^\mu = 2im\bar{\psi}\gamma^5\psi . \quad (24)$$

Due to the severe restrictions for γ -matrices in two dimensions, these currents have actually only two independent components,

$$j_V^0 = j_A^1 , \quad j_V^1 = j_A^0 , \quad (25)$$

or

$$j_A^\mu = \epsilon^{\mu\nu} j_{V,\nu} . \quad (26)$$

This intimate relationship between vector and axial currents is the key for understanding the existence of massless mesons and baryons (see Sec. 3.3).

2.3 Scalar bosons

Bosons are quantized canonically with equal-time commutation relations

$$[\pi(x), \phi(y)] = -i\delta(x - y) . \quad (27)$$

Whereas the free massive scalar field has no special features as compared to 3+1 dimensions and satisfies the Klein-Gordon equation

$$(\partial_\mu \partial^\mu + m^2)\phi = 0 , \quad (28)$$

massless bosons are quite delicate. The simplest object in 3+1 dimensional quantum field theory, the massless scalar field, becomes the most subtle one in 1+1 dimensions due to severe infrared divergences.¹⁰ As pointed out by Coleman,¹¹ formally, the integral appearing in the free two-point function

$$\langle 0 | \phi(x) \phi(0) | 0 \rangle = \int \frac{d^2 k}{(2\pi)} e^{ikx} \delta(k^2) \Theta(k_0) \quad (29)$$

is IR divergent, as can be seen by performing the k^0 -integration,

$$\int_0^\infty \frac{dk^1}{2\pi k^1} \cos(k^1 x^1) e^{ik^1 x^0} . \quad (30)$$

Since this is also the simplest example of a Goldstone boson in 3+1 dimensions (broken symmetry: $\phi \rightarrow \phi + c$),¹² one expects trouble with the Goldstone theorem in two dimensions. This is indeed what happens: There is a rigorous no-go theorem which forbids SSB of a continuous symmetry in two dimensions (Coleman theorem¹¹). A similar phenomenon is known in statistical physics: there is no long range order in two-dimensional systems (at least with short range interactions¹³). The strong infrared fluctuations destroy the order, for instance in a crystal, a magnet or a superfluid. There is a different type of long range order though which we discuss in the next subsection.

2.4 Long range order

The absence of long range order in 1+1 dimensional QFT or two-dimensional statistical physics could be a fatal blow to our investigation — what interesting phase structure can possibly be left? To understand the way out, let us first come back to the essence of two-dimensionality alluded to in the preceding subsection: Long range order cannot be maintained over arbitrarily large distances due to strong fluctuations of the Goldstone mode; there is no SSB. A nice example for this effect are atoms in a plane which want to form a crystal.¹⁴ The

amplitude of fluctuations of each atom around its equilibrium position grows logarithmically with L , if L is the extension of the crystal. The calculation involves a similar infrared divergence as in the 2-point function (29),

$$\langle \vec{u}^2 \rangle \sim \int \frac{d^2k}{(2\pi)^2} \frac{1}{\omega^2(k)} \sim \int_{2\pi/L}^{\Lambda} \frac{dk}{k} , \quad (31)$$

($\Lambda = 1/a$, inverse lattice spacing). In order to circumvent this no-go theorem one can go to the large N limit, invoking a diverging number of degrees of freedom at each point. This was demonstrated by Witten^{15,16} for the chiral GN model, a case very pertinent to the present study. After integrating out the fermions with the help of a complex scalar auxiliary field $\Phi = \Phi_0 e^{i\theta}$, one gets the following effective low-energy action for the Goldstone mode θ ,

$$\mathcal{L}_{\text{eff}} = \frac{N}{4\pi} (\partial_\mu \theta)^2 . \quad (32)$$

Chiral symmetry breaking can be probed by the correlator

$$\langle \bar{\psi}\psi(x) \bar{\psi}\psi(y) \rangle \rightarrow \langle \Phi^*(x) \Phi(y) \rangle . \quad (33)$$

It approaches a constant $|\Phi_0|^2$ for $|x - y| \rightarrow \infty$ if the symmetry is broken. Without SSB, one expects an exponential decay

$$\langle \Phi^*(x) \Phi(y) \rangle \sim e^{-M|x-y|} . \quad (34)$$

Here, a different behavior is found,

$$\langle \Phi^*(x) \Phi(y) \rangle \sim \langle e^{-i\theta(x)} e^{i\theta(y)} \rangle \sim e^{-2\pi G(x-y)/N} \sim \frac{1}{|x-y|^{1/N}} . \quad (35)$$

G is the free massless boson propagator, logarithmic in two dimensions. Exponentiation of this propagator yields a power law behavior for the propagator. Evidently, there is no SSB at any finite N , in agreement with the no-go theorem, but there is a loophole at $N = \infty$ since

$$\langle \Phi^*(x) \Phi(y) \rangle \sim 1 + \frac{1}{N} \ln |x-y| + O(1/N^2) . \quad (36)$$

The correlator becomes more and more long-range until it cannot be distinguished from a constant, in the limit $N \rightarrow \infty$. A similar phenomenon is known from two-dimensional xy spin-model^{17,18,19} under the name of topological order.

2.5 Gauge fields

Gauge symmetry implies redundant variables; this is nowhere as clear as in a two dimensional world where, due to the absence of transverse directions, one might guess that all degrees of freedom of a gauge field are “pure gauge”. This is not quite true — there are left-over quantum mechanical degrees of freedom stemming from gauge invariant zero-mode fields. They can only be discussed reasonably well on a finite interval of length L . Evidently, pure gauge theories are a totally different story in 1+1 and 3+1 dimensions, as are the corresponding interactions between static charges.

2.5.1 Abelian gauge fields

For the U(1) gauge theory, Lagrangian and field strength tensor look as usual,

$$\mathcal{L} = -\frac{1}{4}F_{\mu\nu}F^{\mu\nu} , \quad F_{\mu\nu} = \partial_\mu A_\nu - \partial_\nu A_\mu . \quad (37)$$

In two dimensions however, an antisymmetric tensor has only one independent component, a Lorentz scalar (the electric field); there is no magnetic field. Canonical quantization in the Weyl gauge ($A_0 = 0$) reveals that the electric field $E = \partial_0 A^1$ is conjugate to (minus) the vector potential A^1 ,

$$[E(x), A^1(y)] = i\delta(x - y) . \quad (38)$$

The Gauss law in this gauge has to be implemented as a constraint on the physical states (this is possible since $G(x)$ is conserved),

$$G(x)|\rangle = \partial_1 E(x)|\rangle = 0 . \quad (39)$$

This leaves only the 0-mode of A_1 , the spatially constant electric field, as physical variable. Switching to finite L , we have

$$a = \frac{1}{L} \int_0^L dx A^1(x) , \quad e = \int_0^L dx E(x) \quad (40)$$

with

$$H = \frac{1}{2L} e^2 , \quad [e, a] = i . \quad (41)$$

Since the integer part of $\frac{gLa}{2\pi}$, g being the electric charge of static sources, can also be gauged away by a periodic gauge transformation

$$U = e^{i2\pi nx/L} , \quad (42)$$

pure QED reduces to quantum mechanics of a particle on a circle.²⁰ If we couple static charges to the gauge field, this changes Gauss’s law into $G =$

$\partial_x E - e\rho$. The “longitudinal” electric field (i.e., the x -dependent part) is the Coulomb field of the static charge, which is linear in one space dimension. For comparison with Yang-Mills theory below, assume two charges $\pm g$ on a circle of length L at points x, y ; then the change in energy is

$$\Delta E = g^2 K(x - y) \quad (43)$$

with the periodic Coulomb potential

$$\begin{aligned} K(x - y) &= \langle x | \frac{1}{\partial_x^2} | y \rangle = -\frac{L}{4\pi^2} \sum_{n \neq 0} \frac{1}{n^2} e^{i2\pi n(x-y)/L} \\ &= -\frac{L}{12} + \frac{1}{2}|x - y| - \frac{1}{2L}(x - y)^2 . \end{aligned} \quad (44)$$

Pure QED is confining in 1+1 dimensions for rather trivial reasons. In the limit $L \rightarrow \infty$, the fact that the potential to order g^2 is linear also follows on purely dimensional grounds, since $[g] = L^{-1}$. Finally, we note that one has to impose the residual Gauss law ($Q| \rangle = 0$); only the charge 0 sector survives on the circle.

2.5.2 Non-Abelian gauge fields

Consider the Lagrangian of Yang-Mills theory with a $SU(N)$ gauge group on a circle,^{21,22,23}

$$\mathcal{L} = -\frac{1}{4} F_{\mu\nu}^a F^{a\mu\nu} , \quad (45)$$

and

$$F_{\mu\nu}^a = \partial_\mu A_\nu^a - \partial_\nu A_\mu^a - gf^{abc} A_\mu^b A_\nu^c . \quad (46)$$

Whereas canonical quantization in the Weyl gauge is as straightforward as in the Abelian case, the resolution of Gauss’s law becomes more intricate due to its non-linearity

$$G^a(x) = (DE)^a(x) = \partial_x E^a - gf^{abc} A^{1,b} E^c . \quad (47)$$

Generically, the covariant derivative has $N - 1$ zero modes; the projections of E onto these are the physical (quantum mechanical) variables e^p .²⁴ They are non-hermitean due to the projection onto A^1 -dependent basis vectors. The corresponding gauge invariant coordinates are the eigenphases of the path ordered integrals (untraced Polyakov loops) around the compact space direction,

$$\mathcal{P} = P e^{ig \int_0^L dx A^1(x)} = V e^{igaL} V^\dagger , \quad a = a^p t^p . \quad (48)$$

One finds

$$[e^p, a^q] = i\delta_{pq} \quad (49)$$

and the Hamiltonian

$$H_a = \frac{1}{2L} e^{p\dagger} e^p = -\frac{1}{2L} \frac{1}{\mathcal{J}(a)} \frac{\partial}{\partial a^p} \mathcal{J}(a) \frac{\partial}{\partial a^p} . \quad (50)$$

This form makes explicit the fact that the variables are curvilinear coordinates — H_a is just the Laplacian on the $SU(N)$ group manifold, the Jacobian $\mathcal{J}(a)$ being the reduced Haar measure (Vandermonde determinant for unitary matrices)

$$\mathcal{J}(a) = \prod_{i>j} \sin^2 \left(\frac{1}{2} gL(a_{ii} - a_{jj}) \right) . \quad (51)$$

Convenient angular variables are

$$\varphi_i = gLa_{ii} \quad (52)$$

with the constraint $\sum_i \varphi_i = 0$ for $SU(N)$. If one introduces the analogue of a “radial wavefunction”

$$\Phi(\varphi) = \frac{u(\varphi)}{\sqrt{\mathcal{J}(\varphi)}} , \quad (53)$$

the Laplacian is reduced to cartesian form (except for a center of mass correction in the $SU(N)$ case, as opposed to $U(N)$), and a constant effective potential appears,

$$H = -\frac{g^2 L}{4} \left(\sum_{i=1}^N \frac{\partial^2}{\partial \varphi_i^2} - \frac{1}{N} \left(\sum_{i=1}^N \frac{\partial}{\partial \varphi_i} \right)^2 \right) - \frac{Ng^2 L(N^2 - 1)}{48} . \quad (54)$$

The reduced wave function $u(\varphi)$ now has to satisfy the boundary conditions

$$u(\varphi) = 0 \quad \text{if} \quad \varphi_i = \varphi_j . \quad (55)$$

The ground state is simply $\Phi_0 = \text{const.}$, normalizable owing to the compactness of the variables, with $E_0 = 0$. To get the excited states for any N , it is advantageous to reinterpret this problem in terms of free, non-relativistic fermions on a circle²⁵ (the Pauli principle is enforced by Eq. (55)) with periodic (anti-periodic) boundary conditions for odd (even) N . Then the wavefunctions are Slater determinants of single particle wave functions

$$\psi_m(\varphi) = \frac{1}{\sqrt{2\pi}} e^{im\varphi} \quad (56)$$

with m integer for odd, half integer for even N . The energy is

$$E = \frac{g^2 L}{4} \left(\sum_m^{\text{occ}} m^2 - \frac{1}{N} \left(\sum_m^{\text{occ}} m \right)^2 \right) - \frac{Ng^2 L(N^2 - 1)}{48}, \quad (57)$$

where the sums run over all occupied orbits. By filling the lowest N single particle states, one can easily ascertain that the ground state wavefunction is constant and that the ground state energy vanishes. The configuration space is determined by the fundamental domain, the smallest region bounded by zeros of the Jacobian. We can choose

$$\varphi_1 < \varphi_2 < \dots < \varphi_N \quad (58)$$

and the center of mass constraint $\sum_i \varphi_i = 0$ for $SU(N)$ (this represents a more complete gauge fixing). Since the ordering is on a circle rather than a line, it still leaves a residual gauge freedom, namely cyclic permutations of color labels. This residual Z_N symmetry is expected on topological grounds due to

$$\Pi_1(SU(N)/Z_N) = Z_N. \quad (59)$$

This is the well-known center symmetry of pure Yang Mills theory which plays an important role at finite temperature.²⁶ By way of illustration, take $SU(2)$: There is only one independent angular variable, $\varphi = (\varphi_1 - \varphi_2)/2 \in [0, \pi]$. Then, YM_2 reduces to quantum mechanics of a particle in an infinite square well with

$$H = -\frac{g^2 L}{8} \frac{\partial^2}{\partial \varphi^2} - \frac{g^2 L}{8} \quad (60)$$

and

$$u_n(\varphi) = \sqrt{\frac{2}{\pi}} \sin n\varphi, \quad \mathcal{J}(\varphi) = \sin^2 \varphi, \quad E_n = \frac{g^2 L}{8} (n^2 - 1). \quad (61)$$

The Z_2 center symmetry is just parity. A detailed discussion of the $SU(3)$ case with two independent variables can be found in Ref. 27. At very large N , since the φ_i repel each other (cf. Eq. 55) and live on a circle, they will tend to distribute themselves along the circle like a pearl necklace, with fluctuations which are $1/N$ suppressed in amplitude. This observation will become important later on for the 't Hooft model at finite temperature.

The existence of zero mode gluons also complicates the interaction between static charges, at least for finite L . If one puts a static $q\bar{q}$ -pair on a circle, the Coulomb potential evidently involves D^{-2} (covariant derivatives) rather than

∂^{-2} , so that the Coulomb interaction gets modified by the gauge field remnants. The Coulomb potential can be transformed to coordinate space,^{28,29}

$$\begin{aligned} K_{ij}(z) &= -L \sum_n \frac{1}{(2\pi n - \varphi_j + \varphi_i)^2} e^{i2\pi n z/L} \\ &= -\frac{L}{4} e^{i(\varphi_j - \varphi_i)z/L} \left(\frac{1}{\sin^2(\varphi_i - \varphi_j)/2} - \frac{2}{L}|z| + i\frac{2}{L}z \cot(\varphi_i - \varphi_j)/2 \right) \end{aligned} \quad (62)$$

for $i \neq j$, whereas it is identical to the Abelian one, Eq. (44), for $i = j$. Since the φ_i are dynamical variables, one is not yet through but still has to solve a fairly complicated quantum mechanical $(N - 1)$ -body problem with a two-body potential defined by the Coulomb interaction. This reflects the fact that due to color spin dynamics, charges are never static in the non-Abelian case, even if they are nailed down in space. A full analytic solution is available for the $SU(2)$ case,²⁸ where a dynamical quantum mechanical supersymmetry is at work.³⁰ It explains why the potential is strictly linear (at all L , not just in the limit $L \rightarrow \infty$), and why – for vanishing separation of the charges – all excited states are doubly degenerate whereas the ground state is non-degenerate and has strictly zero energy, see Fig. 1. In the limit $L \rightarrow \infty$, all excited states move up to infinite energy, the gauge field dynamics get frozen, and the difference between QED_2 and YM_2 disappears.

The discussion about the zero mode gauge fields may seem a bit pedantic: Why bother about finite L at all? The reason is of course that we are interested among other things in the finite temperature problem. The physics relevance of the Polyakov loop is beyond doubt there.

Finally, the fact that the left-over gluon variables are eigenphases of path-ordered integrals has been used in the literature to emphasize the string picture: Closed strings that wrap around the compact direction in pure Yang-Mills theory, open strings with quarks at the ends if one includes matter fields in the fundamental representation.^{29,31,32} We shall not exploit this picture here any further.

2.6 Renormalization

From the kinetic term in the Lagrangian in two dimensions, one infers that Dirac fermion, scalar boson and vector fields have dimensions

$$[\psi_i] = L^{-1/2}, \quad [\phi] = [A^\mu] = L^0. \quad (63)$$

In self-interacting fermion theories, a quartic self-interaction has dimensionless coupling constant and is therefore perturbatively renormalizable (GN model)

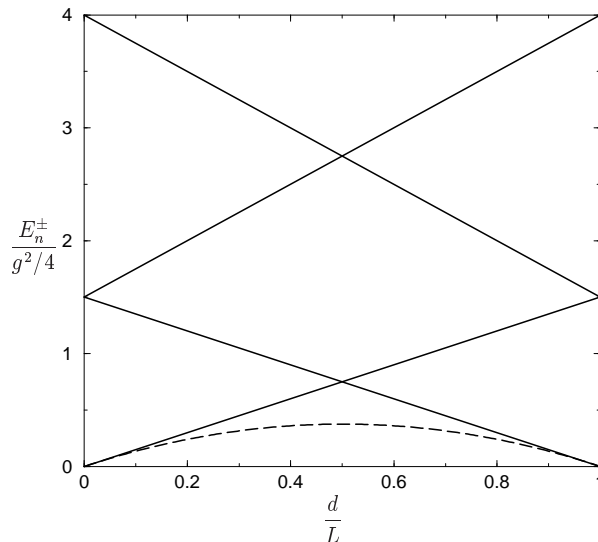


Figure 1: Interaction energy of static quarks at distance d on a circle of length L . Dashed line: QED₂, cf. Eq. (44); solid lines: SU(2) YM₂ (cf. Refs. 28, 30).

unlike in four dimensions (NJL model). Self-interacting bosons can have interactions of arbitrary high order with couplings of positive mass dimension and are all super renormalizable (e.g. sine-Gordon model). The gauge coupling has dimension of mass, therefore gauge theories like the Schwinger model or QCD₂ are also super-renormalizable.

In the U(1) theory, an axial anomaly occurs, as is well known from the Schwinger model. In one-flavor SU(N) QCD₂, there is no axial anomaly.

Pure fermionic theories of GN type are asymptotically free; they share this property with QCD and are rather exceptional in this respect. The β -function is negative (see Sec. 3.1.1). If the bare mass is put equal to zero (as in the original GN model), dimensional transmutation occurs like in pure Yang-Mills theory in four dimensions: A massless theory generates mass dynamically. All dimensionless ratios can be predicted without free parameter, only the physical fermion mass is needed as an input.³

In the massive GN model, there are two distinct parameters of dimension mass (matching the two bare parameters Ng^2, m_0): The physical fermion mass m and the ratio $m_0/(Ng^2)$. The first parameter is directly observable via the spectrum. The second parameter is also observable: In the chiral GN model, it determines the mass of the would-be Goldstone boson, cf. Sec. 3.3. In the

non-chiral GN model, it can be measured via the $\bar{q}q$ scattering length which is proportional to Ng^2/m_0 . In the limit $m_0 \rightarrow 0$, the pion mass goes to zero and the scattering length in the non-chiral model diverges. In this way, the second parameter disappears and all observables can be expressed in terms of m only.

QCD₂ is trivially asymptotically free, being super-renormalizable. The perturbative (short distance) interaction is determined by dimensional considerations.

2.7 Soluble models of interest for QCD

The first generation of soluble models like the Thirring model³³ or the massless Schwinger model² from ± 1960 were not yet rich enough for the questions we are interested in. Although they can be solved exactly and have certain interesting non-perturbative aspects, they essentially describe free theories with a trivial S -matrix. If one tries to make them non-trivial by adding e.g. a mass term or flavor, one loses solvability. The Schwinger model has confinement, but provides no model for hadrons.

From this point of view, 't Hooft's idea of the $1/N$ expansion³⁴ is very nice indeed. By invoking a large number of fermion species and using $1/N$ as a small parameter, one finds highly non-trivial results already to leading order. Semiclassical methods become applicable and yield systematic, reliable results. All symmetries like Poincaré invariance, chiral symmetry, gauge invariance are preserved. The phenomenological arguments in favor of the large N limit for QCD (Zweig rule etc.^{35,36,37}) naturally play no role in two dimensions, where it is a purely theoretical tool.

Models based on the large N expansion can be considered as second generation field theory models, also historically. The two models we are particularly interested in came up in 1974, the GN³ and the 't Hooft model⁴. The GN model generalizes the Thirring model to N flavors, while the 't Hooft model generalizes the Schwinger model to the non-Abelian SU(N) gauge group with a large number of colors. They acquire a rich physical content, as we hope to convince the reader in the remainder of this article. Here, we only mention the following basic facts: The GN models describe self-interacting massless fermions with a point-like four-fermion interaction. Depending on the particular variant, they can have either a discrete or a continuous chiral symmetry; in the latter case, the GN model may be thought of as the NJL model³⁸ in two dimensions. Mass terms which violate chiral symmetry explicitly can be included as well without loss of solvability (at large N). The 't Hooft model is QCD₂ with SU(N) color in the limit $N \rightarrow \infty$, with massless or massive quarks in the fundamental representation. As mentioned above, the model on the infinite line has no gluon

degrees of freedom, but is also a self-interacting fermion theory, here with a linear Coulomb potential characteristic for the two dimensional world (in an appropriate gauge). Unlike the GN models, this model shows confinement, which makes it particularly interesting from the point of view of QCD. The fact that also in real life (in four dimensions), the NJL model and QCD are used in parallel nowadays for certain questions of strong interaction physics makes this pair of models a good match and immediately suggests many questions to be asked. Throughout this work, we do not consider any embellishments or generalizations (e.g. flavor, more complicated interactions, different matter fields) of these models which have occasionally been invoked. The nice thing about the original models is just the contrast between the simplicity of the Lagrangian and the complexity of the phenomena it produces, and we do not want to spoil this property.

Finally, we should point out that the main goal of the present study are questions of hot and dense matter in these toy models. For this purpose, the large N limit is not only a technical trick leading to solvability of the models, but is in fact instrumental for enabling chiral symmetry breakdown in two dimensions. This is the reason why another aspect of the GN model will play no role here, its integrability.^{39,40,41} A lot of progress has been made towards solving the finite N model exactly. Here, we shall restrict ourselves to the large N limit so that the corresponding difference between the non-integrable 't Hooft model and the integrable GN models will not play any role, but a common approach for both models will be used throughout.

3 Two dimensional models at zero temperature and chemical potential

3.1 Gross-Neveu models

We cannot discuss finite temperature or density without first reviewing the particle content of the theory. Originally, the GN model has been solved with the help of semi-classical functional methods,³ supplemented by inverse scattering techniques from soliton theory for the baryons.⁴² This approach can be rigorously justified in the large N limit. Typically, one introduces auxiliary bosonic fields and integrates out the fermions (Gaussian integral over Grassmann variables), then applies a saddle point approximation to the remaining bosonic functional integral. More recently, an alternative to the inverse scattering method has been proposed, based on the Gel'fand-Dikii equation.⁴³ Here, in order to have a coherent scheme for all questions that interest us as well as for pedagogical reasons, we shall make use of time honored concepts well known from atomic and nuclear physics, such as the HF and random phase

approximation (RPA), although in a fully relativistic setting.^{44,45,46} In contrast to the functional integral methods, we thereby handle fermions more directly and, since we work canonically, can also more readily address questions of the vacuum structure (Dirac sea). Needless to say, the equations one eventually solves are always the same (HF or Schwinger-Dyson, RPA or Bethe-Salpeter equations). More than anything else the choice is a question of language.

3.1.1 Vacuum, physical fermion

The Lagrangian of the GN model family, including a bare fermion mass term and suppressing color labels, reads³

$$\mathcal{L} = \bar{q} i\gamma^\mu \partial_\mu q + \frac{1}{2} g^2 \left[(\bar{q}q)^2 - \lambda (\bar{q}\gamma^5 q)^2 \right] - m_0 \bar{q}q . \quad (64)$$

The original model with discrete chiral symmetry $q \rightarrow \gamma^5 q$ is recovered for $\lambda = 0, m_0 = 0$; the choice $\lambda = 1, m_0 = 0$ corresponds to the NJL-type model with continuous chiral symmetry; the m_0 term breaks both chiral symmetries explicitly. To leading order in $1/N$, the Hartree approximation can be used, replacing $\bar{q}q$ in the Euler-Lagrange equation

$$i\gamma^\mu \partial_\mu q + g^2 (\bar{q}q - \lambda (\bar{q}\gamma^5 q)\gamma^5) q - m_0 q = 0 \quad (65)$$

by its vacuum expectation value (the Fock term is $1/N$ suppressed). The non-zero value of the order parameter for chiral symmetry signals SSB. We first assume $\langle \bar{q}\gamma^5 q \rangle = 0$,

$$\{i\gamma^\mu \partial_\mu - m_0 + Ng^2 \rho_s\} q(x) = 0 . \quad (66)$$

A physical fermion mass appears,

$$m = m_0 - Ng^2 \rho_s , \quad \rho_s = \frac{1}{N} \langle \bar{q}q \rangle , \quad (67)$$

as dictated by covariance. The essence of the Hartree approximation is to impose a self-consistency condition, here on the scalar density ρ_s of the vacuum. Using the free fermion spinors of Eq. (15) above we get

$$\begin{aligned} \rho_s = -\frac{(m - m_0)}{Ng^2} &\stackrel{!}{=} \int_{-\Lambda/2}^{+\Lambda/2} \frac{dk}{2\pi} \bar{v}(k)v(k) \\ &= -\int_{-\Lambda/2}^{+\Lambda/2} \frac{dk}{2\pi} \frac{m}{\sqrt{k^2 + m^2}} \simeq -\frac{m}{2\pi} \log \frac{\Lambda^2}{m^2} . \end{aligned} \quad (68)$$

As usual, this is also a variational solution obtained by minimizing the vacuum energy in the space of Slater determinants. The Hartree- or gap equation,

$$m = m_0 + m \frac{Ng^2}{2\pi} \ln \frac{\Lambda^2}{m^2} , \quad (69)$$

contains much information. For $m_0 = 0$ (discrete or continuous model), it has two solutions, either $m = 0$ or

$$1 = \frac{Ng^2}{2\pi} \ln \frac{\Lambda^2}{m^2} . \quad (70)$$

The broken symmetry solution is always lower in energy density by

$$\mathcal{E}_{\text{vac}} - \mathcal{E}_{\text{vac}}^{\text{free}} = -\frac{Nm^2}{4\pi} . \quad (71)$$

The gap equation for the broken phase does not determine m , as is clear from the fact that the theory contains no dimensionful parameter. If m is adjusted (to the “observed” fermion mass, whatever that means in two dimensions), then the gap equation is a renormalization condition which tells us how Ng^2 (the bare coupling constant) depends on the cutoff Λ . Correspondingly, the physical mass has the dependence

$$m = \Lambda \exp \left\{ -\frac{\pi}{Ng^2} \right\} \quad (72)$$

familiar from similar dependences in real QCD and in line with the renormalization group. All physical quantities with dimension of mass have to depend in the same way on g, Λ . The essential singularity in g at $g = 0$ underlines the power of the $1/N$ expansion as compared to ordinary perturbation theory in g . Dimensionless quantities can be predicted without any parameter, at $m_0 = 0$. Apart from this phenomenon of dimensional transmutation, the other remarkable feature which we find here is asymptotic freedom (AF).^{47,48} One can determine the β -function of the GN model in an elementary way as follows: The physical fermion mass m should be cut-off independent, therefore

$$\Lambda \frac{d}{d\Lambda} m(\Lambda, g(\Lambda)) = \left(\Lambda \frac{\partial}{\partial \Lambda} + \Lambda \frac{dg}{d\Lambda} \frac{\partial}{\partial g} \right) m = 0 . \quad (73)$$

Set

$$\Lambda \frac{dg}{d\Lambda} = \beta(g) \quad (74)$$

and find, by inserting m from Eq. (72),

$$\beta(g) = -\frac{Ng^3}{2\pi} < 0 \quad (75)$$

or AF (to this order, the result is independent of the renormalization scheme). More elaborate computations of the higher loop beta-functions^{49,50} do not play a role in the large N limit. We shall return to the issue of AF in connection with $q\bar{q}$ scattering, where a running coupling constant will be defined.

For $m_0 = 0$ and the case of continuous chiral symmetry, the assumption $\langle \bar{q}\gamma^5 q \rangle = 0$ is too restrictive; one gets a continuum of vacua related by $U(1)$ transformations and labeled by a chiral angle φ ,

$$\langle \bar{q}q \rangle = -\frac{m}{g^2} \cos \varphi, \quad \langle \bar{q}i\gamma^5 q \rangle = \frac{m}{g^2} \sin \varphi. \quad (76)$$

For non-vanishing bare mass m_0 , the gap equation (69) signals the appearance of a second physical parameter $\frac{m_0}{Ng^2}$, in addition to the overall scale set by m . Its relevance for scattering and bound state observables will become clear later on.

3.1.2 Baryons

It would be premature to conclude from the preceding section that the GN model at $N \rightarrow \infty$ reduces to a free, massive fermion theory. As observed by Witten,³⁶ baryons have to be considered at large N and can be treated in HF approximation, like the vacuum. They correspond to a different kind of HF solution which breaks translational invariance. Their mass diverges like N , the baryon-baryon interaction also scales like N , and these effects have to be taken into account in leading order. Baryons were found originally with functional techniques and inverse scattering methods.⁴² Since we now know the scalar potential, we can use it to verify Witten's picture of baryons as relativistic HF solutions — this is what we propose to do here.⁴⁶ We consider the discrete chiral model first, since the continuous model has in addition totally different, light baryons, see Sec. 3.3 below.

If we restrict ourselves to baryons made up of $n \leq N$ quarks, it is sufficient to take into account one positive energy “valence” level filled with n fermions, together with the completely filled Dirac sea. The Hartree equation without invoking translational invariance becomes

$$\{i\gamma^\mu \partial_\mu + Ng^2 \rho_s(x)\} q(x) = 0 \quad (77)$$

where the scalar density now refers to the baryon state $|B\rangle$,

$$\rho_s(x) = \frac{1}{N} \sum_{i=1}^N \langle B | \bar{q}_i(x) q_i(x) | B \rangle. \quad (78)$$

We introduce the single particle energies and eigenfunctions of the Dirac Hamiltonian corresponding to Eq. (77),

$$\left\{ \gamma^5 \frac{1}{i} \frac{\partial}{\partial x} - \gamma^0 N g^2 \rho_s(x) \right\} \psi_\alpha^{(\pm)}(x) = \pm \epsilon_\alpha \psi_\alpha^{(\pm)}(x) . \quad (79)$$

Then $\rho_s(x)$ is given by

$$\rho_s(x) = \frac{n}{N} \bar{\psi}_0^{(+)}(x) \psi_0^{(+)}(x) + \sum_\alpha \bar{\psi}_\alpha^{(-)}(x) \psi_\alpha^{(-)}(x) \quad (80)$$

where $\psi_0^{(+)}$ is the valence state. Dashen *et al.*⁴² have found two different types of solutions for the scalar density, the “kink” and the “double kink” (or rather kink-antikink). Let us start with the less exotic double kink, characterized by the following scalar potential:

$$S(x) \equiv -N g^2 \rho_s(x) = m \{1 + y (\tanh \xi_- - \tanh \xi_+)\} \quad (81)$$

with the definitions

$$y = \sin \theta , \quad \theta = \frac{\pi}{2} \frac{n}{N} , \quad (82)$$

$$\xi_\pm = y m x \pm \frac{1}{2} \text{artanh } y . \quad (83)$$

$S(x)$ has the form of a potential well and approaches for $x \rightarrow \pm\infty$ the asymptotic value m , i.e., the physical fermion mass. Varying y or equivalently the degree of occupation n/N , $S(x)$ changes from a $1/\cosh^2(y m x)$ shape at small y to a Woods-Saxon like shape at $y \simeq 1$,

$$S(x) \sim \left(1 + e^{(|x|-R)/c}\right)^{-1} , \quad (84)$$

with skin thickness c and radius R given by

$$c = \frac{1}{2m} , \quad R = -\frac{1}{2m} \log \frac{\cos \theta}{2} \quad (y \rightarrow 1) , \quad (85)$$

respectively. We proceed to verify the self-consistency of this scalar potential. After a straightforward solution of the Dirac equation (77) with potential (81), one finds the following results: The normalized wavefunctions of the discrete (valence) states are given by (in a basis where $\gamma^0 = -\sigma_1, \gamma^1 = i\sigma_3$)

$$\psi_0^{(\pm)}(x) = \frac{\sqrt{ym}}{2} \begin{pmatrix} \frac{1}{\cosh \xi_-} \\ \mp \frac{1}{\cosh \xi_+} \end{pmatrix} \quad (86)$$

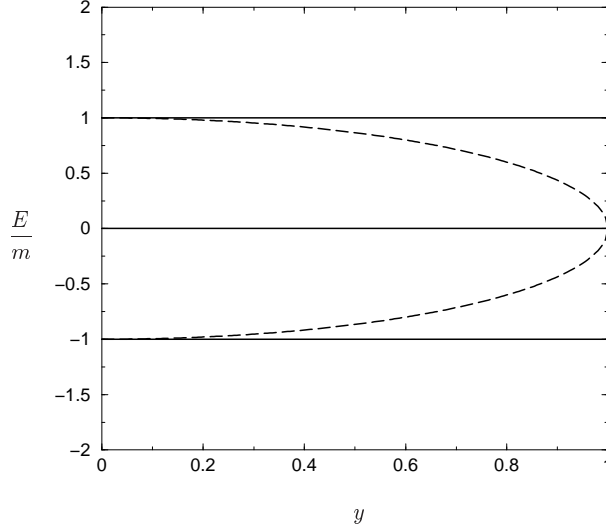


Figure 2: Single particle spectrum belonging to the baryon in the GN model. Continuum states fill the outer region $|E/m| > 1$; dashed curves inside the gap are valence levels; y measures the occupation number of the positive energy valence state, cf. Eq. (82).

with eigenvalues

$$E_0^{(\pm)} = \pm m \sqrt{1 - y^2} . \quad (87)$$

The continuum states are

$$\psi_k^{(\pm)}(x) = \frac{1}{\sqrt{2}E(k)(ik + ym)} \begin{pmatrix} (ik - m)(ik - ym \tanh \xi_-) \\ \pm E(k)(ik - ym \tanh \xi_+) \end{pmatrix} e^{ikx} , \quad (88)$$

with

$$E(k) = \sqrt{k^2 + m^2} . \quad (89)$$

They are reflectionless, a characteristic feature of time independent solutions.⁵¹
^{52,53} The spectrum of the Dirac Hamiltonian therefore consists of the usual positive and negative energy continua starting from $\pm m$ and a pair of discrete states inside the mass gap at energies given by Eq. (87), see Fig. 2. These latter states are of course a prerequisite for obtaining bound baryons. The discrete negative energy state has to be filled completely (N fermions), its positive energy partner with $n \leq N$ fermions (remember that, unlike in QCD, there is no restriction to color singlets). Reinserting Eqs. (86,88) into (81), one can then verify the self-consistency of the solution. This requires the use of the vacuum gap equation (69) to eliminate infinities.⁴⁶

Finally, one has to compute the mass of the baryon. This is somewhat delicate because of the vacuum subtraction. The single particle energies of two systems must be subtracted: One of the systems has only continuum states, whereas the other system has one extra pair of discrete states. The easiest way of doing this is to enclose the system in a finite box, thereby discretizing all states, and to use the well-known relation between phase shifts and density of states. In this way, one recovers the result of Dashen *et al.*⁴² for the baryon mass,

$$M_B = \frac{2Nym}{\pi} = nm \left(\frac{\sin \theta}{\theta} \right) . \quad (90)$$

Let us briefly compare this exact result to the non-relativistic approach (in the present model, the number of valence quarks governs the degree of relativity). In the non-relativistic Hartree approximation, we start from the Schrödinger equation for a particle of mass m , interacting with the other particles through a δ -function potential. The Hartree equation then reduces to the non-linear Schrödinger equation,⁵⁴

$$\left\{ -\frac{1}{2m} \frac{\partial^2}{\partial x^2} - ng^2 |\phi_0|^2 \right\} \phi_0(x) = E_0 \phi_0(x) , \quad (91)$$

with the following bound state solution,

$$\phi_0(x) = \sqrt{\frac{\kappa}{2}} \frac{1}{\cosh \kappa x} , \quad (92)$$

$$\kappa = \frac{1}{2} ng^2 m , \quad E_0 = -\frac{\kappa^2}{2m} . \quad (93)$$

The baryon mass turns out to have the value

$$M_B = nm \left(1 - \frac{1}{6} \left(\frac{ng^2}{2} \right)^2 \right) . \quad (94)$$

If we choose

$$g^2 = \frac{\pi}{N} , \quad (95)$$

both M_B and the scalar density in the full calculation and in the non-relativistic limit agree up to $O(y^2)$. The reason why the GN model corresponds to a specific choice of the coupling constant is that it involves only one parameter, whereas the non-relativistic model has two independent parameters, the fermion mass and the coupling constant.

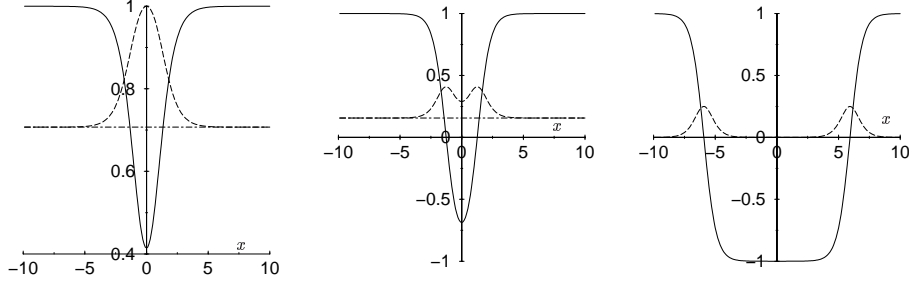


Figure 3: Scalar potential S (solid), valence fermion density ρ_f^0 (dashed) and valence energy E_0 (dash-dotted lines) for GN model baryon and three different occupation fractions, $n/N = 0.5$ (left), 0.9 (middle), and 0.99999 (right). In units of m .

Now turn to the opposite, extreme relativistic limit. As θ approaches $\pi/2$, the effects of the Dirac sea become overwhelming. Eventually, the baryon goes over into a well separated kink anti-kink pair. Although the scalar density becomes flat, the fermion density for the discrete state is concentrated near the surface, since

$$\rho_f^0 = \psi_0^\dagger(x)\psi_0(x) = \frac{ym}{4} \left(\frac{1}{\cosh^2 \xi_-} + \frac{1}{\cosh^2 \xi_+} \right). \quad (96)$$

In the limit $y \rightarrow 1$, the two kinks are completely decoupled, see Fig. 3.

If one looks at a single kink now, one finds another type of baryon of the GN model, referred to as Callan-Coleman-Gross-Zee kink in the literature.⁵⁵ It has the scalar potential

$$S(x) = m \tanh(xm). \quad (97)$$

This solution has many unusual features: $S(x)$ interpolates between the two different vacua related by the discrete γ^5 -transformation. Unlike the double kink baryon which is only stabilized by the binding of fermions, the single kink is topologically stable. The fact that a kink type potential can bind particles is a well-known, purely relativistic effect which has no analogue in non-relativistic quantum mechanics. The discrete state corresponding to Eq. (86) becomes

$$\psi_0(x) = \sqrt{\frac{m}{2}} \begin{pmatrix} \frac{1}{\cosh mx} \\ 0 \end{pmatrix}, \quad (98)$$

with eigenvalue $E_0 = 0$, while the continuum wavefunctions replacing Eq. (88) are

$$\psi_k^{(\pm)}(x) = \frac{1}{\sqrt{2E(k)}} \begin{pmatrix} ik - m \tanh mx \\ \pm E(k) \end{pmatrix} e^{ikx}. \quad (99)$$

The valence state has evidently vanishing scalar density so that there is no feedback at all to the Hartree potential. This is consistent with the fact that the mass of the kink baryon is independent of the number n of valence fermions. The self-consistency for the scalar potential can again be verified using the vacuum Hartree condition (69). As expected intuitively, the mass is $1/2$ of the double kink mass in the limit $y \rightarrow 1$

$$M_B|_{\text{kink}} = \frac{Nm}{\pi} , \quad (100)$$

in agreement with Dashen *et al.*⁴²

3.1.3 Mesons

In this section, we shall rederive the known fermion-antifermion bound state (meson) of the GN model, using the relativistic RPA. This meson has zero binding energy in the large N limit, i.e., its mass is just twice the physical fermion mass.³ We discuss only the discrete chiral symmetry case here, without bare mass; the NJL type model with its massless Goldstone mode will be treated in Sec. 3.3. We derive the RPA equations using an equations of motion approach^{44,45} and solve them analytically for mesons with arbitrary momentum, thereby demonstrating explicitly the covariance of the spectrum.⁴⁶

In RPA, the meson is described in terms of particle-hole excitations on top of the HF vacuum. We therefore start from the equation of motion of the following operator bilinear in the fermion fields,

$$Q_{\alpha\beta}(x, y) = \frac{1}{N} \sum_i q_{i\beta}^\dagger(y) q_{i\alpha}(x) . \quad (101)$$

Using the equation of motion for q , Eq. (65), and neglecting $1/N$ suppressed terms, we find

$$\begin{aligned} i \frac{\partial}{\partial t} Q(x, y) &= -i \left\{ \frac{\partial}{\partial y} Q(x, y) \gamma^5 + \frac{\partial}{\partial x} \gamma^5 Q(x, y) \right\} \\ &\quad - N g^2 \left\{ \text{tr} (\gamma^0 Q(x, x)) \gamma^0 Q(x, y) - Q(x, y) \gamma^0 \text{tr} (\gamma^0 Q(y, y)) \right\} \end{aligned} \quad (102)$$

Furthermore, we expand the operator $Q(x, y)$ around its vacuum expectation value

$$Q(x, y) = \langle 0 | Q(x, y) | 0 \rangle + \frac{1}{\sqrt{N}} \tilde{Q}(x, y) + \dots \quad (103)$$

where the c -number part corresponds to the density matrix of the vacuum,

$$\langle 0 | Q(x, y) | 0 \rangle = \rho(x - y) . \quad (104)$$

Inserting (103) into (102) and equating terms with the same power in $1/\sqrt{N}$, we get to zeroth order the following alternative formulation of the Hartree equation,

$$i\frac{\partial}{\partial t}\rho(x) = -i\frac{\partial}{\partial x}[\gamma^5, \rho(x)] - Ng^2\text{tr}(\gamma^0\rho(0))[\gamma^0, \rho(x)] = 0 \quad (105)$$

and to order $1/\sqrt{N}$ the linearized equation of motion for the fluctuation \tilde{Q} ,

$$\begin{aligned} i\frac{\partial}{\partial t}\tilde{Q}(x, y) &= -i\left\{\frac{\partial}{\partial y}\tilde{Q}(x, y)\gamma^5 + \frac{\partial}{\partial x}\gamma^5\tilde{Q}(x, y)\right\} \\ &\quad - Ng^2\left\{\text{tr}(\gamma^0\rho(0))\gamma^0\tilde{Q}(x, y) - \tilde{Q}(x, y)\gamma^0\text{tr}(\gamma^0\rho(0))\right. \\ &\quad \left.+ \text{tr}(\gamma^0\tilde{Q}(x, x))\gamma^0\rho(x-y) - \rho(x-y)\gamma^0\text{tr}(\gamma^0\tilde{Q}(y, y))\right\}. \end{aligned} \quad (106)$$

Switching to momentum variables,

$$\begin{aligned} \rho(k) &= \int dx e^{-ikx}\rho(x) \\ \tilde{Q}(k', k) &= \int dx \int dy e^{-ik'x+iky}\tilde{Q}(x, y), \end{aligned} \quad (107)$$

the Hartree equation simplifies to

$$[h(k), \rho(k)] = [k\gamma^5 + m\gamma^0, \rho(k)] = 0 \quad (108)$$

where $h(k)$ denotes the single particle Dirac Hamiltonian and where we have again introduced the physical fermion mass, Eq. (67). The Hartree solution of Sec. 3.1.1 corresponds to

$$\rho(k) = v(k)v^\dagger(k) = \frac{1}{2} - \frac{m}{2E(k)}\gamma^0 - \frac{k}{2E(k)}\gamma^5 \quad (109)$$

and obviously satisfies Eq. (108). In order to convert Eq. (106) into the canonical form of the RPA, we first have to project the operator \tilde{Q} onto self-consistent Hartree spinors. In the present case this simply amounts to a change of basis from massless to massive free spinors. We define the “particle-hole” and “hole-particle” components of the operator \tilde{Q} as

$$\begin{aligned} \tilde{Q}_{12}(k', k) &= u^\dagger(k')\tilde{Q}(k', k)v(k) \\ \tilde{Q}_{21}(k', k) &= v^\dagger(k')\tilde{Q}(k', k)u(k). \end{aligned} \quad (110)$$

Using the commutation relations, the corresponding “particle-particle” and “hole-hole” operators \tilde{Q}_{11} and \tilde{Q}_{22} can be shown to be of higher order in $1/\sqrt{N}$ and can therefore be neglected. The resulting system of coupled equations is sandwiched between the vacuum $|0\rangle$ and a one meson state $\langle n, P|$, where P denotes the total momentum and n the type of meson. We define the transition matrix-elements

$$\begin{aligned}\langle n, P|\tilde{Q}_{21}(k', k)|0\rangle &= 2\pi\delta(P - k + k')X_n(P, k) , \\ \langle n, P|\tilde{Q}_{12}(k', k)|0\rangle &= 2\pi\delta(P - k + k')Y_n(P, k) .\end{aligned}\quad (111)$$

Then, using the Heisenberg equation of motion in order to replace time derivatives by energies, we obtain

$$\mathcal{E}_n(P)X_n(P, k) = E(k - P, k)X_n(P, k) \quad (112)$$

$$\begin{aligned}-Ng^2\bar{v}(k - P)u(k) \int \frac{dk'}{2\pi} \{ \bar{v}(k')u(k' - P)Y_n(P, k') \\ + \bar{u}(k')v(k' - P)X_n(P, k') \} \\ \mathcal{E}_n(P)Y_n(P, k) = -E(k - P, k)Y_n(P, k) \\ + Ng^2\bar{u}(k - P)v(k) \int \frac{dk'}{2\pi} \{ \bar{v}(k')u(k' - P)Y_n(P, k') \\ + \bar{u}(k')v(k' - P)X_n(P, k') \}\end{aligned}\quad (113)$$

with

$$E(k', k) = E(k') + E(k) . \quad (114)$$

These are the final RPA equations. Taking into account the symmetry relation

$$\bar{u}(k)v(k') = -\bar{v}(k)u(k') \quad (115)$$

which holds for the spinors (15), they can be cast into the familiar matrix form of the RPA,

$$\begin{pmatrix} A & B \\ -B & -A \end{pmatrix} \begin{pmatrix} X \\ Y \end{pmatrix} = \mathcal{E} \begin{pmatrix} X \\ Y \end{pmatrix} . \quad (116)$$

It is illustrated graphically in Fig. 4. Characteristic of the RPA (as opposed to the Tamm-Dancoff approximation (TDA)) are the backward going bubbles (corresponding to Y -components) which account for ground state correlations. Since the integral kernels are separable, one can solve these equations algebraically. After a few straightforward steps⁴⁶ one arrives at the eigenvalue equation

$$1 = \frac{Ng^2}{2} \int \frac{dk}{2\pi} \left(\frac{1}{E(k - P)} + \frac{1}{E(k)} \right) \frac{4m^2 + P^2 - E^2(k - P, k)}{\mathcal{E}_n^2(P) - E^2(k - P, k)} . \quad (117)$$

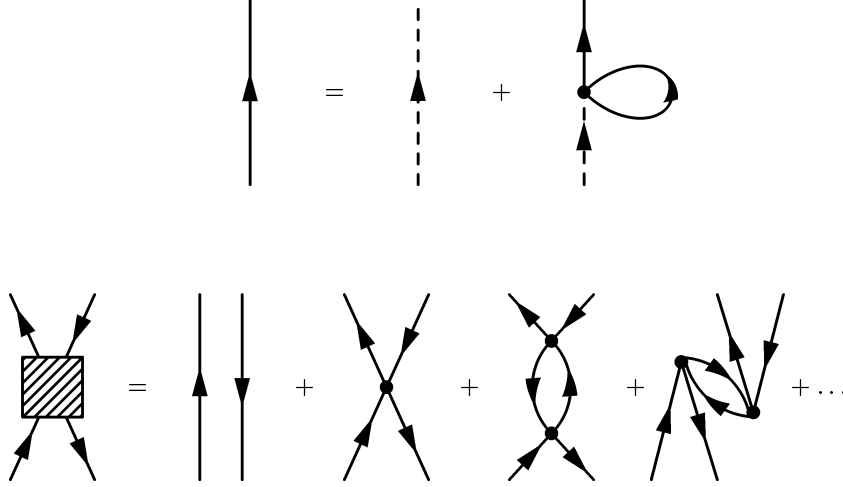


Figure 4: Diagrammatic illustration of HF (upper part) and RPA (lower part) for the GN model. Dashed lines: bare (massless) quark propagator, solid lines: dressed (massive) quark propagator.

Clearly, the choice

$$\mathcal{E}_0^2(P) = 4m^2 + P^2 \quad (118)$$

converts this into the vacuum Hartree equation. This shows that there is a marginally bound meson with mass $2m$, and that the spectrum is covariant.

It is instructive to compute also the $q\bar{q}$ scattering matrix in this approach⁵⁶. The scattering matrix can easily be found, since we are dealing with a separable potential. With the Mandelstam variable $s = 2P\mathcal{E}$, find

$$-\frac{1}{\tau(s)} = -\frac{\sqrt{2}}{\pi m^2} \sqrt{1-\eta} \left(\log \frac{1-\sqrt{1-\eta}}{1+\sqrt{1-\eta}} + i\pi \right) \quad (119)$$

in the scattering regime with $\eta = 4m^2/s < 1$. (τ is normalized such that $\tau = -Ng^2m^2/\sqrt{8}$ in tree approximation). $\tau(s)$ has the expected pole at $s = 4m^2$ corresponding to the threshold bound state. By going to large s , we can check asymptotic freedom in a very physical manner,

$$\tau(s) \approx \frac{\pi m^2}{\sqrt{2}} \frac{1}{\log(m^2/s)}. \quad (120)$$

The interaction shows the logarithmic decrease in the UV characteristic for asymptotically free theories. A running coupling constant can be defined by

comparison with the tree approximation ($s = \mu^2$),

$$Ng_{\text{eff}}^2(\mu) = \frac{2\pi}{\log \mu^2/m^2} . \quad (121)$$

This illustrates once again the usefulness of the GN model as toy model for QCD.

3.2 't Hooft model

The 't Hooft model⁴ is defined as the large N limit of 1+1 dimensional $SU(N)$ gauge theory with quarks in the fundamental representation,

$$\mathcal{L} = \bar{q} i \not{D} q - \frac{1}{2} \text{tr} F_{\mu\nu} F^{\mu\nu} , \quad \not{D} = \gamma^\mu (\partial_\mu + i g A_\mu) . \quad (122)$$

In the axial gauge, the gluons are gauged away, leaving behind a theory of fermions interacting via a Coulomb potential which is linearly rising in one space dimension. 't Hooft originally solved this model for the meson spectrum, using light-cone coordinates and the light-cone gauge. This was the first practical demonstration of the power of the $1/N$ expansion for gauge theories.³⁴ Working diagrammatically, he identified planar diagrams without quark loops as being of leading order in $1/N$ (nested rainbow graphs and ladders) and summed them up by solving (light-cone) Schwinger-Dyson and Bethe-Salpeter equations. He thus found an infinite tower of mesons lying on a kind of Regge trajectory. Early applications of this model dealt with issues of confinement, asymptotic freedom, form factors, scattering etc.^{57,58,59,60,61} For some time, the precise character of the 't Hooft limit was somewhat disputed (strong vs. weak coupling, order of limits, 't Hooft boundary condition, IR regularization of the quark self-energy, Wu's alternative meson equation⁶²). Studies in ordinary coordinates followed where the vacuum and baryons can be dealt with in a more direct way;^{63,64,65,44,45} they fully confirmed the original light-cone results for the meson spectrum. During the last few years, various extensions of the 't Hooft model were found useful as laboratory for QCD related questions, such as adjoint quarks^{66,67} (a toy model for gluons and strings), heavy quarks, operator product expansion, duality etc.^{68,69,70} In line with our main subject, we propose to go through the same three topics as in Sec. 3.1 for the GN model — the vacuum, baryons and mesons. The light sector (mesons and baryons which become massless in the chiral limit) will be deferred to Sec. 3.3 where we will cover this aspect in a unified way for both models.

3.2.1 Vacuum, confinement

We start with a brief reminder of the vacuum, chiral symmetry breaking and the role of confinement in the 't Hooft model.^{44,45} Since this latter aspect is

intimately related to infrared singularities (absent in the GN model), we work in a finite interval of length L , taking the limit $L \rightarrow \infty$ at the end whenever possible. Fermions are assumed to obey antiperiodic boundary conditions. We introduce a bilinear operator which describes color singlet dynamics to leading order in large N (cf. GN model in Sec. 3.1.3),

$$Q(p', p) = \frac{1}{N} \sum_i \begin{pmatrix} a_i^\dagger(p) a_i(p') & b_i^\dagger(p) a_i(p') \\ a_i^\dagger(p) b_i(p') & b_i^\dagger(p) b_i(p') \end{pmatrix}. \quad (123)$$

The a_i, b_i are annihilation operators for right- and left-handed quarks. The Hamiltonian for the 't Hooft model in the axial gauge has the form

$$\begin{aligned} H &= \sum_{p,i} \frac{2\pi}{L} (p + 1/2) \left(a_i^\dagger(p) a_i(p) - b_i^\dagger(p) b_i(p) \right) \\ &+ \frac{g^2 L}{16\pi^2} \sum_{ij, n \neq 0} \frac{j_{ij}(n) j_{ji}(-n)}{n^2} + m \sum_{p,i} \left(a_i^\dagger(p) b_i(p) + b_i^\dagger(p) a_i(p) \right). \end{aligned} \quad (124)$$

The currents $j_{ij}(n)$ can be taken in the $U(N)$ form at large N ,

$$j_{ij}(n) = \sum_p \left(a_j^\dagger(p) a_i(p+n) + b_j^\dagger(p) b_i(p+n) \right). \quad (125)$$

H is expressed in terms of Q as

$$\begin{aligned} H &= \frac{2\pi}{L} N \sum_p \left(p + \frac{1}{2} \right) \text{tr} \gamma^5 Q(p, p) + m N \sum_p \text{tr} \gamma^0 Q(p, p) \\ &+ \frac{N^2 g^2 L}{16\pi^2} \sum_{n \neq 0, rs} \frac{1}{n^2} \text{tr} \{ \delta_{rs} Q(r, r) - Q(s, r) Q(r-n, s-n) \}, \end{aligned} \quad (126)$$

whereas the equation of motion for Q becomes

$$\begin{aligned} i\partial_t Q(p', p) &= \frac{2\pi}{L} \left((p' + 1/2) \gamma^5 Q(p', p) - (p + 1/2) Q(p', p) \gamma^5 \right) \\ &+ m [\gamma^0, Q(p', p)] + \frac{N g^2 L}{8\pi^2} \sum_{n \neq 0, p''} \frac{1}{n^2} \{ Q(p', p'') Q(p'' - n, p - n) \\ &\quad - Q(p' - n, p'' - n) Q(p'', p) \}. \end{aligned} \quad (127)$$

Expansion of Q around its c -number part (vacuum expectation value)

$$\begin{aligned} Q(p', p) &= \langle 0 | Q(p', p) | 0 \rangle + \frac{1}{\sqrt{N}} \tilde{Q}(p', p) + \dots \\ &= \delta_{p'p} \rho(p) + \frac{1}{\sqrt{N}} \tilde{Q}(p', p) + \dots \end{aligned} \quad (128)$$

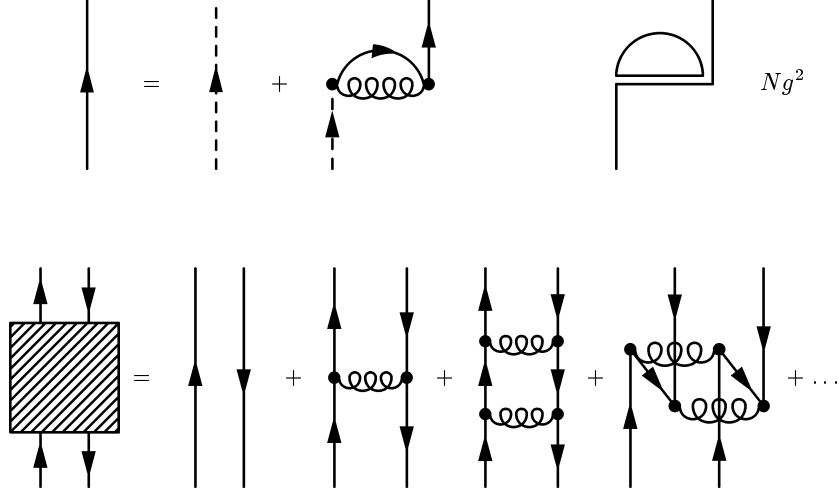


Figure 5: Same as Fig. 4, but for 't Hooft model in axial gauge. Curly lines: Static Coulomb potential. The extra diagram in 't Hooft's double line representation (upper right) explains the dominance of the Fock term at large N .

yields, to leading order, the HF equation

$$[h_{HF}, \rho(p)] = 0 \quad (129)$$

with the single particle HF Hamiltonian

$$h_{HF} = \frac{2\pi}{L}(p + 1/2)\gamma^5 + m\gamma^0 - \frac{Ng^2L}{8\pi^2} \sum_{n \neq 0} \frac{1}{n^2}(\rho(p-n) - 1/2) . \quad (130)$$

In contrast to the GN model where the Hartree term dominates, here only the Fock term survives at large N , see Fig. 5 (the Coulomb interaction acts like a color exchange force). Solving the HF equation self-consistently is equivalent to summing up nested rainbow graphs in a Schwinger-Dyson equation.^{4,63} On general grounds, the vacuum density matrix ρ can be parametrized as

$$\rho(p) = \frac{1}{2} + \gamma^0 \rho_0(p) - i\gamma^1 \rho_1(p) + \gamma^5 \rho_5(p) \quad (131)$$

where ρ_1 is only allowed if $m = 0$. Charge conjugation requires $\rho_{0,1}$ to be even, ρ_5 to be odd functions of momenta. The Slater determinant condition $\rho^2(p) = \rho(p)$ characteristic for HF then translates into

$$\rho_0^2(p) + \rho_1^2(p) + \rho_5^2(p) = \frac{1}{4} . \quad (132)$$

Consider first the case of massive quarks. For $m \neq 0$, ρ_1 vanishes and we can set

$$\rho_0 = -\frac{1}{2} \sin \theta(p) , \quad \rho_5 = -\frac{1}{2} \cos \theta(p) . \quad (133)$$

Comparing

$$\rho(p) = v(p)v^\dagger(p) \quad (134)$$

with the HF spinors of Sec. 2.2 (Eq. 15), $\theta(p)$ is recognized as the Bogoliubov angle. The HF equation now becomes

$$\frac{2\pi}{L}(p+1/2) \sin \theta(p) - m \cos \theta(p) + \frac{Ng^2L}{16\pi^2} \sum_{n \neq 0} \frac{1}{n^2} \sin(\theta(p) - \theta(p-n)) = 0 , \quad (135)$$

i.e., a nonlinear integral equation in the limit $L \rightarrow \infty$. For $m = 0$, ρ_1 can be non-zero. As in the chiral GN model, there is now a continuum of vacua parametrized by a chiral angle φ ,

$$\begin{pmatrix} \rho_0(p) \\ \rho_1(p) \\ \rho_5(p) \end{pmatrix} = -\frac{1}{2} \begin{pmatrix} \sin \theta(p) \cos \varphi \\ \sin \theta(p) \sin \varphi \\ \cos \theta(p) \end{pmatrix} . \quad (136)$$

The gap equation (135) remains valid provided we set $m = 0$. The chiral condensates are

$$\langle \bar{q}q \rangle = -\frac{N}{L} \sum_p \sin \theta(p) \cos \varphi , \quad \langle \bar{q} i\gamma^5 q \rangle = \frac{N}{L} \sum_p \sin \theta(p) \sin \varphi . \quad (137)$$

Although the gap equation (135) for the 't Hooft model has to be solved numerically,^{65,44,45} the value of the quark condensate is known analytically, owing to an indirect determination via sum rules and the 't Hooft equation for mesons;⁷¹ it is (for $\varphi = 0$)

$$\langle \bar{q}q \rangle_v = -\frac{N}{\sqrt{12}} \left(\frac{Ng^2}{2\pi} \right)^{1/2} . \quad (138)$$

(This formula has been generalized to the case of finite bare quark mass.⁷²) In Fig. 6, we show a few typical results for the Bogoliubov angle for several values of the quark mass and compare them to the free theory. For larger quark masses, the interaction effects are very small and can be treated perturbatively.

So far, there seems to be little difference between the GN and 't Hooft models — superficially, the vacuum looks in both cases as if the fermions had acquired a dynamical mass, although momentum dependent in the 't Hooft

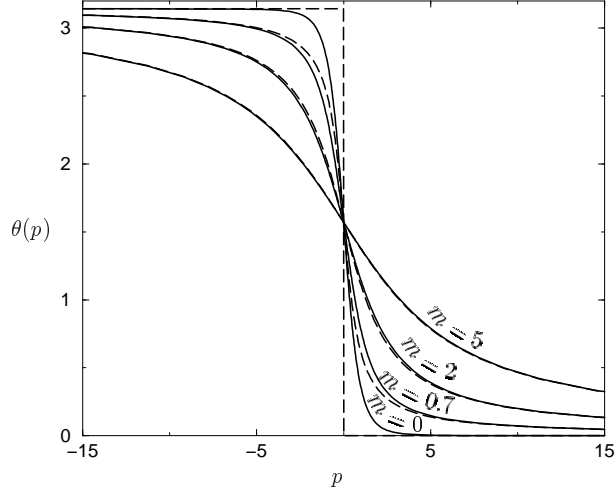


Figure 6: Bogoliubov angles for QCD₂ (solid curves) compared to free theory (dashed curves) as a function of momentum, for several bare quark masses. Units are such that $Ng^2 = 2\pi$.

case. How does confinement of quarks manifest itself? In QCD₂, there are no massive quarks in the spectrum, and we have to understand how their appearance can be avoided in an independent particle picture like the HF approximation. As already suspected by 't Hooft, the answer lies in the IR divergence of the quark self-energy.

We first remark that the gap equation (135) has no IR problem in the limit $L \rightarrow \infty$: The Coulomb interaction term has only a simple pole which can be regulated with a principal value prescription (or symmetric cut-off). The IR divergence discussed in the literature concerns the quark self-energies or, in our language, the HF single particle energies which have to be interpreted physically as removal energies (Koopmans' theorem⁷³). We can deduce them by varying the vacuum energy functional

$$\begin{aligned}
E_{HF}/N &= - \sum_p \frac{2\pi}{L} (p + 1/2) \cos \theta(p) - m \sum_p \sin \theta(p) \\
&\quad + \frac{Ng^2 L}{32\pi^2} \sum_{n \neq 0, p} \frac{1}{n^2} (1 - \cos(\theta(p) - \theta(p - n))) \quad (139)
\end{aligned}$$

with respect to the occupation number of level p and find

$$\omega(p) = \frac{2\pi}{L}(p + 1/2) \cos \theta(p) + m \sin \theta(p) + \frac{Ng^2L}{16\pi^2} \sum_{n \neq 0} \frac{1}{n^2} \cos(\theta(p) - \theta(p - n)) \quad (140)$$

or, in the thermodynamic limit $L \rightarrow \infty$ (setting $q = 2\pi(p + 1/2)/L$),

$$\omega(q) = q \cos \theta(q) + m \sin \theta(q) + \frac{Ng^2}{4} \int \frac{dq'}{2\pi} \frac{\cos(\theta(q) - \theta(q'))}{(q - q')^2} . \quad (141)$$

Due to the double pole, the integral is badly IR divergent. To exhibit the divergence, let us isolate the divergent part of the sum in Eq. (140) before taking the limit $L \rightarrow \infty$,

$$\omega(q) = q \cos \theta(q) + m \sin \theta(q) + \frac{Ng^2}{4} \int \frac{dq'}{2\pi} \frac{\cos(\theta(q) - \theta(q')) - 1}{(q - q')^2} + \frac{Ng^2L}{48} . \quad (142)$$

The principal value prescription for the quadratic pole advocated by Bars and Green⁶³ and Li *et al.*⁶⁵ amounts to throwing away the divergent constant $Ng^2L/48$. As a consequence, one gets an awkward sign change (tachyonic behavior) in the single particle energies at small p and m . The usual excuse is to say that these self-energies have no physical meaning, being gauge dependent and non-covariant. Indeed, this difficulty has no direct consequence for the vacuum properties — as pointed out above, the gap equation is free of IR divergences. Moreover, the calculation of color singlet mesons is also IR safe, as pointed out by 't Hooft (his IR cutoff parameter λ is related to our box size L by $\lambda = 12/\pi L$)⁴⁵: The infinite self-energy term is cancelled by an equally infinite piece in the Coulomb interaction.

Since the emergence of the constant $Ng^2L/48$ in the single particle energy (142) but not in the vacuum energy (139) is a subtle but rather important point, let us briefly recall the argument given in Ref. 45 (see also Ref. 74). In many-body language, the Coulomb interaction produces both one- and two-body terms in H . If the single particle energies are decomposed accordingly as

$$\omega(p) = \omega^{(1)}(p) + \omega^{(2)}(p) , \quad (143)$$

then the HF ground state energy is

$$\langle 0|H|0\rangle = -N \sum_p \left(\omega^{(1)}(p) + \frac{1}{2} \omega^{(2)}(p) \right) . \quad (144)$$

As is well known, the factor $1/2$ is necessary to avoid double counting of the 2-body interaction term. In the 't Hooft model, one finds

$$\begin{aligned}\omega^{(1)}(p) &= \frac{2\pi}{L} \left(p + \frac{1}{2} \right) \cos \theta(p) + m \sin \theta(p) - \frac{Ng^2L}{48} , \\ \omega^{(2)}(p) &= \frac{Ng^2L}{16\pi^2} \sum_{n \neq 0} \frac{1}{n^2} (1 + \cos(\theta(p) - \theta(p+n))) .\end{aligned}\quad (145)$$

Remembering that $\sum_{n \neq 0} 1/n^2 = \pi^2/3$, we see that in the ground state energy (144) the IR tamed combination $(\cos(\theta(p) - \theta(p+n)) - 1)/n^2$ appears whereas in the quark self-energy (143), the 1-term in $\omega^{(2)}$ is cancelled and an IR divergence (quadratic pole for $L \rightarrow \infty$) survives.

Why bother about this IR divergence at all? As one proceeds to other applications of the 't Hooft model than the meson spectrum, it is no longer true that the quark removal energies do not show up in any physical quantity. The prime example is finite temperature field theory in the large N expansion by means of the standard generalization of HF to finite T .⁷⁵ Here, the thermal occupation factors depend crucially on the single particle energies.⁶⁴ If these are made finite by some ad-hoc prescription, quarks will manifest themselves through contributions to the pressure of order N , in conflict with confinement. We shall return to this issue in more detail in Sec. 4.3. Summarizing, we believe that the divergence of the quark single particle energies simply reflects confinement. In fact this may be the only way how confinement can be realized in the independent particle picture characteristic for the leading order in a $1/N$ expansion.

3.2.2 Baryons

Since their structure is very different, we distinguish between those baryons which become massless in the chiral limit and those which stay massive. The first ones are closely related to Goldstone bosons and will be deferred to Sec. 3.3, where they will be discussed for the chiral GN model as well. Here, we briefly sketch what is known about the “normal” type of baryons in the 't Hooft model.

Several papers deal with QCD₂ baryons for a small number of colors, like $N = 2$ (where they are degenerate with mesons⁷⁶) or $N = 3$.⁷⁷ We concentrate on the large N limit instead where baryons are described in relativistic HF approximation. An analytic solution like in the GN model seems to be out of the question. The work closest in spirit to our description of the GN model baryons (cf. Sec. 3.1.2) is Ref. 44. In this work, a numerical approach based on a lattice discretization of space and the use of staggered fermions has been employed. The HF equation is solved in position space, both at strong

($Ng^2 \gg m$) and weak ($Ng^2 \ll m$) coupling. One valence level is taken into account in addition to the Dirac sea. Unlike in the GN model where the filling fraction n/N can be varied, here one has to fill the valence level completely with N quarks in order to form a color singlet baryon. For heavy quarks, the HF equation reduces to the non-relativistic one with a linearly rising potential and the sea becomes irrelevant; the HF equation for the valence level then becomes

$$\left(-\frac{1}{2m}\frac{\partial^2}{\partial x^2} + \frac{Ng^2}{4} \int dy |x-y| |\varphi(y)|^2\right) \varphi(x) = \epsilon \varphi(x) . \quad (146)$$

For moderately heavy quarks, significant relativistic effects were found. The $B = 2$ sector was also explored, with the result that two $B = 1$ baryons were observed interacting via an exponentially decreasing repulsive potential.

3.2.3 Mesons

Originally, 't Hooft determined the meson spectrum by solving the Bethe-Salpeter equation in light-cone gauge, summing up all planar diagrams without quark loops. He found an infinite tower of mesons with masses which behave asymptotically like

$$\mu^2(n) \rightarrow \pi^2 n + O(\ln n) . \quad (147)$$

This should be contrasted to the GN models with one or two mesons only; the difference obviously reflects confinement (Regge behavior). In the chiral limit, a massless meson appears (see Sec. 3.3). These results have subsequently been confirmed in normal coordinates, using the axial gauge. The necessary equations were first derived by Bars and Green⁶³ and later solved numerically by several groups.^{65,45} The equal-time approach turns out to be significantly more involved than the light-cone approach. Nevertheless, since we cannot use light-cone quantization for all the questions which interest us and wish to stay within one common framework, we have to outline this approach here.

As before, we consider small oscillations around the HF solution in the space of Slater determinants. The quantized modes of these oscillations are just the RPA modes. The RPA equation is identical to the Bethe-Salpeter equation in a diagrammatic large N approximation.⁶³ To derive it, we return to the equation of motion for the bilinear quark operator $Q(p, p')$, Eq. (127), insert the expansion (128) and focus onto the next-to-leading order in $1/\sqrt{N}$,

$$\begin{aligned} i\partial_t \tilde{Q}(p', p) &= h_{HF}(p') \tilde{Q}(p', p) - \tilde{Q}(p', p) h_{HF}(p) \\ &+ \frac{Ng^2 L}{8\pi^2} \sum_{n \neq 0} \frac{1}{n^2} \{ \rho(p') \tilde{Q}(p' - n, p - n) - \tilde{Q}(p' - n, p - n) \rho(p) \} . \end{aligned} \quad (148)$$

Expanding \tilde{Q} in the HF spinors, as in Sec. 3.1.3 Eq. (110) and (111), and setting

$$\begin{aligned}\langle n, K | \tilde{Q}_{21}(p', p) | 0 \rangle &= \delta_{K, p-p'} \Phi_+^n(K, p) , \\ \langle n, K | \tilde{Q}_{12}(p', p) | 0 \rangle &= \delta_{K, p-p'} \Phi_-^n(K, p)\end{aligned}\quad (149)$$

then yields the two coupled equations

$$\begin{aligned}\pm E(K) \Phi_{\pm}(K, p) &= (\omega_0(p - K) + \omega_0(p)) \Phi_{\pm}(K, p) \\ &\quad - \frac{Ng^2L}{8\pi^2} \sum_{p'(\neq p)} \frac{1}{(p - p')^2} \{s(p, p', K) \Phi_{\mp}(K, p') \\ &\quad + c(p, p', K) \Phi_{\pm}(K, p')\}\end{aligned}\quad (150)$$

with the definitions

$$\begin{aligned}s(p, p', K) &= \sin\left(\frac{\theta(p') - \theta(p)}{2}\right) \sin\left(\frac{\theta(p - K) - \theta(p' - K)}{2}\right) , \\ c(p, p', K) &= \cos\left(\frac{\theta(p') - \theta(p)}{2}\right) \cos\left(\frac{\theta(p - K) - \theta(p' - K)}{2}\right) .\end{aligned}\quad (151)$$

Eqs. (150) have the standard RPA form of Eq. (116), with

$$\begin{aligned}A_{pp'}(K) &= \delta_{pp'}(\omega_0(p - K) + \omega_0(p)) - \frac{Ng^2L}{8\pi^2} \frac{(1 - \delta_{pp'})}{(p - p')^2} c(p, p', K) , \\ B_{pp'}(K) &= -\frac{Ng^2L}{8\pi^2} \frac{(1 - \delta_{pp'})}{(p - p')^2} s(p, p', K) .\end{aligned}\quad (152)$$

The diagrammatic content of these equations is sketched in Fig. 5 (see Sec. 3.2.1). Using a slightly different language, Bars and Green⁶³ interpret them in terms of forward and backward going strings. The covariance of the spectrum is a non-trivial issue if one works canonically in normal coordinates, but can be checked either numerically or via the $1/N$ expansion of the Poincaré algebra. Meson wavefunctions (or rather RPA amplitudes) can be found in the literature for a few low-lying states⁶⁵ In the limit of heavy quarks, the RPA reduces to the non-relativistic Schrödinger equation with a linear potential. The light-cone TDA ('t Hooft equation) on the other hand can be recovered by going to the infinite momentum frame⁶³ (backward going bubbles are suppressed, see also Sec. 3.3).

3.3 Chiral limit and Goldstone modes

Since QCD₂ or the chiral GN model in the massless limit break chiral symmetry spontaneously (at least at infinite N), the appearance of a boson whose mass behaves like the square root of the bare quark mass has to be expected. This has a lot in common with four dimensional theories and makes these models good toy models for QCD. However, the chiral limit is somewhat obscured by a certain pathology of two dimensional theories which gives rise to a much greater variety of (decoupled) massless states. In particular, non-interacting massless mesons and baryons already appear at finite N where the Coleman theorem certainly forbids talking about Goldstone bosons. Our main interest here is in the large N limit where we will derive both massless mesons and baryons. However, before doing so, we also briefly explain the more pathological aspects of two dimensional theories leading to massless states at finite N as well.

The identification of massless excitations in two dimensional field theories is one of the tasks where light-cone quantization is particularly elegant. Due to the light-cone dispersion relation $p_+ = \frac{m^2}{2p_-}$, a massless state in two dimensions has zero energy at all momenta. Therefore its presence can be associated with a *local* symmetry of the Hamiltonian. In the chiral limit the right-handed fermions drop out of the light-cone Hamiltonian $P^+ = H - P$.^{78,79,45} Since the Coulomb interaction admits local chiral transformations, P^+ is invariant under local phase transformations of right-handed quarks. Free, massless bosons then must appear and it is sufficient to identify the winding number of their field with baryon number to infer the existence of free, massless baryons as well. The IR trouble of Coleman's theorem is avoided by the fact that the massless modes decouple.

The essence of the argument can of course also be phrased without recourse to light-cone quantization.¹⁵ Let us return to the fermion currents discussed in Sec. 2.2. Vector current conservation allows us to set

$$j_V^\mu = \epsilon^{\mu\nu} \partial_\nu \phi \quad (153)$$

with a scalar field ϕ . If the axial current is non-anomalous, we get in the limit $m \rightarrow 0$ (see j_A^μ above, Eq. (24))

$$\partial_\mu j_A^\mu = \square \phi = 0 \quad , \quad (154)$$

i.e., the announced massless boson. This purely classical argument can easily be promoted to the quantum level within the canonical framework.⁸⁰ Define the right-handed current as

$$j_R(q, t) = \frac{1}{2}(j_V^0(q, t) + j_V^1(q, t)) \quad (155)$$

where Heisenberg operators, Fourier transformed with respect to the space coordinate x are used. In the chiral limit, vector and axial vector current conservation imply

$$[j_R(q, t), H] = qj_R(q, t) . \quad (156)$$

Besides, if P denotes the momentum operator, we have trivially

$$[j_R(q, t), P] = qj_R(q, t) . \quad (157)$$

For any energy-momentum eigenstate $|i\rangle$ with eigenvalues (E_i, P_i) , we thus get

$$\begin{aligned} H j_R(q, t)|i\rangle &= (E_i - q)j_R(q, t)|i\rangle , \\ P j_R(q, t)|i\rangle &= (P_i - q)j_R(q, t)|i\rangle . \end{aligned} \quad (158)$$

Thereby decoupled massless bosons can be added to or removed from any stationary state. Similarly, left moving massless bosons can be related to the left-handed current.

Let us now turn to the large N limit and discuss the emergence of massless particles there. Again we benefit from the experience in many-body theory. The Goldstone theorem has a close correspondence which we may invoke here (remember that it also holds in non-relativistic theories): If the HF ground state breaks a continuous symmetry spontaneously, the RPA develops a gapless mode. The basic argument can be given in two lines, using the language of linear response theory (without external force).⁸¹ Take the equation of motion for the one-body density matrix,

$$i\dot{\rho} = [h(\rho), \rho] . \quad (159)$$

Expand ρ around its ground state expectation value, $\rho = \rho^{(0)} + \delta\rho$, and linearize

$$i\delta\dot{\rho} = [h(\rho^{(0)}), \delta\rho] + \left[\frac{\delta h}{\delta \rho} \delta\rho, \rho^{(0)} \right] . \quad (160)$$

This equation has the form of the RPA, cf. the above derivation in the equations of motion approach in Sec. 3.1.3. If the ground state density matrix ρ breaks a continuous symmetry, we find that the deformation $\delta\rho$ corresponding to the symmetry transformation (e.g. a chiral rotation) solves the RPA equation with zero energy. The backward going ph-bubbles are crucial for getting the zero modes; as is well known, the TDA does not have this property.

These insights enable us to construct the Goldstone boson type solution of the RPA equation explicitly. In the case of QCD₂, the RPA amplitudes of the “pion” can easily be obtained by projecting the right-handed current onto HF

spinors. Since these depend only on the Bogoliubov angle, the pion amplitudes are intimately related to the broken symmetry vacuum. One finds^{80,82}

$$\begin{aligned}\Phi_+^\pi(K, p) &= \sqrt{\frac{2\pi}{K}} \cos(\theta(p)/2) \sin(\theta(p - K)/2) , \\ \Phi_-^\pi(K, p) &= \sqrt{\frac{2\pi}{K}} \sin(\theta(p)/2) \cos(\theta(p - K)/2) .\end{aligned}\quad (161)$$

The chiral GN model can be analyzed in a similar manner. Generalizing the derivation of the RPA equation, Sec. 3.1.3, to the chirally invariant model, one finds an integral equation with a two-term separable kernel (instead of one-term in the model with discrete chiral symmetry) and correspondingly two bound states, the threshold bound state at $2m$ (the “ σ ”) and a massless one (the “ π ”). The pion has the same structure as in Eq. (161), except that the Bogoliubov angles now refer to the GN vacuum. They are just the Bogoliubov angles of the free, massive fermions given in Eq. (16). In this particular case, we are in the rare position of having complete analytical control over a meson (the π) in an arbitrary Lorentz frame. In Fig. 7, we illustrate the disappearance of the backward components as one boosts the pion to higher momenta (in the rest frame, both are exactly equal). At very high momenta, the constant wave function familiar from the light-cone meson equation emerges.⁴ In the infinite momentum limit, the ’t Hooft and GN model pions become identical, although their “wave functions” (161) differ in any other frame due to different Bogoliubov angles. This illustrates nicely how the vacuum decouples in the infinite momentum frame, one of the celebrated advantages of the light-cone approach (triviality of the vacuum). Connected to this is the disappearance of the backward amplitudes — the RPA reduces to the TDA in the infinite momentum frame, the other characteristic benefit on the light-cone.

We now turn to the issue of baryons which become massless in the chiral limit, a phenomenon which does not happen in 3+1 dimensions. The best way of thinking about them is in terms of coherent, topological excitations of the pion field. Like the massive baryons discussed in Secs. 3.1.2 and 3.2.2, they are accessible through the relativistic HF approximation. In order to find these solutions in the first place, another point of view has turned out to be very useful. It is closely related to bosonization,⁸³ but since only the chiral field is bosonized, it is conceptually and technically much simpler. It is also similar in spirit to the Skyrme picture of baryons in 3+1 dimensions.⁸⁴

Following Salcedo *et al.*,⁴⁴ we start from a variational ansatz for the baryon near the chiral limit. The interaction part of the ground state energy functional

$$E[\rho] = N \int dx \text{tr} \left[\left(-i\gamma^5 \vec{\partial}_x + m\gamma^0 \right) \rho(x, x) \right]$$

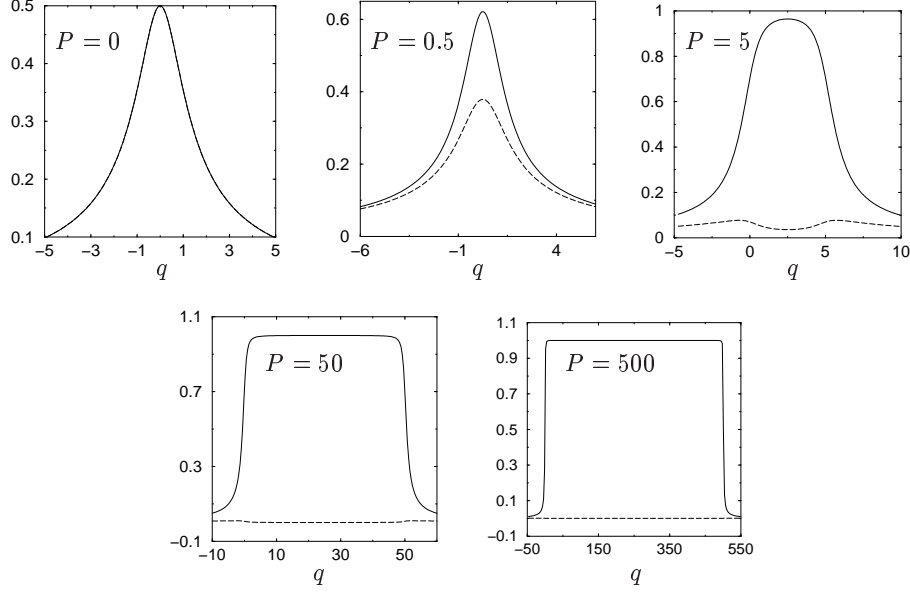


Figure 7: Forward (solid lines) and backward (dashed lines) RPA amplitudes $\Phi_{\pm}^{\pi}(P, q)$ of the pion in the chiral GN model, for pion momenta P from 0 to 500 (in units of m). This illustrates the evolution from the rest frame to the “infinite momentum frame”.

$$+ \frac{N^2 g^2}{8} \int dx dy |x - y| \text{tr} (\rho(x, y) \rho(y, x)) \quad (162)$$

(where $\vec{\partial}_x$ acts only on the first variable of $\rho(x, x)$) is invariant under any *local* chiral transformation. Let us perform a local chiral rotation of the vacuum density matrix,

$$\rho'(x, y) = e^{i\chi(x)\gamma^5} \rho^v(x - y) e^{-i\chi(y)\gamma^5}. \quad (163)$$

We can use the following general decomposition of the baryon density matrices ρ^v and ρ'

$$\rho = \frac{1}{2} \rho_e + \gamma^0 \rho_0 - i\gamma^1 \rho_1 + \gamma^5 \rho_5 \quad (164)$$

with corresponding superscripts. In the vacuum, $\rho_e = \delta(x - y)$, due to translational invariance all components depend only on $x - y$ and ρ_1 vanishes unless $m = 0$. If the vacuum breaks chiral symmetry, the ansatz (163) yields a new density matrix which can be inserted into Eq. (162); $\chi(x)$ is then determined by minimizing E . In order to understand the emergence of baryon number out

of winding number, we need the short distance singularities of ρ^v which are the same as in the free theory,

$$\begin{aligned}\rho_0(x) &= -\frac{m}{2\pi}K_0(m|x|) \sim \frac{m}{2\pi}\ln(m|x|) , \\ \rho_5(x) &= \frac{m}{2\pi i}\text{sgn}(x)K_1(m|x|) \sim \frac{1}{2\pi i x} .\end{aligned}\quad (165)$$

Using

$$\begin{aligned}\rho'_e(x, y) &= \cos(\chi(x) - \chi(y))\rho_e^v(x - y) + 2i\sin(\chi(x) - \chi(y))\rho_5^v(x - y) , \\ \rho'_5(x, y) &= \cos(\chi(x) - \chi(y))\rho_5^v(x - y) + \frac{i}{2}\sin(\chi(x) - \chi(y))\rho_e^v(x - y) ,\end{aligned}\quad (166)$$

one then finds

$$\begin{aligned}\lim_{y \rightarrow x} [\rho'_e(x, y) - \rho_e^v(x - y)] &= \frac{1}{\pi}\partial_x \chi(x) , \\ \lim_{y \rightarrow x} \partial_x [\rho'_5(y, x) - \rho_5^v(x - y)] &= \frac{i}{4\pi}(\partial_x \chi(x))^2 .\end{aligned}\quad (167)$$

Similarly,

$$\rho'_0(x, x) \mp i\rho'_1(x, x) = \frac{\langle \bar{q}q \rangle_v}{2N} e^{\mp i2\chi(x)} \quad (168)$$

where $\langle \bar{q}q \rangle_v$ refers to the vacuum. If we invoke a finite spatial box of length L for these topological considerations, the baryon number gets identified with the winding number of the chiral field,

$$B = \int_0^L dx [\rho'_e(x, x) - \rho_e^v(0)] = \frac{1}{\pi}(\chi(L) - \chi(0)) . \quad (169)$$

This is an integer if the baryon goes over into the vacuum at 0 and L . For small quark mass, find

$$E[\rho'] = E[\rho^v] + N \int dx \left\{ \frac{1}{2}(\partial_x \phi)^2 + m \frac{\langle \bar{q}q \rangle_v}{N} [\cos(\sqrt{4\pi}\phi(x)) - 1] \right\} \quad (170)$$

with the rescaled field

$$\phi(x) = -\frac{1}{\sqrt{\pi}}\chi(x) \quad (171)$$

and $\langle \bar{q}q \rangle_v$ referring to the vacuum in the chiral limit. $E[\rho']$ is minimized if ϕ satisfies the sine-Gordon equation⁵⁴

$$\partial_x^2 \phi + \sqrt{4\pi}m \frac{\langle \bar{q}q \rangle_v}{N} \sin(\sqrt{4\pi}\phi(x)) = 0 . \quad (172)$$

The solution with baryon number one is just the famous sine-Gordon kink,

$$\phi(x) = -\frac{2}{\sqrt{\pi}} \arctan \exp\left(\frac{x}{x_B}\right). \quad (173)$$

It is localized with spatial extent x_B ,

$$x_B = \left(-4\pi m \frac{\langle \bar{q}q \rangle_v}{N}\right)^{-1/2} \quad (174)$$

and has mass

$$M_B = 8N \left(-\frac{m}{4\pi} \frac{\langle \bar{q}q \rangle_v}{N}\right)^{1/2}. \quad (175)$$

If one linearizes the sine-Gordon equation (in the limit $m \rightarrow 0$), one can immediately read off the Gell-Mann, Oakes, Renner relation (GOR)⁸⁵

$$m_\pi^2 = -4\pi m \frac{\langle \bar{q}q \rangle_v}{N} \quad (176)$$

for the Goldstone boson. We have thus derived an effective low energy theory near the chiral limit. Since the potential energy does not enter Eq. (170) but only the kinetic energy and mass term, the resulting low energy effective theory is universal for a whole class of such chiral models.

In the limit $m \rightarrow 0$, both the pion and the baryon become massless; the baryon gets completely delocalized. This could actually have been anticipated from current conservation: $\partial_1 j_A^1 = 0$ holds for any stationary state and in two dimensions, j_A^1 is just the baryon density j_V^0 (cf. Sec. 2.2).

An attempt to illustrate the baryon structure in the chiral limit has been made in Fig. 8. For $m = 0$, $\chi(x)$ becomes simply a linear function and the scalar and pseudoscalar condensates

$$\langle \bar{q}q \rangle = \langle \bar{q}q \rangle_v \cos(2\pi(x-x_0)/L), \quad \langle \bar{q}i\gamma^5 q \rangle = -\langle \bar{q}q \rangle_v \sin(2\pi(x-x_0)/L), \quad (177)$$

can be regarded as projections of a spiral of radius $\langle \bar{q}q \rangle_v$ winding around once. This picture will be generalized later on and turn out to be useful for characterizing baryonic matter in two dimensional chiral models.

In Ref. 44 the Skyrme type picture of the baryon was compared to the exact numerical solution for light quarks and good agreement was found also for small, finite quark masses. It was pointed out that these results support the Skyrme picture of the baryon more than the bag picture in two dimensions.

Finally, let us come back to the question of validity of the variational calculation based on the ansatz (163). In the massless limit, it is easy to

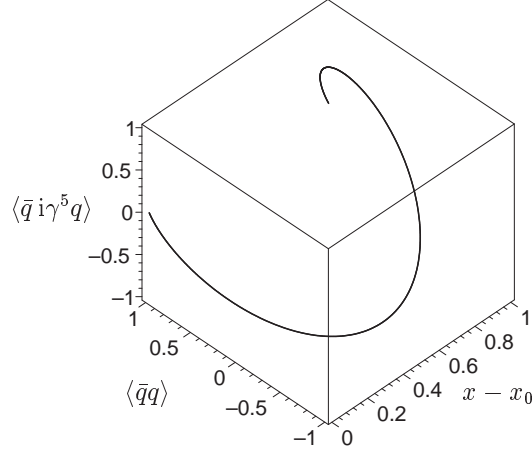


Figure 8: Attempt to visualize the topological structure of the massless baryon in terms of a “chiral spiral” winding around once. Condensates in units of $\langle \bar{q} q \rangle_v$, x in units of L .

convince oneself that Eq. (163) with a linear function $\chi(x)$ solves the HF equation exactly. Thus for instance in the 't Hooft model, the massless HF equation reads⁴⁴

$$-i(\gamma_5)_{\alpha\beta} \frac{\partial}{\partial x} \varphi_{\beta}^{(n)}(x) + \frac{Ng^2}{4} \int dy |x-y| \rho'_{\alpha\beta}(x,y) \varphi_{\beta}^{(n)}(y) = \omega_n \varphi_{\alpha}^{(n)}(x) . \quad (178)$$

Upon substituting

$$\varphi_{\alpha}^{(n)}(x) = \left(e^{-i\pi x \gamma_5 / L} \right)_{\alpha\beta} \tilde{\varphi}_{\beta}^{(n)}(x) \quad (179)$$

as we are instructed to do by Eq. (163), we discover that $\tilde{\varphi}^{(n)}$ does indeed solve the HF equation, the only change being that the single particle energy ω_n gets replaced by $\omega_n + \pi/L$. The same argument goes through in the chiral GN model, or in any field theory where the interaction term has a local chiral invariance for that matter. This shows that the result becomes exact in the chiral limit (to leading order in the $1/N$ expansion, of course).

4 Finite temperature

4.1 Finite temperature versus finite extension

We briefly discuss the relation between field theories at finite extension and finite temperature.⁸⁶ Equivalence between relativistic theories at finite exten-

sion and finite temperature is formally almost trivial but gives rise to some of the most intriguing consequences of covariance. By rotational invariance in the Euclidean, the value of the partition function of a system with finite extension L in one space direction and β in the time direction is invariant under the exchange of these two parameters,

$$Z(\beta, L) = Z(L, \beta) , \quad (180)$$

provided bosonic (fermionic) fields satisfy periodic (antiperiodic) boundary conditions in both time and compact space coordinate. Sending one of the parameters (β, L) to infinity, relativistic covariance connects the thermodynamic properties of a canonical ensemble with the properties of the pure state of the vacuum corresponding to the same physical system but at finite extension. In particular, as a consequence of (180), energy density and pressure are related by

$$\epsilon(\beta, L) = -p(L, \beta) . \quad (181)$$

For a system of non-interacting particles this equation can be used to relate quantitatively the Stefan-Boltzmann law with the Casimir effect — phenomena which at first glance would not seem to be related at all.⁸⁷ Another application of this discrete relativistic symmetry worth mentioning are quark propagators and the interpretation of lattice data in “funny space”.⁸⁸ In four dimensional QCD, the confinement-deconfinement phase transition and the chiral phase transition, when quarks are present, appear as “quantum phase transitions” if one swaps space and Euclidean time. They are driven by changes in quantum rather than thermal fluctuations which in turn are induced by changes of a parameter of the system (L) .^{89,90} We have found it useful to apply this technique to the two dimensional models at hand to see how it works in detail in the presence of interaction effects. Consistency between finite extension and thermal field theory calculations provides a non-trivial test of the approximations used and will help us to clarify the role of confinement in the ’t Hooft model. For the case of two dimensions with one extension taken to be infinite, the symmetry is illustrated in Fig. 9.

To leading order in the large N limit, it is easy to include finite temperature and chemical potential since the required generalization of our main tool, the HF approximation, is well known.⁷⁵ Let us focus on finite temperature here since finite density and chemical potential will be the subject of Secs. 5 and 6. The main difference to the temperature zero case is that for systems in thermal equilibrium, one is no longer dealing with a pure state but with a mixed state. The concepts of independent particles and single particle states remain valid. Whereas at $T = 0$ each orbit is either empty or occupied (sharp

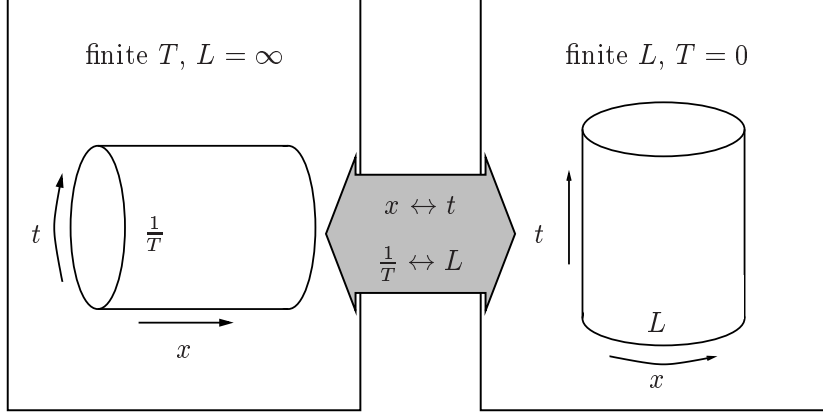


Figure 9: Correspondence between relativistic field theories at finite temperature and finite extension.

Fermi surface), at finite T the occupation number is given by the thermal occupation probability (Dirac-Fermi distribution⁹¹). The one-body density matrix no longer satisfies the projector property $\rho^2 = \rho$ characteristic for a single Slater determinant but assumes the form

$$\rho = N_+ uu^\dagger + N_- vv^\dagger , \quad (182)$$

with occupation numbers

$$N_\pm = \frac{1}{e^{\pm\beta\epsilon} + 1} . \quad (183)$$

Using

$$N_+ + N_- = 1 , \quad N_+ - N_- = -\tanh \frac{\beta\epsilon}{2} , \quad (184)$$

one can write

$$\rho = \frac{1}{2} + (\gamma^0 \rho_0 + \gamma^5 \rho_5) \tanh \frac{\beta\epsilon}{2} . \quad (185)$$

where ρ_0, ρ_5 are given in terms of Bogoliubov angles in the same way as at zero temperature (in the chiral limit, there could be a ρ_1 -term in addition.) In contrast to the $T = 0$ case now the single particle energies ϵ become physically relevant and will appear explicitly in the self-consistency equation, simply because excited states do play a role in the thermal equilibrium. The alternative scenario, namely HF at $T = 0$ but finite extension, does not require any new

tools, at least for the GN model. In the case of the 't Hooft model, the situation will turn out to be more involved due to the different gluon dynamics in a finite box (cf. Sec. 4.3).

4.2 GN model on a cylinder

Before embarking on the details of the finite temperature GN model, we have to come back once more to the issue of SSB in lower dimensional systems.⁹² Since the thermodynamic limit can be taken only with respect to one dimension now, there are further restrictions as compared to those of Sec. 2.4. According to the Mermin-Wagner theorem, even a discrete symmetry should be immediately restored at $T = 0^+$. The restoration of chiral symmetry at finite temperature is expected to be driven by the presence of kinks and antikinks^{93,94} for any large but finite N . If however the limit $N \rightarrow \infty$ is taken before the thermodynamic limit, these configurations are suppressed and one is left with the mean field theory where a second order phase transition at a critical temperature $T_c \neq 0$ becomes possible. Similarly, for the continuous model, for large but finite N at $T \neq 0$, the almost long range order disappears. Only if $N \rightarrow \infty$ is taken first, mean field theory applies and one finds the same critical temperature as in the discrete model. The non-analytic structure revealed by the phase diagram of the infinite N GN model depends on the diverging number of fermion components like in reduced models.^{95,96}

Barducci *et al.*⁹² advocate to include a small bare fermion mass, thereby eliminating kink-antikink configurations in the thermodynamic limit. Since their results go over rather smoothly into those obtained in mean field theory at $m = 0$, we see nothing wrong in considering the chiral limit directly for some questions.

First consider finite extension which requires only minimal modifications of the HF approach for the vacuum discussed in Sec. 3.1.1. Since the fermion momenta are discretized due to the antiperiodic boundary conditions, the gap equation (68) (self-consistency requirement for the scalar density) has to be replaced by

$$m = \frac{2Ng^2}{L} \sum_{n=0}^{N_\Lambda} \frac{m}{\sqrt{m^2 + k_n^2}} \quad (186)$$

with

$$N_\Lambda = \frac{L\Lambda}{4\pi} , \quad k_n = \frac{\pi}{L}(2n+1) . \quad (187)$$

As the finite extension does not affect any UV properties, we can renormalize the theory in the limit $L \rightarrow \infty$. Denoting the physical mass on the infinite line

by m_0 and using Eqs. (68) and (186), we obtain

$$\lim_{\Lambda \rightarrow \infty} \left(\int_0^{\Lambda/2} \frac{dk}{2\pi} \frac{1}{\sqrt{m_0^2 + k^2}} - \frac{1}{L} \sum_{n=0}^{N_\Lambda} \frac{1}{\sqrt{m^2 + k_n^2}} \right) = 0. \quad (188)$$

This equation is now free of divergences but cannot be solved analytically in general. To find the critical length below which chiral symmetry gets restored it is sufficient to set $m = 0$ and solve for L ,

$$\frac{1}{2} \ln \frac{\Lambda}{m_0} = \sum_{n=0}^{N_\Lambda} \frac{1}{2n+1}. \quad (189)$$

The sum can be performed,

$$\sum_{n=0}^{N_\Lambda} \frac{1}{2n+1} = \frac{1}{2} (C + \ln 4N_\Lambda) + O(1/N_\Lambda^2) \quad (190)$$

($C \approx 0.5772$ Euler constant) yielding the critical length

$$L_c = \frac{\pi}{m_0} e^{-C}. \quad (191)$$

A bare fermion mass m_b can easily be taken into account if one replaces the gap equation (188) by

$$\left(\frac{m_b}{2Ng^2} \right) \left(\frac{1}{m_0} - \frac{1}{m} \right) + \lim_{\Lambda \rightarrow \infty} \left(\int_0^{\Lambda/2} \frac{dk}{2\pi} \frac{1}{\sqrt{m_0^2 + k^2}} - \frac{1}{L} \sum_{n=0}^{N_\Lambda} \frac{1}{\sqrt{m^2 + k_n^2}} \right) = 0. \quad (192)$$

Note the appearance of the new parameter $\frac{m_b}{Ng^2}$ in addition to m_0 . Numerical solutions of this gap equation for different quark masses are shown in Fig. 10, exhibiting a second order phase transition in the chiral limit and a cross-over phenomenon for non-zero bare masses. Since it explicitly violates chiral symmetry, the bare quark mass plays a role analogous to that of an external magnetic field in the ferromagnetic phase transition. Finally, we reemphasize that to this order in the $1/N$ expansion the calculation is identical for the GN models with discrete or continuous chiral symmetry.

We now switch to the equivalent finite temperature calculation to familiarize ourselves with the corresponding generalization of the HF approximation. As indicated in Sec. 4.1, the gap equation of thermal HF has to be modified by T -dependent occupation numbers which “smear out” the Fermi surface,

$$m - m_b = Ng^2 \int \frac{dk}{2\pi} \frac{m}{\epsilon(k)} \tanh \frac{\beta \epsilon(k)}{2}, \quad \epsilon(k) = \sqrt{m^2 + k^2}. \quad (193)$$

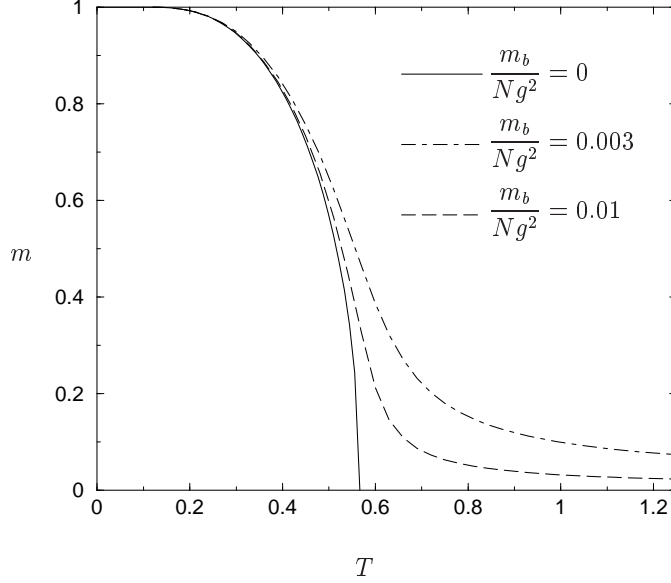


Figure 10: Temperature dependence of dynamical fermion mass for several values of bare mass, in the GN model. In units of m_0 .

The tanh was derived in Eq. (185). Renormalizing at $T = 0$ then yields the following equation for the T -dependence of the physical fermion mass,

$$0 = m_b \left(\frac{1}{m_0} - \frac{1}{m} \right) + N g^2 \int \frac{dk}{2\pi} \left(\frac{\tanh \frac{1}{2} \beta \sqrt{m^2 + k^2}}{\sqrt{m^2 + k^2}} - \frac{1}{\sqrt{m_0^2 + k^2}} \right). \quad (194)$$

The integral in (194) converges and we recover the well known results obtained by functional integration methods^{97,93} in particular a second order phase transition at a critical temperature T_c which coincides with L_c^{-1} from Eq. (191). Bosonic excitations are $1/N$ suppressed and play no role at this stage. Hence just like in the finite extension case, there is no distinction yet between GN models with continuous and discrete chiral symmetry.

It is interesting to compare the two approaches leading to the gap equations (192) and (194) respectively at an intermediate stage to understand how covariance “works”. The crucial identity which ensures the equivalence of the

finite L and finite T calculations is

$$\int_{-\Lambda/2}^{\Lambda/2} \frac{dk}{\sqrt{m^2 + k^2}} \tanh\left(\frac{1}{2}\beta\sqrt{m^2 + k^2}\right) \stackrel{!}{=} \frac{4\pi}{L} \sum_{n=0}^{N_\Lambda} \frac{1}{\sqrt{m^2 + k_n^2}} \quad (195)$$

for $\beta = L$. Eq. (195) can be verified with the help of Cauchy's theorem. The integrand has simple poles in the upper half plane at

$$k = i\sqrt{m^2 + ((2n+1)\pi/\beta)^2}, \quad (n = 0 \dots N_\Lambda) \quad (196)$$

with residues $-2i/(\beta\sqrt{m^2 + ((2n+1)\pi/\beta)^2})$. Thereby, a continuous average involving thermal occupation numbers can be converted into a sum characteristic for a finite interval. This is of course reminiscent of the imaginary time approach with Matsubara frequencies although different in detail (in the canonical approach) due to the interchange of frequencies and momenta. In the Euclidean path integral formalism, we would expect no difference whatsoever.

So far we have concentrated on the dynamical mass or equivalently the chiral condensate. Other bulk thermodynamic observables can easily be calculated from the thermodynamic potential. Let us therefore consider the two functions which are minimized with respect to m in the two approaches. At finite extension in the chiral limit, it is the HF vacuum energy density

$$\frac{\mathcal{E}}{N} = \frac{m^2}{2Ng^2} - \frac{1}{L} \sum_n \sqrt{m^2 + k_n^2} \quad (197)$$

(cf. Sec. 3.1.1). The gap equation (186) follows from the condition $\partial\mathcal{E}/\partial m = 0$. In the finite T case on the other hand, we have to minimize the thermodynamic potential ϕ or free energy density \mathcal{F} related to the partition function via

$$\frac{\phi}{L} = \mathcal{F} = -\frac{1}{\beta L} \ln \text{tr} e^{-\beta H} \quad (198)$$

and equal to the negative of the pressure. In the GN model at the HF level, the Hamiltonian is given by that of the free, massive theory plus a c -number term correcting for double counting of the two-body interaction,

$$H = H_m^{(0)} + \frac{Lm^2}{2g^2}. \quad (199)$$

Therefore the partition function can be evaluated following the textbook approach for a free Fermi gas,⁹¹

$$\frac{\mathcal{F}}{N} = \frac{m^2}{2Ng^2} - \int \frac{dk}{2\pi} \left[\epsilon(k) + \frac{2}{\beta} \ln \left(1 + e^{-\beta\epsilon(k)} \right) \right]. \quad (200)$$

Differentiating with respect to m reproduces Eq. (194) (here for $m_b = 0$). Since we have already verified that the two gap equations are identical, it is sufficient to check that \mathcal{E} and \mathcal{F} coincide for one value of m (upon identifying L and β) to establish that the two functions agree everywhere as expected on general grounds (cf. Eq. (181)). We choose $m = 0$ where all calculations can be done in closed form. For the energy density in the finite interval we find, using heat kernel regularization (as usually done in treating the Casimir effect),

$$\frac{\mathcal{E}}{N} = -\frac{\pi}{6L^2} . \quad (201)$$

For finite temperature Eq. (200) yields

$$\frac{\mathcal{F}}{N} = -\frac{\pi}{6\beta^2} . \quad (202)$$

i.e., the Stefan-Boltzmann law. In both cases, the same L - resp. β -independent quadratically divergent term has been dropped. This illustrates the above mentioned correspondence between the Casimir effect and the Stefan-Boltzmann law and completes the demonstration that compressed and hot relativistic systems are fully related by covariance for the case of the GN model.

In order to derive other bulk thermodynamic observables it is useful to renormalize the thermodynamic potential.^{92,95} Using the gap equation at zero temperature one can write

$$\left. \frac{\mathcal{F}}{N} \right|_{\text{ren}} = \frac{m^2}{4\pi} \left(\ln \left(\frac{m^2}{m_0^2} \right) - 1 \right) + \frac{m_0^2}{4\pi} - \frac{2}{\beta} \int \frac{dk}{2\pi} \ln \left(1 + e^{-\beta\epsilon(k)} \right) . \quad (203)$$

Following Barducci *et al.*⁹² we have added a constant “bag term” $m_0^2/4\pi$ in order to normalize the (unobservable) vacuum pressure to zero. The derivative $\partial\mathcal{F}_{\text{ren}}/\partial m$ reproduces the renormalized gap equation (194). From this, the bulk thermodynamical observables can be obtained. For temperatures below the phase transition, pressure and internal energy density are

$$\frac{p}{N} = -\frac{m^2}{4\pi} \left(\ln \left(\frac{m^2}{m_0^2} \right) - 1 \right) - \frac{m_0^2}{4\pi} + \frac{2}{\beta\pi} \int_0^\infty dk \ln \left(1 + e^{-\beta\epsilon(k)} \right) \quad (204)$$

$$\frac{\varepsilon}{N} = \frac{m^2}{4\pi} \left(\ln \left(\frac{m^2}{m_0^2} \right) - 1 \right) + \frac{m_0^2}{4\pi} + \frac{2}{\pi} \int_0^\infty dk \frac{\epsilon(k)}{1 + e^{\beta\epsilon(k)}} \quad (205)$$

where m has to be evaluated at the minimum of \mathcal{F} (solution of the gap equation). In the region above T_c , the results are simply

$$\frac{p}{N} = \frac{\pi T^2}{6} - \frac{m_0^2}{4\pi} , \quad (206)$$

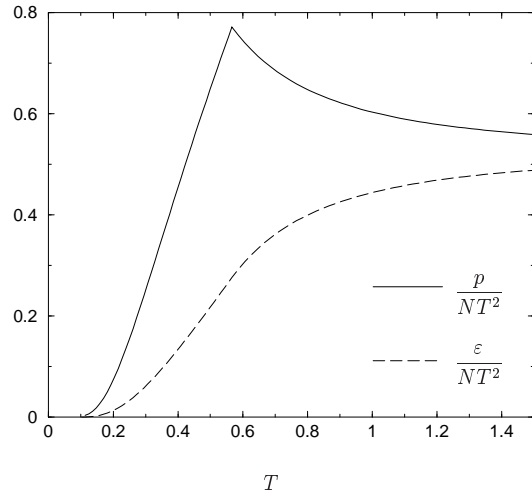


Figure 11: Pressure (solid line) and internal energy density (dashed line) per color in the GN model, dividing out the T^2 dependence of the Stefan-Boltzmann law. In units of m_0 ; adapted from Ref. 92.

$$\frac{\varepsilon}{N} = \frac{\pi T^2}{6} + \frac{m_0^2}{4\pi}. \quad (207)$$

In Fig. 11, pressure and internal energy density have been plotted after dividing out the T^2 dependence of the Stefan-Boltzmann law, so as to enhance interaction effects.

In conclusion, both finite extension and finite temperature calculations agree perfectly for the GN model. Covariance of the single particle energies is certainly the key feature behind this result.

4.3 't Hooft model on a cylinder, decompactification

The behavior of the 't Hooft model at finite temperature is rather controversial. McLerran and Sen⁹⁸ argue that there is no deconfining phase transition, except possibly at infinite temperature. Ming Li,⁶⁴ using standard finite temperature field theory methods, concludes that chiral symmetry may get restored in the limit $T \rightarrow \infty$. In both of these studies, severe infrared problems were encountered, either in the form of divergent diagrams or ambiguous quark self energies. Hansson and Zahed⁹⁹ address the question of the N -dependence of thermodynamic quantities. Several studies have considered QCD₂ on a spatial circle at zero temperature. As explained above, this can also be reinterpreted as finite

temperature calculations for a spatially extended system. Lenz *et al.*⁴⁵ observe a chiral phase transition in the massless 't Hooft model at some critical length, strongly reminiscent of the GN model. Dhar *et al.*^{29,31,32} treat the zero mode gluons in a more ambitious way than Ref. 45 using technology developed in the framework of matrix models and string theory, but are not able to fully solve the resulting complicated equations. They propose that the gauge variables get decompactified by the fermions in complete analogy with the Schwinger model,²⁰ a claim which has recently been disputed by Engelhardt.¹⁰⁰

Let us first consider finite temperature HF. Here, the single particle energies enter through the equilibrium thermal occupation numbers. If we used the principal value prescription with tachyonic behavior at small momenta⁶⁴ (Sec. 3.2.1), we would necessarily get a non-trivial temperature dependence in leading order of the $1/N$ expansion (T -dependent condensate and pressure of order N). Physically, this would imply that the quarks get deconfined. Color singlet mesons which might contribute to thermodynamic observables can show up only in next-to-leading order in $1/N$. We have argued before that the HF single particle energies (interpreted as removal energies) should include the constant $Ng^2L/48$ diverging in the thermodynamic limit (cf. Sec. 3.2.1). If this is kept, $e^{-\beta\epsilon} \rightarrow 0$ and all thermal factors become independent of T . As a consequence,

$$\frac{\partial}{\partial T} \lim_{N \rightarrow \infty} \frac{\langle \bar{q}q \rangle}{N} = 0, \quad \lim_{N \rightarrow \infty} \frac{p}{N} = 0. \quad (208)$$

A system of independent quarks cannot be heated up due to confinement. This leaves no room for a chiral phase transition, not even in the limit $T \rightarrow \infty$.

Let us now turn to the finite extension alternative. The 't Hooft model on a line reduces to a purely fermionic theory with linear Coulomb interaction, see Sec. 3.2. If we simply take this theory and put it on a finite interval with antiperiodic boundary conditions for the quarks, we can repeat the HF calculation of the vacuum (Sec. 3.2.1) numerically, in analogy to what we did analytically in the GN model (Sec. 4.2). This calculation has in fact been done long ago, although for reasons totally unrelated to finite temperature.^{45,101} A second order phase transition to a chirally restored phase was found at a critical interval length of $L_c \approx 19.4/\sqrt{Ng^2}$. Here, the quark self-energies cannot be responsible since they do not enter the gap equation which is perfectly well behaved in the IR, see Sec. 3.2.1. So something must have gone wrong with covariance — the equivalence of finite extension and finite temperature which we have verified in the GN model seems to have been lost in the gauge theory.

The solution to this puzzle was found only recently.¹⁰² It turns out that as soon as one considers finite L , it is not true that the gluons in QCD₂ can be completely eliminated in favor of a static Coulomb potential between quarks.

The large N limit of the zero mode gluons (discussed for pure Yang-Mills in Sec. 2.5) needs to be refined. Eventually, the finite interval calculation yields the same null-result as the thermal HF approach. In effect, the zero mode gluons make it impossible to compress the quark system, in the same way as the IR-divergent single particle energies make it impossible to heat the system up (to leading order in $1/N$). We are familiar with the fact that gauge theories can hide their microscopic degrees of freedom; it is perhaps less well known that they can even hide the structure of space-time, making a cylinder look like an infinite plane (“decompactification”¹⁰²). Since this is a novel and unexpected phenomenon, it may be worth going briefly through the analysis.

It is easy to include dynamical fermions into the pure Yang-Mills theory of Sec. 2.5. We again work canonically on a spatial circle of length L in the gauge $\partial_1 A_1 = 0$, $(A_1)_{ij} = \delta_{ij} \frac{\varphi_i}{gL}$ diagonal in color. The Hamiltonian reads^{45,24,27}

$$H = H_g + H_f + H_C , \quad (209)$$

with the gauge field kinetic energy

$$H_g = -\frac{g^2 L}{4} \sum_i \frac{\partial^2}{\partial \varphi_i^2} , \quad (210)$$

the quark kinetic energy

$$\begin{aligned} H_f = & \sum_{n,i} \frac{2\pi}{L} \left(n + \frac{\varphi_i}{2\pi} \right) \left(a_i^\dagger(n) a_i(n) - b_i^\dagger(n) b_i(n) \right) \\ & + m \sum_{n,i} \left(a_i^\dagger(n) b_i(n) + b_i^\dagger(n) a_i(n) \right) , \end{aligned} \quad (211)$$

and the Coulomb interaction

$$H_C = \frac{g^2 L}{4} \sum_{n,i,j} \frac{j_{ij}(n) j_{ji}(-n)}{(2\pi n - \varphi_j + \varphi_i)^2} . \quad (212)$$

The notation for the quark operators and currents is the same as in Sec. 3.2. As discussed in Sec. 2.5 due to the curved configuration space of the φ_i and the $SU(N)$ Haar measure originally appearing in H_g , this Hamiltonian has to be supplemented by the following boundary condition for the wavefunctionals,

$$\Psi(\varphi_1, \dots, \varphi_N; \text{fermions}) = 0 \quad \text{if} \quad \varphi_i = \varphi_j \bmod 2\pi . \quad (213)$$

In Ref. 45 quantization was performed after complete classical gauge fixing. Thereby, the fact that the φ_i are curvilinear coordinates was ignored. This

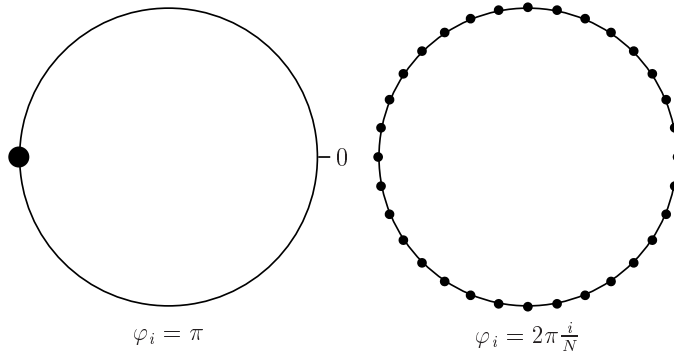


Figure 12: Preferred gluon background field configuration, determining quark boundary conditions for 't Hooft model on a spatial circle. Left: Neglecting the Jacobian. Right: Taking into account the repulsion due to the Vandermonde determinant (“pearl necklace”).

led to the assumption that all the φ_i are frozen at the value π in the large N limit. In the resulting purely fermionic theory, the only remnant of the gluons are antiperiodic boundary conditions for the quarks in the compact space direction. In the meantime, this whole approach has been put on a more rigorous basis by first quantizing in the Weyl gauge and then resolving the Gauss law quantum mechanically.²⁴ This made it clear that the φ_i are parameters on the group manifold with corresponding Jacobian, the $SU(N)$ reduced Haar measure. When solving the theory, it is then possible to restrict oneself to the smallest region in field space bounded by zeros of the Jacobian, see Ref. 27 where the consequences for $SU(2)$, $SU(3)$ have been explored in the case of adjoint fermions. How can this be generalized to the large N limit? A definite choice of “fundamental domain” obviously means that the φ_i always remain ordered, say $0 \leq \varphi_1 \leq \varphi_2 \leq \dots \leq \varphi_N \leq 2\pi$. If we think of the gluons as particles on a circle, they cannot cross each other and become closely packed in the limit $N \rightarrow \infty$. Their fluctuations are suppressed by $1/N$, simply due to lack of space. The only degree of freedom left, the collective rotation of this “pearl necklace”, is a $U(1)$ factor which anyway is not present in the $SU(N)$ theory. This suggests that the correct choice for the gluon background field as seen by the fermions is not $\varphi_i = \pi$, but rather the continuum limit of the lattice points

$$\varphi_i = 2\pi \frac{i}{N}, \quad (i = 1 \dots N) \quad (214)$$

(see Fig. 12). Instead of antiperiodic boundary conditions, the fermions then acquire color dependent boundary conditions which interpolate smoothly be-

tween the phases 0 and 2π ,

$$\psi_k(L) = e^{i2\pi k/N} \psi_k(0) , \quad (k = 1 \dots N) . \quad (215)$$

In the thermodynamic limit $L \rightarrow \infty$, both of these choices of the gluon field configuration, $\varphi_i = \pi$ or Eq. (214), will become indistinguishable and yield the well-known results. We now show that at finite L the effects of the gluons on the quarks is radically different in these two cases, and that it is the spread out distribution (214) which is in fact the correct one.

In such a gluonic background field, the fermions can be treated in a relativistic HF approximation along the lines explained in Sec. 3.2.1 except that the Bogoliubov angle acquires a color index. The gap equation then becomes

$$\frac{2\pi}{L}(n+\alpha_i) \sin \theta_i(n) - m \cos \theta_i(n) + \frac{g^2 L}{16\pi^2} \sum_{n',j} \frac{\sin(\theta_i(n) - \theta_j(n-n'))}{(n' - \alpha_j + \alpha_i)^2} = 0 \quad (216)$$

where we have switched to the slightly more convenient variable $\alpha_i = \frac{\varphi_i}{2\pi} \in [0, 1]$ for the gluons. If $\alpha_i = 1/2$ as chosen in Ref. 45, $\theta_i(n)$ becomes i -independent and we recover the old gap equation considered in that work. Now, we assume $\alpha_i = i/N$ and perform the large N limit before solving the gap equation. Since α_i becomes a continuous variable, we replace $\theta_i(n) \rightarrow \theta_\alpha(n)$ and $\sum_j \rightarrow N \int_0^1 d\alpha'$, with the result

$$\begin{aligned} & \frac{2\pi}{L}(n+\alpha) \sin \theta_\alpha(n) - m \cos \theta_\alpha(n) \\ & + \frac{Ng^2 L}{16\pi^2} \sum_{n'} \int_0^1 d\alpha' \frac{\sin(\theta_\alpha(n) - \theta_{\alpha'}(n-n'))}{(n' - \alpha' + \alpha)^2} = 0 . \end{aligned} \quad (217)$$

This infinite set of coupled integral equations collapses into a single, one-dimensional integral equation, if we set

$$\theta_\alpha(n) = \theta(n+\alpha) . \quad (218)$$

Since n is integer and $\alpha \in [0, 1]$, this step in effect decompactifies the original spatial circle. With this ansatz, the notation $n+\alpha = \nu$, $n-n'+\alpha' = \nu'$ (where ν, ν' are dimensionless, continuous variables) and the substitution $\sum_{n'} \int_0^1 d\alpha' \rightarrow \int_{-\infty}^{\infty} d\nu'$, we obtain

$$\frac{2\pi}{L} \nu \sin \theta(\nu) - m \cos \theta(\nu) + \frac{Ng^2 L}{16\pi^2} \int d\nu' \frac{\sin(\theta(\nu) - \theta(\nu'))}{(\nu - \nu')^2} = 0 . \quad (219)$$

The simple pole in the integral has been regularized by the principal value prescription. After rescaling the variables via

$$\frac{2\pi}{L}\nu := p, \quad \frac{2\pi}{L}\nu' := p', \quad (220)$$

where p, p' have the dimension of momenta, we recover exactly the continuum version of the HF equation, namely

$$p \sin \theta \left(\frac{Lp}{2\pi} \right) - m \cos \theta \left(\frac{Lp}{2\pi} \right) + \frac{Ng^2}{4} \int \frac{dp'}{2\pi} \frac{\sin \left(\theta \left(\frac{Lp}{2\pi} \right) - \theta \left(\frac{Lp'}{2\pi} \right) \right)}{(p - p')^2} = 0. \quad (221)$$

Denoting the Bogoliubov angle of the continuum 't Hooft model by $\theta_{\text{cont}}(p)$, we conclude that

$$\theta(\nu) = \theta_{\text{cont}} \left(\frac{2\pi}{L}\nu \right), \quad (222)$$

or, in terms of the original, color dependent Bogoliubov angle,

$$\theta_i(n) \approx \theta_{\text{cont}} \left(\frac{2\pi}{L} \left(n + \frac{i}{N} \right) \right), \quad (N \rightarrow \infty). \quad (223)$$

This last relation becomes exact in the limit $N \rightarrow \infty$ only. In this limit, the color- and L -dependent Bogoliubov angles for the 't Hooft model on the circle of length L are all given by one universal function, namely the momentum dependent Bogoliubov angle of the 't Hooft model on the infinite line. We emphasize that this universality only holds for the “pearl necklace” type distribution of gauge variables, Eq. (214). If the φ_i are all set equal to π , there is no analytic way known how to relate $\theta(n)$ for different L values, but one has to solve the gap equation numerically for each L .⁴⁵

The upshot of this simple exercise is the following: In the large N limit, the gluon variables influence the fermion boundary conditions in such a way that the circle gets replaced by a line — they decompactify space-time (see Fig. 13; this only works for gauge invariant variables, where one sums over all colors). The length L of the spatial circle becomes an irrelevant parameter. To confirm this last point, let us evaluate the condensate as an example of an observable,

$$\langle \bar{q}q \rangle = -\frac{1}{L} \sum_{n,i} \sin \theta_i(n) = -\frac{N}{L} \sum_n \int_0^1 d\alpha \sin \theta(n + \alpha) = -N \int \frac{dp}{2\pi} \sin \theta_{\text{cont}}(p). \quad (224)$$

The sum over the discrete momenta and the color sum in the large N limit conspire to produce the continuum result, independently of the starting L value.

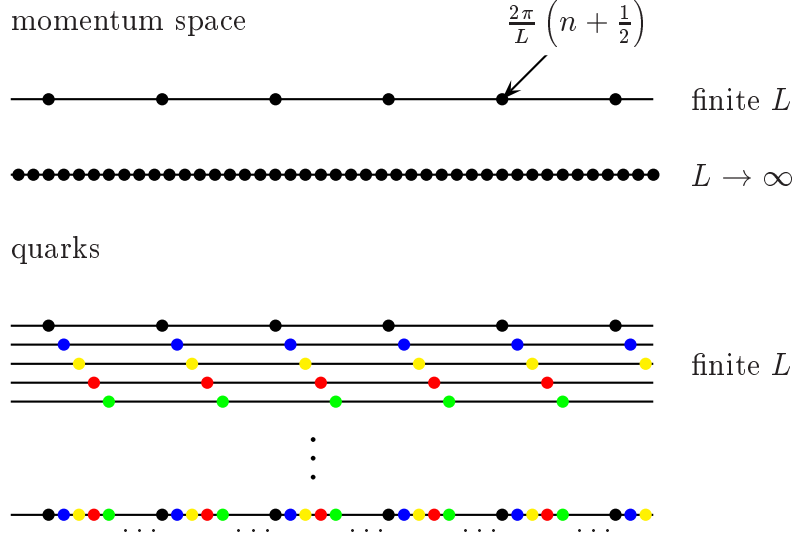


Figure 13: Sketch (in momentum space) of how color-dependent quark boundary conditions in a finite interval may simulate a theory on the infinite line, in the limit $N \rightarrow \infty$ (“decompactification”).

In the alternative thermodynamic interpretation, the condensate becomes independent of temperature to leading order in $1/N$, now in perfect agreement with the finite temperature HF result.

Notice that so far, we have discussed the influence of the gauge fields on the quarks which is indeed dramatic. Vice versa, we do not expect the quarks to influence significantly the gluon zero point motion, again due to the effects of the Jacobian. The kinetic energy H_g will give the same result as in pure Yang Mills theory. Since this contribution to the energy density is L -independent, it again yields zero pressure, reflecting the absence of physical gluonic excitations in 1+1 dimensions.

4.4 $1/N$ corrections at finite T , role of pions

In the present section, we wish to discuss the role of the pions at low temperature. Since this has to do with the next order in the $1/N$ expansion and cannot be covered systematically here, we will content ourselves with briefly reviewing the state of the art and indicating the issues which have attracted most attention recently.

The importance of pions for low temperature QCD was pointed out by Leutwyler and collaborators^{103,104} some time ago. In the vicinity of the chiral limit, pions are naturally the lightest bosons and as such preferred degrees of freedom at low temperature. Using chiral perturbation theory, interaction effects in the pion gas can be computed reliably to rather high order. An extrapolation of the temperature dependence of the chiral condensate even gives a surprisingly good prediction for the critical temperature of the QCD chiral phase transition. Glueballs (if they exist in nature) are much too heavy to matter at low temperatures, quarks are anyway ruled out due to confinement.

The situation is somewhat different in the case of the NJL model which does not exhibit confinement. However also here thermal excitation of a $q\bar{q}$ pair is strongly suppressed as compared to pions at low T . It was soon recognized that the popular $1/N$ expansion is somewhat misleading physically: To leading order, the pions do not contribute at all to thermodynamic observables, they are dominated by the quarks due to their color weight factor (entropy). For any finite N , one can estimate a temperature below which pions dominate, but for $N \rightarrow \infty$ this temperature moves to 0. Zhuang, Klevansky and Hüfner^{105,106} and others have developed techniques to go to next-to-leading order in the $1/N$ expansion, e.g. in the thermodynamic potential. They take into account fluctuations about the mean field which correspond diagrammatically to a ring sum and physically to mesonic contributions. Both $q\bar{q}$ bound states and scattering phase shifts enter. Since a meson in the NJL model can decay into quarks, a “mixed phase” arises at intermediate temperatures where mesons as well as quarks play a role. This problem was also investigated by Barducci *et al.*^{107,108} including the temperature dependence of meson masses.

The same issues are relevant for the lower dimensional models which are the subject of the present work as well. Since these are toy models anyway, one usually takes the limit $N \rightarrow \infty$ seriously (not as an approximation of $N = 3$), at least this is the point of view which we have adopted here. In this case, one might argue that the pions have no influence on the phase diagram of the chiral GN model. In the strict chiral limit, this is a rather extreme picture: N has to be so large that massive fermions win over massless pions in spite of their exponential suppression through the Boltzmann factors, but as a mathematical limit it is perhaps acceptable.

It is instructive to think about the $1/N$ corrections (meson effects) in the “rotated” picture of finite extension field theory. There, in next-to-leading order one would have to evaluate the RPA vacuum in a finite interval, in clear correspondence to the bubble sum of Zhuang *et al.*¹⁰⁵ Unlike the thermodynamic calculation, this does not require any new formalism since the RPA technique is well established. Fermionic and mesonic degrees of freedom are

then treated consistently and it is also clear that scattering states as well as bound states enter. Such a calculation has not yet been carried out for the GN model. The thermodynamic treatment of the $1/N$ corrections has been presented by Barducci *et al.*¹⁰⁹ showing low temperature dominance of pion-like excitations in the massive GN model at finite N . Introducing a bare quark mass enables the authors to vary the degree of explicit chiral symmetry breaking.

Let us finally come back to the 't Hooft model. Here, due to confinement, the quarks do not contribute at all to the pressure at order N so that the mesonic contributions are in fact the leading ones. Since in the large N limit one has non-interacting mesons, one can use the thermodynamics of the ideal Bose gas to analyze this situation. Near the chiral limit, the pion will naturally stick out at low temperatures.

A theoretical question of some interest is the corresponding finite interval RPA calculation in the 't Hooft model. Here, we do not expect that the mechanism which leads to “decompactification” in leading order remains intact, otherwise one would also not get any meson contribution to the pressure. This must mean that the fluctuations of the zero mode gluons come into the picture. It would be interesting to study this in more detail since it would teach us something about the gluon dynamics at large but finite N and perhaps help to settle some of the difficult issues raised by Dhar *et al.*^{29,31,32} in connection with the string picture of QCD₂.

5 Finite density

In the present section, we address the problem of finite baryon density or chemical potential in the GN and 't Hooft models. Since the physics issues are quite different from those at finite temperature (Sec. 4), we restrict ourselves to the $T = 0$ case here and try to clarify the structure of cold baryonic matter first. Ultimately, we are of course interested in the phase diagram of our soluble models in the whole (T, μ) -plane; this will be the subject of Sec. 6. Whereas the GN model at finite density has received a lot of attention in the literature,^{97,93,95,110,92} the corresponding extension of the 't Hooft model has remained essentially unexplored until very recently.^{64,74} Throughout this section, our main focus will be on the relationship between the structure of the single baryon and that of baryonic matter.

5.1 GN model as a Fermi gas

To determine the ground state of the GN model at finite density, we can again use the HF method expected to become exact in the large N limit. As we shall

see, this does not mean that one should trust the results of a HF calculation blindly: If the ground state breaks some symmetry, the HF equations will develop different solutions and one may easily miss the solution with the lowest energy due to erroneous assumptions. Anyway, to start our investigation let us first assume translational invariance and only offer the system the chance to break chiral symmetry. We thus simply fill a number of positive energy plane wave states on top of the Dirac sea until we reach the desired baryon density. This is the standard approach to the finite density GN model, phrased in many-body language. Although we have in mind primarily the chiral GN model, the corresponding calculation would in fact be identical for the model with discrete symmetry only.

We denote the fermion density per color (or baryon density) by $\rho_B = p_f/\pi$ (p_f : Fermi momentum). At the mean field level, the fermions acquire a physical mass m which has to be determined self-consistently. The ground state energy density per color is then given by

$$\frac{\mathcal{E}}{N} = -2 \int_{p_f}^{\Lambda/2} \frac{dk}{2\pi} \sqrt{m^2 + k^2} + \frac{m^2}{2Ng^2} \quad (225)$$

where Λ is the UV cutoff. The first term sums up the single particle energies for all occupied states (the Dirac sea plus all positive energy states with $|p| < p_f$), the second term corrects for double counting of the interaction. We renormalize the theory at $p_f = 0$, cf. Sec. 3.1.1, and denote the physical fermion mass in the vacuum by m_0 . Using the vacuum gap equation (69) to renormalize the matter ground state energy density, Eq. (225), we find (dropping an irrelevant infinity)

$$\frac{\mathcal{E}}{N} = -\frac{m^2}{4\pi} + \frac{p_f}{2\pi} \sqrt{p_f^2 + m^2} + \frac{m^2}{2\pi} \ln \left(\frac{p_f + \sqrt{m^2 + p_f^2}}{m_0} \right) . \quad (226)$$

The energy is minimal provided m satisfies

$$m \ln \left(\frac{p_f + \sqrt{m^2 + p_f^2}}{m_0} \right) = 0 , \quad (227)$$

i.e., for

$$m = 0 \quad \text{or} \quad m = m_0 \sqrt{1 - \frac{2p_f}{m_0}} \quad \left(p_f < \frac{m_0}{2} \right) . \quad (228)$$

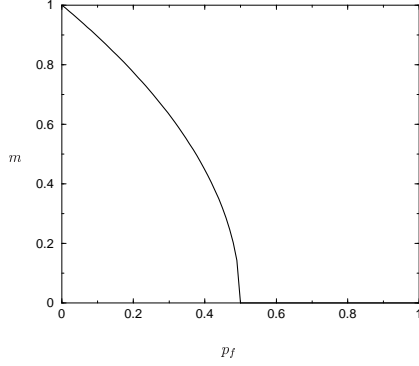


Figure 14: Physical fermion mass as a function of Fermi momentum in the GN model. In units of m_0 .

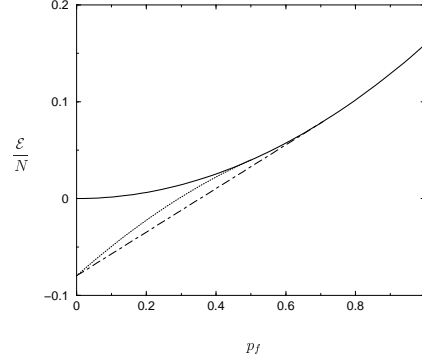


Figure 15: Energy density per color as a function of Fermi momentum in the GN model. Solid curve: Chirally symmetric solution ($m = 0$). Dotted curve: Broken chiral symmetry (m according to Fig. 14). Dash-dotted line: Mixed phase. In units of m_0 .

The corresponding energy densities are

$$\begin{aligned} \left. \frac{\mathcal{E}}{N} \right|_{m=0} &= \frac{p_f^2}{2\pi}, \\ \left. \frac{\mathcal{E}}{N} \right|_{m \neq 0} &= -\frac{m_0^2}{4\pi} + \frac{p_f m_0}{\pi} - \frac{p_f^2}{2\pi} \quad \left(p_f < \frac{m_0}{2} \right). \end{aligned} \quad (229)$$

The physical quark masses (228) and the energy densities (229) are plotted in Figs. 14 and 15. From these figures one might be tempted to conclude that chiral symmetry is broken at low densities and gets restored in a second order phase transition at $p_f = m_0/2$. As is well known, this does not occur, rather there is a first order chiral phase transition at $p_f = m_0/\sqrt{2}$. This can easily be inferred by inspection of the thermodynamic potential of the GN model.^{95,92} At zero temperature, it is possible to understand it also more directly in terms of the following instability. Let us compare the energy densities (229) with the energy density for a system of size L divided into two homogeneous regions I (size ℓ) and II (size $L - \ell$). In region I chiral symmetry is restored; it contains the extra fermions needed to get the prescribed average density (the “MIT bag”¹¹¹). Region II consists of the physical vacuum with broken chiral symmetry, void of excess fermions. The mean energy density obtained in this

way is

$$\frac{\mathcal{E}}{N} = - \left(\frac{L - \ell}{L} \right) \frac{m_0^2}{4\pi} + \frac{L p_f^2}{2\pi \ell} . \quad (230)$$

Minimization with respect to ℓ yields

$$\ell = \frac{\sqrt{2} p_f L}{m_0} \quad (231)$$

valid for $p_f < m_0/\sqrt{2}$, and hence the optimal energy density

$$\frac{\mathcal{E}}{N} = - \frac{m_0^2}{4\pi} + \frac{p_f m_0}{\sqrt{2}\pi} \quad \left(p_f < \frac{m_0}{\sqrt{2}} \right) . \quad (232)$$

As shown in Fig. 15, this solution is lower in energy than the homogeneous one; moreover, it yields the convex hull of \mathcal{E} . It ends exactly at the first order phase transition point $p_f = m_0/\sqrt{2}$ where all space is filled with one big bag. This should be contrasted to the scenario underlying Fig. 14 where the fermion mass decreases continuously. We thus recover the well known mixed phase interpretation of the GN model at finite density, in the zero temperature limit. Notice also that only the total size of regions I and II matters, not how they are subdivided; there could be baryon “droplets” as well.¹¹²

One important point to which we would like to draw the attention of the reader is the behavior of \mathcal{E} near $\rho_B = p_f/\pi = 0$. Since ultimately, at very low density, the fermionic matter problem must reduce to the problem of a single baryon, one would expect

$$\left. \frac{\partial \mathcal{E}}{\partial \rho_B} \right|_{\rho_B=0} = M_B \quad (233)$$

where M_B is the baryon mass. In the present calculation, M_B is not the physical baryon mass, but the mass of an alleged “delocalized” baryon. This is inherent in the translationally invariant HF approach, i.e., the assumption that the single particle orbitals are momentum eigenstates. Using Eq. (233) we obtain in the homogeneous, single phase calculation, Eq. (229), $M_B = N m_0$, consistent with a short range force and a delocalized baryon. The (physically more viable) mixed phase approach, Eq. (232), predicts a baryon mass lower by a factor of $1/\sqrt{2}$ which can be understood in terms of the bag model for the baryon.⁷⁴

However, the GN model possesses bound baryons with lowest mass $N m_0/\pi$ (kink solution for the model with discrete chiral symmetry, cf. Sec. 3.1.2), or even massless baryons (model with continuous chiral symmetry, cf. Sec.

3.3). These binding effects are not $1/N$ suppressed and should be correctly reproduced in a HF approach, in the low density limit. They have obviously been missed here due to our tacit assumption of translational invariance. There is no good reason why such effects should not play a role at higher densities as well. Moreover, differences between the continuous and discrete chirally symmetric GN models based on their different baryon structure and spectra are not at all captured by the Fermi gas approach. In Sec. 5.3 we shall present a cure for this disease. Before that however, let us first repeat the naive calculation for the 't Hooft model where we can also investigate the role of confinement.

5.2 't Hooft model as a Fermi gas

We have discussed the vacuum and baryons in the 't Hooft model in Sec. 3.2. Assuming translational invariance, it is again straightforward to include a finite baryon density into the HF calculation. If p_f denotes the Fermi momentum we only need to replace the density matrix (134) by

$$\begin{aligned}\rho(p) &= \Theta(p_f - |p|)u(p)u^\dagger(p) + v(p)v^\dagger(p) \\ &= \Theta(p_f - |p|) + \Theta(|p| - p_f)v(p)v^\dagger(p)\end{aligned}\quad (234)$$

where we have used the completeness relation for the spinors in the second step. In the expression for the HF ground state energy density at $m = 0$ (139), according to the second line of Eq. (234), we must exclude the region $[-p_f, p_f]$ from the momentum integrations and pick up an additional term due to the change in the baryon density $\text{tr}\rho$,

$$\begin{aligned}\frac{\mathcal{E}}{N} &= - \int \frac{dp}{2\pi} \Theta(|p| - p_f) p \cos \theta(p) \\ &\quad - \frac{Ng^2}{8} \int \frac{dp}{2\pi} \int \frac{dp'}{2\pi} \Theta(|p| - p_f) \Theta(|p'| - p_f) \frac{\cos(\theta(p) - \theta(p')) - 1}{(p - p')^2} \\ &\quad + \frac{Ng^2}{4} \int \frac{dp}{2\pi} \int \frac{dp'}{2\pi} \Theta(p_f - |p|) \Theta(|p'| - p_f) \frac{1}{(p - p')^2} .\end{aligned}\quad (235)$$

This yields at once the following finite density generalization of the gap equation,

$$p \sin \theta(p) + \frac{Ng^2}{4} \int \frac{dp'}{2\pi} \Theta(|p'| - p_f) \frac{\sin(\theta(p) - \theta(p'))}{(p - p')^2} = 0 , \quad (|p| > p_f) , \quad (236)$$

whereas the condensate now becomes

$$\langle \bar{q}q \rangle = -N \int \frac{dp}{2\pi} \theta(|p| - p_f) \sin \theta(p) . \quad (237)$$

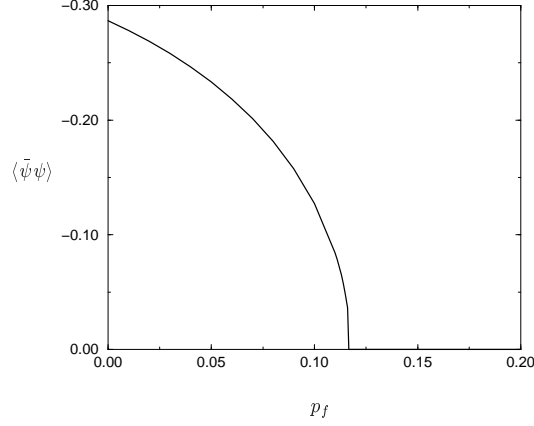


Figure 16: Quark condensate as a function of Fermi momentum in the 't Hooft model, in units where $Ng^2 = 2\pi$.

The gap equation (236) can easily be solved numerically for various p_f . The resulting condensate is shown in Fig. 16. We find that it decreases monotonically with increasing density, disappearing at a critical Fermi momentum

$$p_f^c \approx 0.117 \left(\frac{Ng^2}{2\pi} \right)^{1/2}. \quad (238)$$

This behavior is strikingly similar to the corresponding result for the GN model depicted in Fig. 14, again suggesting some phase transition with restoration of chiral symmetry at high density. Unfortunately, here we are not able to assess whether we are dealing with a first or second order phase transition. The reason lies in the following problem: If we compute the energy density (235) for the 't Hooft model we discover that subtraction of the value at $p_f = 0$ is not sufficient to give a finite result. Unlike in the GN model, the difference is still IR divergent. To be able to proceed, we enclose the system in a box of length L . We then find that the divergence is due to the last term in Eq. (235) (the one which does not involve the Bogoliubov angles) which now contributes the following double sum to the energy per color,

$$\frac{E}{N} \Big|_{\text{div}} = \frac{Ng^2 L}{16\pi^2} \sum_{p \in I} \sum_{n \neq 0, (p-n) \notin I} \frac{1}{n^2}. \quad (239)$$

Here antiperiodic boundary conditions for fermions have been employed in the box regularization, and correspondingly the interval I is defined in the following way,

$$I = [-n_f, n_f] \text{ for } B = 2n_f + 1 \text{ odd, } I = [-n_f - 1, n_f] \text{ for } B = 2n_f + 2 \text{ even.} \quad (240)$$

The result (239) is even more alarming than the non-convex behavior of \mathcal{E} in the GN model, Fig. 15, due to its L -dependence. Adding quarks to the vacuum causes the energy to increase by an infinite amount in the limit $L \rightarrow \infty$. Evaluating the double sums in Eq. (239) for low values of B , we obtain information on the origin of this divergent behavior. For $B = 1$ ($I = [0, 0]$) in particular, the calculated baryon mass (to leading order in L) is

$$M_B = N \left(\frac{Ng^2 L}{48} \right). \quad (241)$$

This is the same relation as $M_B = Nm_0$ in the GN model except that the physical fermion mass is replaced by the infinite constant $Ng^2 L/48$ characteristic of confinement, cf. Eq. (142).

Summarizing, the problems encountered in the GN model with translationally invariant baryonic matter again show up in the 't Hooft model, although in aggravated form. The physics reason is clear: In the GN model the cost of distributing N fermions over the whole space is governed by their physical mass; in the 't Hooft model, due to confinement of quarks, the corresponding quark effective mass diverges with the volume. On the other hand, it is known that both models do possess massless, delocalized baryons in the chiral limit. Evidently, this has to be accounted for, and we conclude that the naive, translationally invariant HF approximation cannot be trusted.

5.3 Breakdown of translational invariance

5.3.1 Strict chiral limit

We now return to the massless baryons introduced in Sec. 3.3 in the chiral limit of two-dimensional field theories. By using literally the same techniques (except for a different value of the baryon number) we can easily find the ground state of the system for any baryon density. As discussed in Sec. 3.3 and illustrated in Fig. 8, the single baryon can be visualized in terms of a “chiral spiral” parametrized by $\chi(x)$ with one single turn in the whole volume. A finite density $\rho_B = B/L = p_f/\pi$ on the other hand implies that

$$\chi(x) = p_f(x - x_0), \quad (242)$$

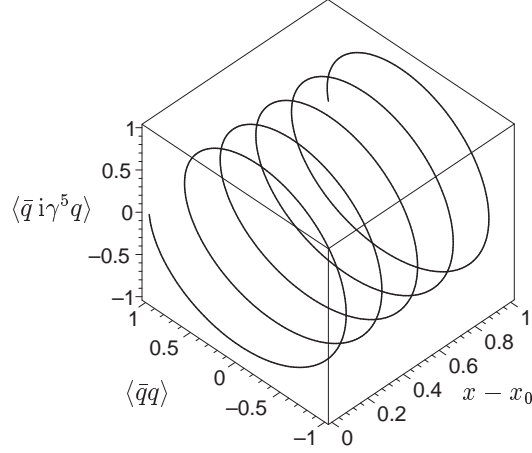


Figure 17: Same as Fig. 8, but for baryonic matter in the chiral GN or 't Hooft model (“chiral spiral”). The wavenumber of the oscillations in the condensates is $2p_f$.

i.e., one full rotation over a physical distance which now has a well defined limit for $L \rightarrow \infty$, namely $2/\rho_B$. The baryon density remains constant in space for the reasons discussed in Sec. 3.3, but the condensates are modulated as

$$\begin{aligned} \langle \bar{q} q \rangle &= \langle \bar{q} q \rangle_v \cos 2p_f(x - x_0) , \\ \langle \bar{q} i \gamma^5 q \rangle &= -\langle \bar{q} q \rangle_v \sin 2p_f(x - x_0) . \end{aligned} \quad (243)$$

They can again be viewed as projections of a chiral spiral of radius $|\langle \bar{q} q \rangle_v|$ onto two orthogonal planes, see Fig. 17.

This state breaks translational symmetry; it is a crystal. In fact, it may be viewed as the simplest possible realization of the old idea of a Skyrme crystal,¹¹³ here in the context of large N two-dimensional field theories. It is meaningless to ask where one baryon begins and ends; each full turn of the spiral adds one unit to the baryon number. Only the condensates reveal that translational symmetry has been broken down to a discrete subgroup. The energy density of this unusual kind of “nuclear matter” is simply (after subtracting the vacuum energy density)

$$\frac{\mathcal{E}}{N} = \frac{p_f^2}{2\pi} . \quad (244)$$

Surprisingly, this is exactly what one would get for a free Fermi gas of massless quarks although Eq. (244) holds for interacting theories where the vacuum has

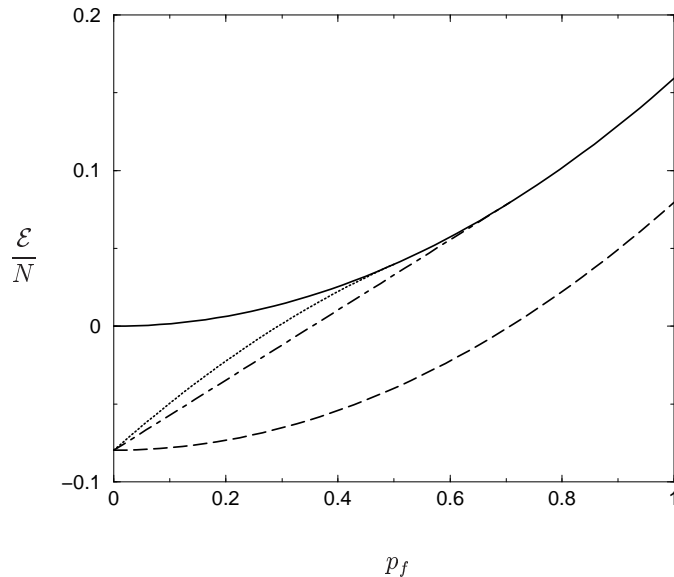


Figure 18: Same as Fig. 15 (GN model), except that the energy density of the Skyrme crystal type of state (the true ground state) has been included as the dashed line.

lower energy due to chiral symmetry breaking. In Fig. 18 we compare the energy density for this state to the ones discussed above for the GN model, where translational symmetry had been assumed. The crystal is always energetically favored, the dependence on p_f is now convex, and there is no trace of a phase transition, neither first nor second order, at any density. The horizontal slope at $p_f = 0$ correctly signals the presence of massless baryons and eliminates the above-mentioned problems with the spurious massive, delocalized baryons. We cannot even draw the corresponding picture for the 't Hooft model, simply because in this case the quark Fermi gas is infinitely higher in energy than the Skyrme crystal for $L \rightarrow \infty$. Nevertheless, all the results for baryonic matter discussed in this section apply to the 't Hooft model as well.

In the high density limit the oscillations of the condensates become more and more rapid. If we are interested only in length scales large as compared to $1/p_f$, the condensates average to zero. In this sense, one might argue that chiral symmetry gets restored at high density, although not in the naive way suggested by Figs. 14 or 15.

Finally, we remark that the “chiral spiral” ground state for fixed baryon

density still preserves one continuous, unbroken symmetry, namely the combination of translation and chiral rotation generated by $P + p_f Q_5$ (P : momentum operator, Q_5 : axial charge). One would therefore expect that RPA excitations on this ground state^{44,45} (or mesons in nuclear matter) will have only one collective, gapless mode, a hybrid of a “phonon” and a “pion”.

5.3.2 Non-vanishing bare quark masses

As discussed in Sec. 3.3 following Ref. 44, a finite bare quark mass can be included in the Skyrme type approach to the baryon; it changes the effective action for the chiral phase $\chi(x)$ from that of a free massless field into a sine-Gordon model. The baryon was identified with the kink solution. It is then clear which type of solution is likely to be a good candidate for baryonic matter: The sine-Gordon kink crystal. It goes over into the results of the previous section in the limit $m \rightarrow 0$ and is an approximate solution to the HF equations (presumably a very accurate one, judging from the results of Ref. 44 for the single baryon). Luckily, the sine-Gordon kink crystal has already been studied thoroughly in the literature, first in solid state physics^{114,115} and more recently as a toy model for the Skyrme crystal,¹¹⁶ in terms of Jacobi elliptic functions and elliptic integrals.¹¹⁷ We take over the results from Ref. 116 which is close in spirit to the present study although the authors apparently did not have in mind two-dimensional large N field theories. Adapting the formulae of their work to our notation, the following steps allow us to generalize the Skyrme crystal of the previous section to small, finite bare quark masses: Let m_π denote the mass of the Goldstone boson, Eq. (176), and $\bar{\rho}_B = p_f/\pi$ the average baryon density (this is our definition of p_f for the case of broken translational symmetry). We then first have to solve the transcendental equation

$$\frac{\pi m_\pi}{p_f} = 2k\mathbf{K}(k) \quad (245)$$

for k where $\mathbf{K}(k)$ is the complete elliptic integral of the first kind. The sine-Gordon kink crystal is then given by the following solution of Eq. (172),

$$\chi(x) = \frac{\pi}{2} + \text{am}(\xi, k) , \quad \xi = \frac{m_\pi}{k}(x - x_0) , \quad (246)$$

($\text{am}(\xi, k)$ is the Jacobian elliptic amplitude function). From this, we can express the baryon density and the various condensates in terms of further Jacobian elliptic functions (dn , sn , cn) as follows,

$$\begin{aligned} \rho_B(x) &= \frac{1}{\pi} \partial_x \chi(x) = \frac{m_\pi}{\pi k} \text{dn}(\xi, k) , \\ \langle \bar{q}q \rangle &= \langle \bar{q}q \rangle_v \cos 2\chi(x) = -\langle \bar{q}q \rangle_v (\text{cn}^2(\xi, k) - \text{sn}^2(\xi, k)) , \\ \langle \bar{q} i \gamma_5 q \rangle &= -\langle \bar{q}q \rangle_v \sin 2\chi(x) = +\langle \bar{q}q \rangle_v 2\text{sn}(\xi, k)\text{cn}(\xi, k) . \end{aligned} \quad (247)$$

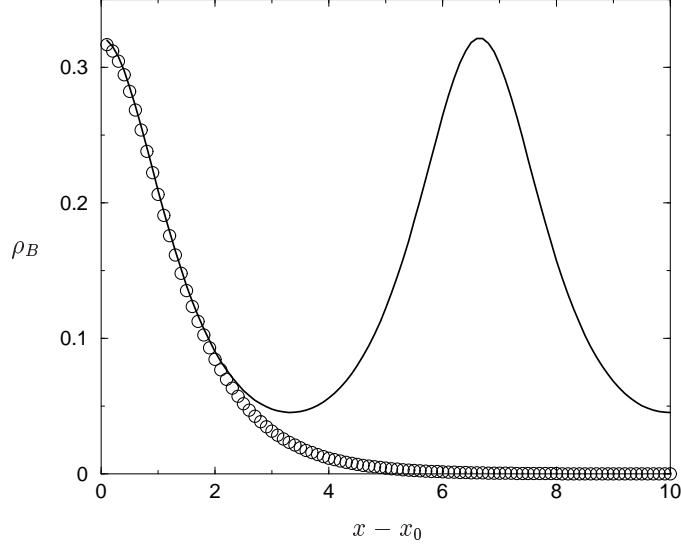


Figure 19: Solid curve: Spatial oscillation of the baryon density in the regime $p_f \ll m_\pi$. Circles: Baryon density for a single baryon for comparison.

Here ξ is as defined in Eq. (246). Finally, the energy per volume of this kind of matter is given by

$$\frac{\mathcal{E}}{N} = \frac{m_\pi p_f}{4\pi^2} \left\{ \frac{8}{k} \mathbf{E}(k) + 4k \left(1 - \frac{1}{k^2} \right) \mathbf{K}(k) \right\} , \quad (248)$$

$\mathbf{E}(k)$ denoting the complete elliptic integral of the second kind.

Let us now illustrate these results in two regimes of interest, namely at low and high density. At low density ($p_f \ll m_\pi$), k in Eq. (245) approaches 1 exponentially, and the baryon density features a chain of well resolved lumps whose shape is determined by the single kink solution (Fig. 19). Likewise, the condensates behave like those of a single baryon: $\langle \bar{q}q \rangle$ changes from the vacuum value outside the baryons to its negative in their center whereas $\langle \bar{q} i \gamma_5 q \rangle$ is peaked in the surface region of each baryon (Figs. 20, 21). These condensates are projections of the distorted “chiral spiral” shown in Fig. 22. The energy (248) for low densities behaves as

$$\mathcal{E} \approx N \frac{2m_\pi p_f}{\pi^2} = M_B \rho_B , \quad (249)$$

showing the expected connection to the baryon mass. At high densities ($p_f \gg$

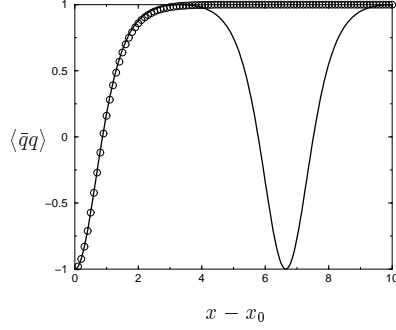


Figure 20: Solid curve: Spatial oscillation of the scalar chiral condensate in the regime $p_f \ll m_\pi$. Circles: Scalar chiral condensate for a single baryon.

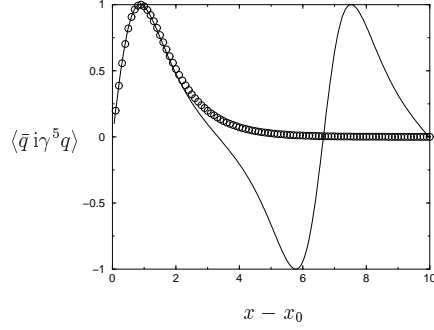


Figure 21: Same as Fig. 20, but for the pseudo-scalar chiral condensate.

m_π), k approaches 0 like

$$k \approx \frac{m_\pi}{p_f} . \quad (250)$$

Thus ξ in Eq. (246) becomes $p_f(x - x_0)$. Moreover, for $k \rightarrow 0$, the Jacobian elliptic functions $\text{am}(\xi, k)$, $\text{sn}(\xi, k)$, $\text{cn}(\xi, k)$ are known to reduce to the argument ξ and the ordinary trigonometric functions $\sin \xi$ and $\cos \xi$, respectively. We thus recover the results for the simple chiral spiral in Sec. 3.3 (the parameter x_0 has to be readjusted to take care of the shift by $\pi/2$ in Eq. (246)). The energy in this case is approximately

$$\frac{\mathcal{E}}{N} \approx \frac{p_f^2}{2\pi} + \frac{m_\pi^2}{8\pi} . \quad (251)$$

The condensates look very much like the sin- and cos-functions of the massless case and need not be plotted. The baryon density oscillates around a constant value, reflecting the strong overlap of the baryons, and are well approximated at high density by

$$\rho_B(x) \approx \frac{p_f}{\pi} \left(1 - \frac{1}{2} \left(\frac{m_\pi}{p_f} \right)^2 \sin^2 p_f(x - x_0) \right) . \quad (252)$$

The behavior of the baryon density $\rho_B(x)$ as one increases p_f (i.e., the mean density) is illustrated in Fig. 23. In the chiral or high-density limit ($m_\pi/p_f \rightarrow 0$) $\rho_B(x)$ eventually becomes x -independent. This provides us with another way of understanding the structure of matter described in the previous section, namely as arising from a chain of very extended, strongly overlapping lumps.

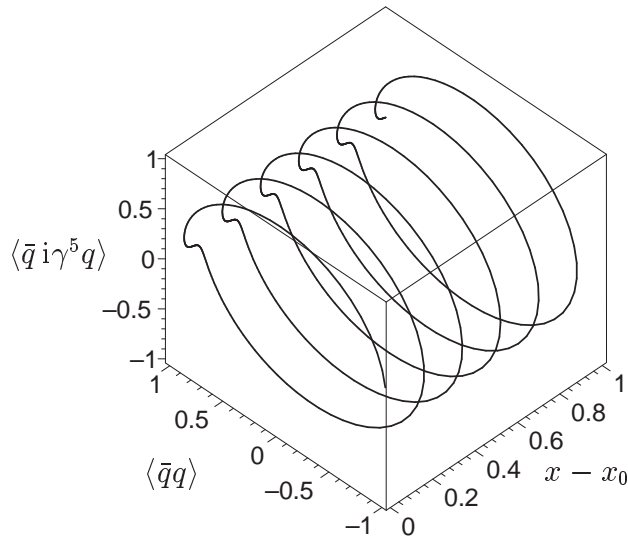


Figure 22: Illustration of the distorted “chiral spiral” for baryonic matter at non-zero bare quark mass (sine-Gordon kink crystal).

5.3.3 Comparison to other works

It is noteworthy that a similar chiral structure of fermionic matter has been reported previously in a variety of models different from the ones discussed here. This indicates that the basic results are more generally valid than our derivation might suggest. Let us briefly go through these works to see what is common and what is different from our case.

The first mention of nonuniform structures we are aware of is Ref. 118 on the massive Schwinger model. Since in the standard Schwinger model baryon charge is confined, one either has to add an inert, uniform background charge to neutralize the system or introduce flavor. In the first case, Fischler *et al.* find that a spatially varying, periodic charge density is induced which they interpret as 1+1 dimensional Wigner crystal.^{119,120} More recently, the massless Schwinger model at finite chemical potential has also been examined and oscillating chiral condensates with wavenumber $k = 2\mu$ were found, by bosonization¹²¹ as well as by functional methods.¹²² In the massless case, the charge density becomes uniform. This phenomenon has obviously a lot in common with our findings, although it is different in detail. In particular, the way to avoid conflict with the no-go theorem for spontaneous symmetry breaking in two dimensions must be different since one cannot invoke large

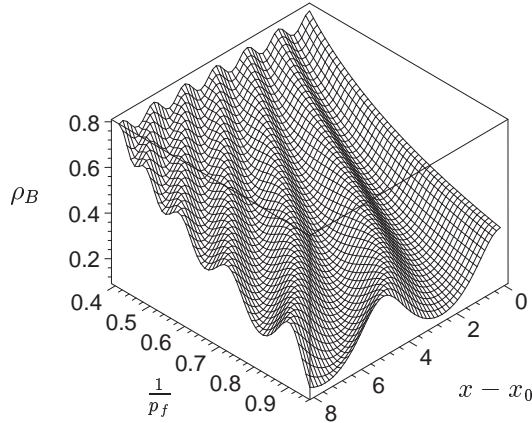


Figure 23: Spatial dependence of the baryon density as it evolves with increasing average density (or Fermi momentum), in units of m_π .

N arguments; presumably, in the $U(1)$ case, the anomaly and the long range Coulomb interaction play a crucial role. In the generalized Schwinger model with two flavors, one can have baryonic charge for neutral systems. Here, Fischler *et al.*¹¹⁸ also arrive at a sine-Gordon equation for the light meson but point out that a possible crystal solution would be destroyed immediately by quantum fluctuations. This is of course avoided in our case by the large N limit.

QCD_2 with flavor at finite chemical potential has been discussed by Christiansen *et al.*¹²³ in the chiral limit. Oscillatory condensates were found within the path-integral approach. Since these authors work at finite N , it is not clear how the no-go theorem is avoided. On the other hand, since we know that QCD_2 does have massless mesons and baryons at finite N , one cannot rule out that there is yet another way of bypassing the Coleman theorem.

Even more surprising are perhaps quite a number of reports about spatially inhomogeneous chiral condensates with exactly the same wave number as in our case, but in 3+1 dimensions. Kutschera *et al.*¹²⁴ have studied quark matter with pion condensates within the σ -model, using a mean-field approximation. Whereas their quark matter is closely analogous to our Fermi gas, the pion condensed state resembles the chiral spiral, especially as far as the condensates are concerned. Another important work is the one by Deryagin *et al.*¹²⁵ on large N QCD in 3+1 dimensions. With the help of a variational calculation, these authors find an instability of cold and dense matter with

respect to formation of an inhomogeneous, anisotropic condensate, a standing wave with wave number 2μ . They point out that unlike color superconductivity, this condensation survives in the $N \rightarrow \infty$ limit. Physically, they interpret their results as condensation of pairs of particles and holes on opposite points of the Fermi surface $|\vec{p}| = \mu$ (“Overhauser effect”¹²⁶). This scenario was subsequently taken up by Shuster *et al.*¹²⁷ and Park *et al.*¹²⁸ who elaborated on the competition between BCS (pp or hh) pairing and Overhauser (ph) pairing. They confirm that the large N limit favors the chiral wave, although it seems very unlikely to be relevant for N values as low as 3.

Let us see how this pairing picture fits into the 1+1 dimensional models considered here. Since relativistic HF is very similar to BCS theory, we can interpret the vacuum result (as encoded in the Bogoliubov angles, cf. Fig. 6, Sec. 3.2.1) as a ph-pairing in a momentum region with a width of order m or $\sqrt{N}g^2$ (for the GN and ’t Hooft models, respectively) and centered around $p = 0$. The crystal solution is obtained by substituting

$$q(x) \rightarrow e^{ip_f x \gamma^5} q(x) , \quad (253)$$

thereby splitting momenta between right-handed and left-handed fermion components by $\pm p_f$. Then, provided that $p_f \gg (m, \sqrt{N}g^2)$, we can indeed describe the result as ph pairing on opposite sides of the Fermi “sphere” (here an interval). However our results also hold for small p_f where this picture is not really applicable.

6 Phase diagram in the (T, μ) -plane

Most of the work done so far on the phase diagram for the two dimensional large N models has been devoted to the original, non-chiral GN model. Its amazingly rich phase diagram has been discussed comprehensively by Wolff⁹⁵ (for $m_b = 0$) and by Barducci *et al.*⁹² (for finite bare quark masses). It has also been invoked for understanding some questions about the statistical physics of polyacetylene,¹²⁹ a linear polymer. We are primarily interested in the role played by chiral symmetry and will therefore concentrate on the chiral GN model. Actually, as far as the conventional Fermi gas approach is concerned, both variants of the GN model yield identical results to leading order in $1/N$.⁹² Apart from briefly reviewing the common lore about the GN model, we will also investigate the novel “crystalline” phase (chiral spiral, cf. Sec. 5.3) and determine which phase is thermodynamically stable. In order to keep things technically as simple as possible, we consider only the $m_b = 0$ case and work to leading order in the $1/N$ expansion throughout this section. Incidentally, the ’t Hooft model will be no issue here: Since in the limit $N \rightarrow \infty$ confinement

suppresses any T -dependence (cf. Sec. 4.3), there is nothing we could add to what has already been said about $T = 0$ and finite density in Sec. 5.

6.1 Chiral GN model with translational invariance

Let us assume unbroken translational invariance and, without loss of generality, $\langle \bar{q} i \gamma^5 q \rangle = 0$. If we are interested in equilibrium thermodynamics at finite temperature and density, it is convenient to work with the grand canonical ensemble where the baryon density is adjusted via a Lagrange multiplier, the chemical potential μ . The HF method can be generalized without any difficulty to finite μ .⁷⁵ Thereby, the HF equation remains unchanged and equal to the free Dirac equation,

$$\left(\gamma^5 \frac{1}{i} \frac{\partial}{\partial x} + m \gamma^0 \right) \varphi_n(x) = \epsilon_n \varphi_n(x) , \quad (254)$$

whereas the chemical potential only enters the gap equation through the standard Fermion occupation numbers

$$-\frac{m}{Ng^2} = \frac{\langle \bar{q} q \rangle}{N} = \sum_n \bar{\varphi}_n(x) \varphi_n(x) \frac{1}{e^{\beta(\epsilon_n - \mu)} + 1} . \quad (255)$$

The solution of the HF equation is once more given by the free, massive Dirac theory with $\epsilon_n = \pm \epsilon(k) = \sqrt{k^2 + m^2}$. The relevant thermodynamic function here is the grand canonical potential often referred to as “effective potential” in this context,

$$V_{\text{eff}} = -\frac{1}{\beta} \ln Z = -\frac{1}{\beta} \ln \text{tr} e^{-\beta(H - \mu N)} . \quad (256)$$

Recalling that the Hamiltonian of the GN model differs from that of the free massive Dirac theory only by a c -number (in leading order in $1/N$) and using the partition function for a free Fermi gas as follows,

$$\begin{aligned} \ln Z &= \ln \prod_n \left(1 + e^{-\beta(\epsilon_n - \mu)} \right) \\ &= L \int \frac{dk}{2\pi} \ln \left[e^{\beta(\epsilon(k) + \mu)} \left(1 + e^{-\beta(\epsilon(k) - \mu)} \right) \left(1 + e^{-\beta(\epsilon(k) + \mu)} \right) \right] , \end{aligned} \quad (257)$$

the effective potential density ($\mathcal{V}_{\text{eff}} = V_{\text{eff}}/L$) per color becomes

$$\frac{\mathcal{V}_{\text{eff}}}{N} = \frac{m^2}{2Ng^2} - \int \frac{dk}{2\pi} \left\{ \epsilon(k) + \mu + \frac{1}{\beta} \ln \left[\left(1 + e^{-\beta(\epsilon(k) - \mu)} \right) \left(1 + e^{-\beta(\epsilon(k) + \mu)} \right) \right] \right\} . \quad (258)$$

In this way, the “vacuum part” ($T = \mu = 0$) can easily be identified and separated from the “matter part” which in turn is made up of particle and anti-particle contributions. Incidentally, the term

$$- \int \frac{dk}{2\pi} \mu \quad (259)$$

in eq. (258) is a pure vacuum term which is usually omitted in the literature; it arises from the infinite fermion density of the Dirac sea. The gap equation (255) can be further worked out to yield

$$m = \frac{Ng^2}{2\pi} \int dk \frac{m}{\epsilon(k)} \left(1 - \frac{1}{e^{\beta(\epsilon(k)-\mu)} + 1} - \frac{1}{e^{\beta(\epsilon(k)+\mu)} + 1} \right), \quad (260)$$

where we have used

$$\bar{u}(k)u(k) = -\bar{v}(k)v(k) = \frac{m}{\epsilon(k)}. \quad (261)$$

Eq. (260) is equivalent to the condition that the effective potential (258) is stationary with respect to m ,

$$\frac{\partial \mathcal{V}_{\text{eff}}}{\partial m} = 0. \quad (262)$$

Renormalization can be performed at $T = 0, \mu = 0$ (physical fermion mass m_0) resulting in the renormalized potential

$$\begin{aligned} \frac{\mathcal{V}_{\text{eff}}}{N} \Big|_{\text{ren}} &= \frac{m^2}{4\pi} \ln \left(\frac{m^2}{m_0^2} \right) + \frac{m_0^2 - m^2}{4\pi} \\ &\quad - \frac{1}{\beta} \int \frac{dk}{2\pi} \ln \left[\left(1 + e^{-\beta(\epsilon(k)-\mu)} \right) \left(1 + e^{-\beta(\epsilon(k)+\mu)} \right) \right]. \end{aligned} \quad (263)$$

By adding the “bag pressure” $m_0^2/(4\pi)$ and dropping the term in Eq. (259), it has been adjusted to vanish in the vacuum. The effective potential (263) contains all the information about the conventional phase diagram of the GN model. (For the path integral derivation and the representation of \mathcal{V}_{eff} in terms of sums over Matsubara frequencies instead of integrals over thermal occupation numbers, we refer to Refs. 95, 110.) For the sake of completeness, we record the expressions for standard thermodynamical bulk observables: The free energy density \mathcal{F} (or, equivalently, minus the pressure p) is equal to \mathcal{V}_{eff} , Eq. (263). The quark density ρ and the entropy density s are obtained by

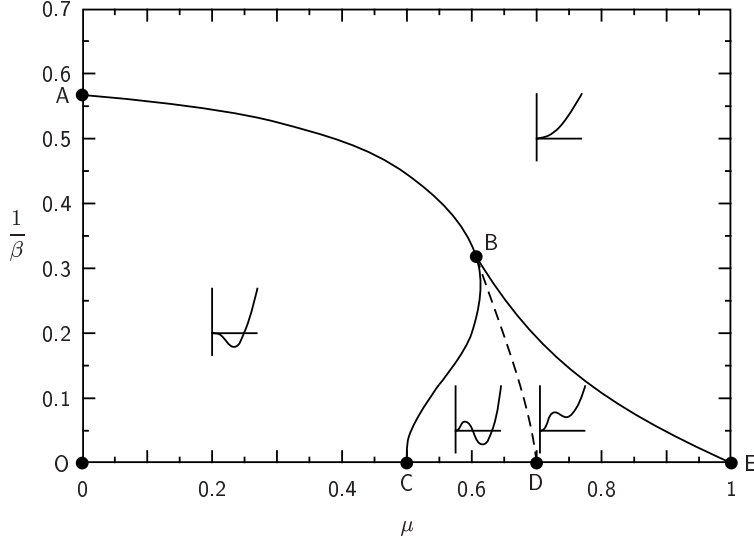


Figure 24: Phase diagram of the (chiral or non-chiral) GN models, assuming unbroken translational symmetry. For a discussion, see text below Eq. (266). Units of m_0 ; adapted from Ref. 95.

differentiating p with respect to μ and T ,

$$\frac{\rho}{N} = \frac{1}{\pi} \int_0^\infty dk \left(\frac{1}{e^{\beta(\epsilon(k)-\mu)} + 1} - \frac{1}{e^{\beta(\epsilon(k)+\mu)} + 1} \right), \quad (264)$$

$$\begin{aligned} \frac{s}{N} &= \frac{1}{\pi} \int_0^\infty dk \ln \left[\left(1 + e^{-\beta(\epsilon(k)-\mu)} \right) \left(1 + e^{-\beta(\epsilon(k)+\mu)} \right) \right] \\ &+ \frac{\beta}{\pi} \int_0^\infty dk \left(\frac{\epsilon(k) - \mu}{e^{\beta(\epsilon(k)-\mu)} + 1} + \frac{\epsilon(k) + \mu}{e^{\beta(\epsilon(k)+\mu)} + 1} \right), \end{aligned} \quad (265)$$

whereas the internal energy density can now be deduced via

$$\varepsilon = Ts - p + \mu\rho. \quad (266)$$

Needless to say, all of these observables have to be evaluated in the absolute minimum of the effective potential with respect to m , i.e., by solving the gap equation.

The phase diagram which one obtains in this way is depicted in Fig. 24, adapted from Ref. 95. The line AB is a critical line of second order transitions (\mathcal{V}_{eff} changes from one minimum to a maximum and a minimum). The point

B is a tricritical point located at $1/\beta = 0.3183$, $\mu = 0.6082$ (all numbers here are in units of m_0); it separates the second order line from a first order line BD along which \mathcal{V}_{eff} has two degenerate minima and a maximum. The endpoint D lies at $\mu = 1/\sqrt{2}$ where the $T = 0$ phase transition occurs, cf. Sec. 5.1. Lines BC and BE are boundaries of metastability; when crossed, the potential acquires or loses a second minimum; point C is at $\mu = 1/2$. In region OABD, chiral symmetry is broken and the quarks are massive; the outside region has unbroken chiral symmetry and massless fermions.

In order to highlight the different behavior of the system when going through a first and second order phase transition, respectively, we have illustrated in Figs. 25 and 26 the evolution of \mathcal{V}_{eff} along the $\mu = 0$ and $T = 0$ axes (this corresponds to the special cases discussed in Secs. 4 and 5, respectively). Also shown is the behavior of the physical fermion mass. In this way, the unstable HF solution which we have found at finite density (with continuously decreasing mass, see Sec. 5.1) can be identified as corresponding to a local maximum of \mathcal{V}_{eff} . In preparing Fig. 26, we have taken advantage of the fact that the integration in Eq. (263) can be carried out at $T = 0$ with the result

$$\begin{aligned} \frac{\mathcal{V}_{\text{eff}}}{N} = & \frac{m^2}{4\pi} \ln \left(\frac{m^2}{m_0^2} \right) + \frac{m_0^2 - m^2}{4\pi} \\ & + \frac{1}{2\pi} \theta(\mu - m) \left[m^2 \ln \left(\frac{\mu + \sqrt{\mu^2 - m^2}}{m} \right) - \mu \sqrt{\mu^2 - m^2} \right]. \end{aligned} \quad (267)$$

6.2 Chiral spiral at finite temperature

We have seen before that the translationally non-invariant finite density solution (constant baryon density, but oscillating condensates in the chiral limit) of the HF equation at $T = 0$ can be obtained from the vacuum solution by a space dependent chiral rotation of the quarks, cf. Sec. 3.3. As already noted by Kao *et al.*¹²¹ for the massless Schwinger model and by Sadzikowski *et al.*¹³⁰ for the σ - and NJL models, the same procedure works at finite temperature as well. We show that the Fermi gas solution at zero chemical potential and finite temperature can be mapped onto the chiral spiral type solution at finite μ and the same T . This will allow us to follow the fate of the crystalline solution as we heat up baryonic matter.

We start from the HF equation at finite T, μ , but neither invoking trans-

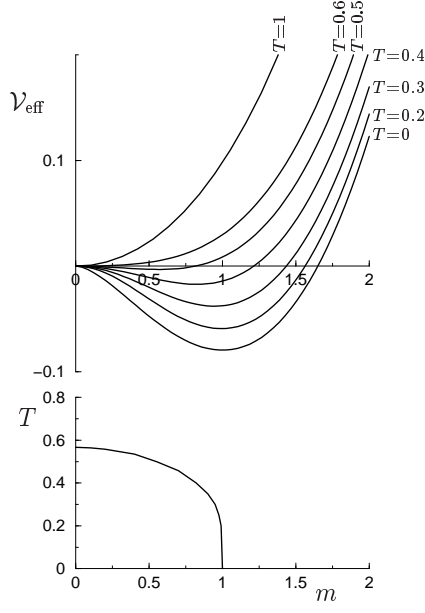


Figure 25: Upper graph: Effective potential density as a function of dynamical fermion mass m at $\mu = 0$ for various temperatures below and above $T_c \approx 0.567$. Lower graph: m as a function of T (i.e., position of minimum in upper curves). Second order phase transition.

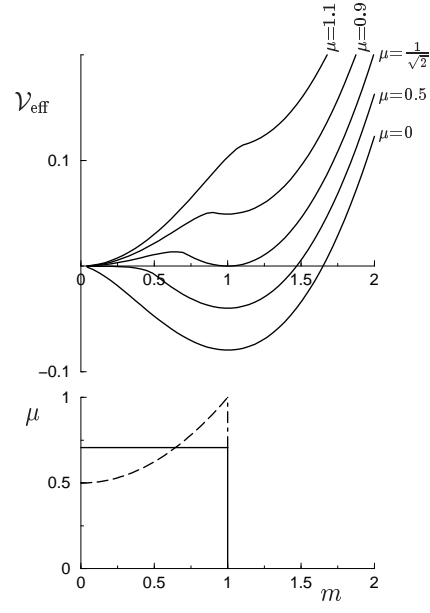


Figure 26: Upper graph: Effective potential density as a function of dynamical fermion mass m at $T = 0$ for various chemical potentials below and above $\mu_c = 1/\sqrt{2}$. Lower graph: m as a function of μ (dashed line: position of maximum, corresponding to Fig. 14; solid line: position of minimum in upper curves). First order phase transition.

lational invariance nor assuming that $\langle \bar{q} i\gamma^5 q \rangle$ vanishes,

$$\left\{ \gamma^5 \frac{1}{i} \frac{\partial}{\partial x} - g^2 (\langle \bar{q}(x) q(x) \rangle \gamma^0 + \langle \bar{q}(x) i\gamma^5 q(x) \rangle i\gamma^1) \right\} \varphi_n(x) = \omega_n \varphi_n(x) . \quad (268)$$

As before, temperature and chemical potential only show up in the self-consistency relations which now read

$$\begin{aligned} \langle \bar{q}(x) q(x) \rangle &= N \sum_n \bar{\varphi}_n(x) \varphi_n(x) \frac{1}{e^{\beta(\omega_n - \mu)} + 1} , \\ \langle \bar{q}(x) i\gamma^5 q(x) \rangle &= N \sum_n \bar{\varphi}_n(x) i\gamma^5 \varphi_n(x) \frac{1}{e^{\beta(\omega_n - \mu)} + 1} . \end{aligned} \quad (269)$$

Guided by the $T = 0$ results (cf. Sec. 5.3.1), we make the following ansatz for the x -dependence of the scalar and pseudo-scalar condensates,

$$\langle \bar{q}(x)q(x) \rangle = -\frac{m}{g^2} \cos(2\mu x) , \quad \langle \bar{q}(x)i\gamma^5 q(x) \rangle = \frac{m}{g^2} \sin(2\mu x) . \quad (270)$$

The HF equation for this particular potential can be turned into

$$\left\{ \gamma^5 \frac{1}{i} \frac{\partial}{\partial x} + m e^{i\mu x \gamma^5} \gamma^0 e^{-i\mu x \gamma^5} \right\} \varphi_n(x) = \omega_n \varphi_n(x) \quad (271)$$

where we have used the fact that

$$e^{i\mu x \gamma^5} \begin{pmatrix} \gamma^0 \\ i\gamma^1 \end{pmatrix} e^{-i\mu x \gamma^5} = \begin{pmatrix} \cos 2\mu x & -\sin 2\mu x \\ \sin 2\mu x & \cos 2\mu x \end{pmatrix} \begin{pmatrix} \gamma^0 \\ i\gamma^1 \end{pmatrix} . \quad (272)$$

A local chiral rotation of the form

$$\varphi_n(x) = e^{i\mu x \gamma^5} \chi_n(x) \quad (273)$$

then eliminates the x -dependence from the HF potential,

$$\left\{ \gamma^5 \frac{1}{i} \frac{\partial}{\partial x} + \mu + m\gamma^0 \right\} \chi_n(x) = \omega_n \chi_n(x) , \quad (274)$$

and enables us to solve the HF equation trivially,

$$\begin{aligned} \chi_n(x) &= e^{ikx} u(k) & (\omega_n = \epsilon(k) + \mu) , \\ \chi_n(x) &= e^{ikx} v(k) & (\omega_n = -\epsilon(k) + \mu) , \end{aligned} \quad (275)$$

with $\epsilon(k) = \sqrt{k^2 + m^2}$ and $u(k), v(k)$ free, massive spinors. Since

$$\chi_n^\dagger(x) i\gamma^1 \chi_n(x) = 0 , \quad (276)$$

the two self-consistency conditions (269) collapse into the single condition

$$-\frac{m}{Ng^2} = \sum_n \chi_n^\dagger(x) \chi_n(x) \frac{1}{e^{\beta(\omega_n - \mu)} + 1} . \quad (277)$$

The additive term μ in ω_n , Eq. (275), just cancels the chemical potential and we have mapped our problem exactly onto the $\mu = 0$, translational invariant HF problem at finite T ,

$$-\frac{m}{Ng^2} = \sum_n \chi_n^\dagger(x) \chi_n(x) \frac{1}{e^{\beta\epsilon_n} + 1} , \quad \epsilon_n = \omega_n - \mu = \pm \sqrt{k^2 + m^2} . \quad (278)$$

The parameter m therefore has to be identified with the physical fermion mass of the translationally invariant vacuum at $\mu = 0$ and the same finite T . We can thereby construct a translationally broken solution of the HF problem for any (β, μ) ; it can be pictured as a chiral spiral whose radius shrinks with increasing temperature until it disappears at $T_c = m_0 e^C / \pi$, cf. Sec. 4.2.

Let us determine the free energy of this new phase. The density of the effective potential per color is still given by eq. (258), or equivalently by

$$\frac{\mathcal{V}_{\text{eff}}}{N} = \frac{m^2}{2Ng^2} - \frac{1}{L\beta} \sum_n \ln \left(1 + e^{-\beta(\omega_n - \mu)} \right) . \quad (279)$$

The double counting term depends only on the radius of the chiral circle and is therefore unchanged (cf. Eq. (270)),

$$\langle \bar{q}q \rangle^2 + \langle \bar{q}i\gamma^5 q \rangle^2 = \frac{m^2}{g^4} . \quad (280)$$

In view of the relation $\omega_n - \mu = \epsilon_n$, it appears superficially as if nothing depended on μ and we got the same result as for the translationally invariant system at zero chemical potential. As we know from the $T = 0$ case, this argument is too rough — the μ -dependence is intimately related to the UV regularization. Let us impose an UV-cut-off on the single particle energies at the bottom of the Dirac sea,

$$\omega_n > -\Lambda/2 \quad \Leftrightarrow \quad |k| < \Lambda/2 + \mu . \quad (281)$$

The entire μ -dependence of \mathcal{V}_{eff} arises from this shift in the cutoff. We can then easily evaluate the difference between the free energy density of the “chiral spiral” at (β, μ) and the standard solution at $(\beta, 0)$,

$$\begin{aligned} \left. \frac{\mathcal{V}_{\text{eff}}(\beta, \mu)}{N} \right|_{\text{spir}} - \left. \frac{\mathcal{V}_{\text{eff}}(\beta, 0)}{N} \right|_{\text{stand}} &= - \int_{-(\Lambda/2 + \mu)}^{\Lambda/2 + \mu} \frac{dk}{2\pi} \sqrt{k^2 + m^2} \\ &\quad + \int_{-\Lambda/2}^{\Lambda/2} \frac{dk}{2\pi} \sqrt{k^2 + m^2} \\ &\approx - \frac{(\Lambda + \mu)\mu}{2\pi} . \end{aligned} \quad (282)$$

This result does not depend on temperature, a feature characteristic for an UV effect. The fermion density per color can be obtained by differentiation with respect to μ ; we find the same result as at zero temperature,

$$\frac{\rho}{N} = - \frac{\partial}{\partial \mu} \frac{\mathcal{V}_{\text{eff}}}{N} = \frac{\Lambda}{2\pi} + \frac{\mu}{\pi} , \quad (283)$$

hence, with the definition of the Fermi momentum adopted in Sec. 5.3.1,

$$\mu = p_f \quad (284)$$

(the term $\sim \Lambda$ in Eq. (283) is the fermion density of the Dirac sea). Summarizing, we can now compare the effective potentials for two solutions of the HF equation at finite (β, μ) . The Fermi gas solution with unbroken translational invariance has already been given in Eq. (263). The crystalline phase on the other hand yields

$$\frac{\mathcal{V}_{\text{eff}}}{N} \Big|_{\text{spir}} = \frac{m^2}{4\pi} \ln \left(\frac{m^2}{m_0^2} \right) + \frac{m_0^2 - m^2}{4\pi} - \frac{2}{\beta} \int \frac{dk}{2\pi} \ln \left(1 + e^{-\beta \epsilon(k)} \right) - \frac{\mu^2}{2\pi}, \quad (285)$$

where we have again dropped the term $-\Lambda\mu/(2\pi)$. In both cases, one still has to minimize the effective potential with respect to m . The depth of the respective minima (or physically minus the pressure) allows us to decide which phase is the stable one. The chiral spiral is favored everywhere over the homogeneous phase, below the critical temperature. This can be shown by a straightforward numerical evaluation, but also deduced analytically from the simple relation

$$\mathcal{V}_{\text{eff}}(\beta, \mu)|_{\text{spir}} = \mathcal{V}_{\text{eff}}(\beta, 0) - N \frac{\mu^2}{2\pi}. \quad (286)$$

As the additional term in Eq. (286) does not depend on m , both $\mathcal{V}_{\text{eff}}(\beta, \mu)|_{\text{spir}}$ and $\mathcal{V}_{\text{eff}}(\beta, 0)$ are minimized by the same m

$$m_{\text{spir}}(\beta, \mu) = m(\beta, 0). \quad (287)$$

The free energy density of the spiral at β and μ evaluated at its minimum $m_{\text{spir}}(\beta, \mu)$ is thus equal to

$$\mathcal{V}_{\text{eff}}(\beta, \mu)|_{\text{spir}, m=m_{\text{spir}}} = \mathcal{V}_{\text{eff}}(\beta, 0)|_{m=m(\beta, 0)} - N \frac{\mu^2}{2\pi}. \quad (288)$$

$\mathcal{V}_{\text{eff}}(\beta, \mu)|_{m=m(\beta, \mu)}$ is a monotonously decreasing function of μ at fixed β (its derivative with respect to μ at fixed β is just $-\rho$). Furthermore from the phase diagram (Fig. 24) it is clear that for any fixed β there is a critical chemical potential μ_c , where chiral symmetry gets restored. Above this critical chemical potential, $\mathcal{V}_{\text{eff}}(\beta, \mu)$ evaluated at its minimum just behaves like the energy density of free fermions in 1+1 dimensions

$$\mathcal{V}_{\text{eff}}(\beta, \mu)|_{m=m(\beta, \mu)} = -N \frac{\mu^2}{2\pi} \text{ for } \mu \geq \mu_c. \quad (289)$$

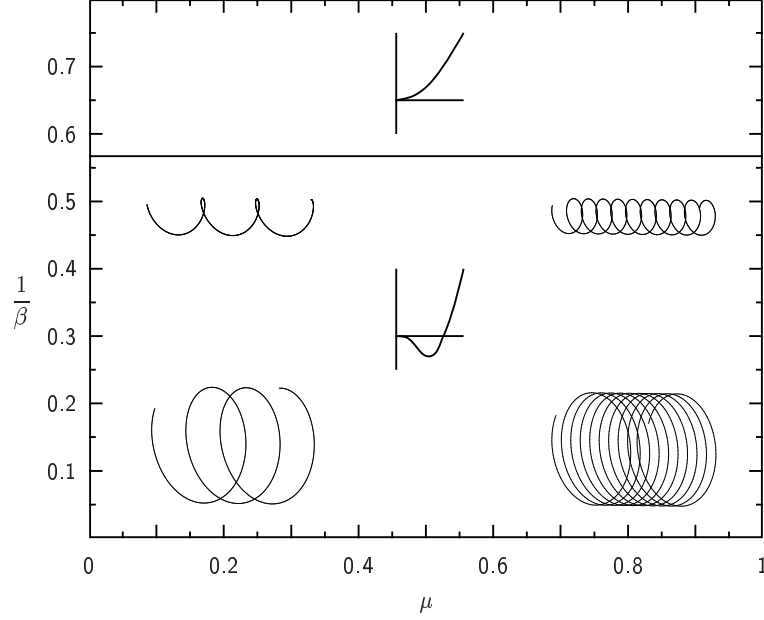


Figure 27: Phase diagram of chiral GN model, based on spatially inhomogeneous solution. The horizontal line at $T_c \approx 0.567$ is a second order line of chiral symmetry restoration. The dependence of radius and helix angle of the chiral spiral on μ and T is indicated qualitatively by means of the inserted drawings.

Comparing Eq. (288) to $\mathcal{V}_{\text{eff}}(\beta, \mu)|_{m=m(\beta, \mu)}$ it is clear that the chiral spiral is always lower in free energy than the homogeneous phase.

Eq. (286) is also useful if one wants to evaluate the thermodynamic observables for the crystal phase

$$\begin{aligned}
 \rho(\beta, \mu)|_{\text{spir}} &= N \frac{\mu}{\pi} , \\
 p(\beta, \mu)|_{\text{spir}} &= p(\beta, 0) + N \frac{\mu^2}{2\pi} , \\
 s(\beta, \mu)|_{\text{spir}} &= s(\beta, 0) , \\
 \varepsilon(\beta, \mu)|_{\text{spir}} &= \varepsilon(\beta, 0) + N \frac{\mu^2}{2\pi} .
 \end{aligned} \tag{290}$$

(At $\mu = 0$, there is no distinction between the Fermi gas and the other phase.) Since the translationally broken phase is the thermodynamically stable phase wherever it exists, the phase diagram of the chiral GN model has only one

horizontal second order line at $T = T_c$ where chiral symmetry is restored and the radius of the chiral spiral shrinks to zero (Fig. 27); no phase transition occurs if we increase the chemical potential. Note that our results are rather different from a recent study of a non-uniform chiral phase in 3+1 dimensional effective field theories (σ -model, NJL model¹³⁰). In our language, these authors use the radius and the helix angle of the chiral spiral as independent variational parameters. Since in 1+1 dimensions baryon number is topologically connected to winding number, we do not seem to have this option but can vary only with respect to the radius (or m).

As a last remark, we wish to comment on the original GN model with only discrete chiral symmetry. The chiral spiral does not exist here and one might think that our analysis does not have anything to say about it. However, the criticism of Sec. 5.1 also applies here. As the non-chiral GN model has (massive) bound baryons, the low density behavior of the energy obtained in standard HF approximation cannot be correct and the phase diagram has to be reconsidered. This is a harder task than for the chiral model since here dynamics is not completely dominated by chiral symmetry. It is quite possible that the first order phase transition survives, but this still has to be worked out in detail.

7 Closing remarks

In this paper, we have illustrated the kind of insights one gets from studies of exactly soluble field theories by means of two classic examples, the GN and the 't Hooft model. The undeniable success of these models stems from a fortunate combination of two very bold substitutions: Replacing the number of spatial dimensions by 1 and the number of colors by ∞ (ironically, both are 3 in real QCD). Without the first choice, there is no solvability; without the 2nd, there are hardly enough interesting phenomena due to rigorous no-go theorems. If one is willing to swallow both of these bitter pills, one is awarded with a striking number of analogies between these toy models and the real world which have led to a long list of QCD-motivated applications. These analogies include such central features of QCD as asymptotic freedom, dimensional transmutation, chiral symmetry breaking, and confinement. In view of the fact that these models have the simplest Lagrangians of certain types which one can write down and are not contrived in any sense, this is quite amazing and underlines their pedagogical value for QCD related questions. Nowadays, it may well be that the study of lower dimensional field theories is a better training ground for students interested in QCD than a standard field theory course based on Feynman diagrams and perturbative QED.

Throughout this work we have tried to emphasize the fact that the solution of these models can be found by rather elementary means — we have deliberately chosen the relativistic HF approach as our main tool. This does not mean though that there are no subtleties: We only mention the emergence of baryon number from the UV regularization, or how zero mode gluons affect the thermodynamics of quarks. Such features make the use of analytical methods particularly important and set the scale for the even more subtle properties to be expected from 4-dimensional QCD.

As far as our more specific subject — finite temperature and density behavior — is concerned, we have found that even after more than 25 years these models are still good for some surprises. The strongest impression for us is the way in which chiral symmetry governs not only the hadron spectrum, but also the phase structure at finite density and temperature. Confinement is most clearly seen in the temperature dependence of observables, whereas the dependence on the chemical potential is dominated by chiral symmetry. Other non-trivial insights are related to the realization of the Skyrme picture in a precise fashion, a triple point in the phase diagram of the non-chiral GN model and inhomogeneous chiral condensates. As a by-product, we have resolved some puzzles in the literature and identified issues where further work is needed, for instance the phase diagram of the non-chiral GN model.

In conclusion, we see no indication that models such as the GN or 't Hooft model are anywhere close to having exhausted their potential as a theoretical laboratory for QCD.

Acknowledgements

We are grateful to Misha Shifman for the invitation to contribute to this Festschrift in honor of Boris Ioffe, thereby forcing us to clarify some issues before a certain deadline. M.T. thanks his collaborators, colleagues and students for most enjoyable and useful interactions on 2d field theory, in particular M. Burkardt, V. Dolman, M. Engelhardt, O. Jahn, M. Kurz, F. Lenz, S. Levit, R. Oderkerk, K. Ohta, R. Pausch, C. Satzinger, B. Schreiber, M. Seeger, A. Smilga, D. Stoll, R. Weingärtner, S. Wörlen, K. Yazaki, and I. Zahed.

References

1. N. Seiberg and E. Witten, *Nucl. Phys. B* **426**, 19 (1994).
2. J. Schwinger, *Phys. Rev.* **128**, 2425 (1962).
3. D.J. Gross and A. Neveu, *Phys. Rev. D* **10**, 3235 (1974).
4. G. 't Hooft, *Nucl. Phys. B* **75**, 461 (1974).
5. D.R. Hartree, *Proc. Camb. Phil. Soc.* **24**, 89 (1928).

6. V.A. Fock, *Z. Phys.* **61**, 126 (1930).
7. M. Blau and G. Thompson, *Trieste HEP Cosmol.*, 0175-244 (1993).
8. E. Abdalla and M.C.B. Abdalla, *Phys. Rep.* **265**, 253 (1996).
9. S.J. Brodsky, H.-C. Pauli, and S.S. Pinsky, *Phys. Rep.* **301**, 299 (1998).
10. N. Nakanishi and I. Ojima, *Covariant operator formalism of gauge theories and quantum gravity*, World Scientific 1991.
11. S. Coleman, *Comm. Math. Phys.* **31**, 259 (1973).
12. C. Itzykson and J.-B. Zuber, *Quantum field theory*, McGraw-Hill 1980.
13. N.D. Mermin and H. Wagner, *Phys. Rev. Lett.* **17**, 1133 (1966).
14. K. Huang, *Quantum Field Theory. From Operators to Path Integrals*, John Wiley 1998, ch. 18.
15. E. Witten, *Nucl. Phys. B* **145**, 110 (1978).
16. I. Affleck, *Nucl. Phys. B* **265**, 448 (1986).
17. J.M. Kosterlitz and D.J. Thouless, *J. Phys. C* **6**, 1181 (1973).
18. J.M. Kosterlitz, *J. Phys. C* **7**, 1046 (1974).
19. V.L. Berezinsky, *Sov. Phys. JETP* **32**, 493 (1971).
20. N.S. Manton, *Ann. Phys. (N.Y.)* **159**, 220 (1985).
21. S.G. Rajeev, *Phys. Lett. B* **212**, 203 (1988).
22. J.E. Hetrick and Y. Hosotani, *Phys. Lett. B* **230**, 88 (1989).
23. J.E. Hetrick, *Int. J. Mod. Phys. A* **9**, 3153 (1994).
24. F. Lenz, H.W.L. Naus, and M. Thies, *Ann. Phys. (N.Y.)* **233**, 51 (1994).
25. J.A. Minahan and A.P. Polychronakos, *Phys. Lett. B* **326**, 288 (1994).
26. B. Svetitsky, *Phys. Rep.* **132**, 1 (1986).
27. F. Lenz, M. Shifman, and M. Thies, *Phys. Rev. D* **51**, 7060 (1995).
28. M. Engelhardt and B. Schreiber, *Z. Phys. A* **351**, 71 (1995).
29. A. Dhar, G. Mandal, and S.R. Wadia, *Nucl. Phys. B* **436**, 487 (1995).
30. M. Seeger and M. Thies, *Phys. Rev. D* **58**, 027701 (1998).
31. A. Dhar, G. Mandal, and S.R. Wadia, *Phys. Lett. B* **329**, 15 (1994).
32. A. Dhar, P. Lakdawala, G. Mandal, and S.R. Wadia, *Int. J. Mod. Phys. A* **10**, 2189 (1995).
33. W.E. Thirring, *Ann. Phys. (N.Y.)* **3**, 91 (1958).
34. G. 't Hooft, *Nucl. Phys. B* **72**, 461 (1974).
35. S. Coleman, Erice lecture 1979, in: *Aspects of symmetry*, Cambridge University press 1985, p. 351.
36. E. Witten, *Nucl. Phys. B* **160**, 57 (1979).
37. A.V. Manohar, in: *Probing the Standard Model of Particle Interactions*, F. David and R. Gupta, eds. (Les Houches 1997).
38. Y. Nambu and G. Jona-Lasinio, *Phys. Rev.* **122**, 345 (1960); **124**, 246 (1961).
39. A.B. Zamolodchikov and A.B. Zamolodchikov, *Phys. Lett. B* **72**, 481

- (1978).
40. N. Andrei and J.H. Lowenstein, *Phys. Rev. Lett.* **43**, 1698 (1979).
 41. N. Andrei and J.H. Lowenstein, *Phys. Lett. B* **90**, 106 (1980); *B* **91**, 401 (1980).
 42. R.F. Dashen, B. Hasslacher, and A. Neveu, *Phys. Rev. D* **12**, 2443 (1975).
 43. J. Feinberg, *Phys. Rev. D* **51**, 4503 (1995).
 44. L.L. Salcedo, S. Levit, and J.W. Negele, *Nucl. Phys. B* **361**, 585 (1991).
 45. F. Lenz, M. Thies, S. Levit, and K. Yazaki, *Ann. Phys. (N.Y.)* **208**, 1 (1991).
 46. R. Pausch, M. Thies, and V.L. Dolman, *Z. Phys. A* **338**, 441 (1991).
 47. D.J. Gross and F. Wilczek, *Phys. Rev. Lett.* **30**, 1343 (1973).
 48. H.D. Politzer, *Phys. Rev. Lett.* **30**, 1346 (1973).
 49. W. Wetzel, *Phys. Lett. B* **153**, 297 (1985).
 50. C. Luperini and P. Rossi, *Ann. Phys. (N.Y.)* **212**, 371 (1991).
 51. S. Shei, *Phys. Rev. D* **14**, 535 (1976).
 52. J. Feinberg and A. Zee, *Phys. Lett. B* **411**, 134 (1997).
 53. J. Feinberg and A. Zee, *Phys. Rev. D* **56**, 5050 (1997).
 54. A.C. Scott, F.Y.F. Chu, and D.W. McLaughlin, *Proc. of the IEEE* **61**, 1443 (1973).
 55. C.G. Callan, S. Coleman, D.J. Gross, and A. Zee, unpublished (referred to by Ref. 42).
 56. M. Thies and K. Ohta, *Phys. Rev. D* **48**, 5883 (1993).
 57. M.B. Einhorn, *Phys. Rev. D* **14**, 3451 (1976).
 58. C.G. Callan, N. Coote, and D.J. Gross, *Phys. Rev. D* **13**, 1649 (1976).
 59. M.B. Einhorn, S. Nussinov, and E. Rabinovici, *Phys. Rev. D* **15**, 2282 (1977).
 60. J. Ellis, *Acta Phys. Polon. B* **8**, 1019 (1977).
 61. J.H. Weis, *Acta Phys. Polon. B* **9**, 1051 (1978).
 62. T.T. Wu, *Phys. Lett. B* **71**, 142 (1977).
 63. I. Bars and M.B. Green, *Phys. Rev. D* **17**, 537 (1978).
 64. M. Li, *Phys. Rev. D* **34**, 3888 (1986).
 65. M. Li, L. Wilets, and M.C. Birse, *J. Phys. G* **13**, 915 (1987).
 66. S. Dalley and I. Klebanov, *Phys. Rev. D* **47**, 2517 (1993).
 67. G. Bhanot, K. Demeterfi, and I. Klebanov, *Phys. Rev. D* **48**, 4980 (1993).
 68. I. Bigi, M. Shifman, N. Uraltsev, and A. Vainshtein, *Phys. Rev. D* **59**, 054011 (1999).
 69. B. Grinstein and R.F. Lebed, *Phys. Rev. D* **59**, 054022 (1999).
 70. M. Burkardt and N. Uraltsev, hep-ph/0005278.

71. A.R. Zhitnitsky, *Phys. Lett. B* **165**, 405 (1985).
72. M. Burkardt, *Phys. Rev. D* **53**, 933 (1996).
73. T.H. Koopmans, *Physica* **1**, 104 (1933).
74. V. Schön and M. Thies, hep-th/0003195.
75. A.L. Fetter and J.D. Walecka, *Quantum theory of many-particle systems*, McGraw-Hill 1971.
76. M. Burkardt, *Multiquarksysteme in der 1+1 dimensionalen QCD*, phd thesis, Universität Erlangen-Nürnberg 1989.
77. M. Durgut, *Nucl. Phys. B* **116**, 233 (1976).
78. D. Amati and E. Rabinovici, *Phys. Lett. B* **101**, 407 (1981).
79. D. Amati, K.-C. Chou, and S. Yankielowicz, *Phys. Lett. B* **110**, 309 (1982).
80. R.P. Oderkerk, *Relativistic hadrons in an external field*, phd thesis, Free University of Amsterdam (VU) 1992.
81. P. Ring and P. Schuck, *The nuclear many-body problem*, Springer, New York 1980.
82. C. Satzinger, *Wiederherstellung der chiralen Symmetrie in QCD₂*, Diplomarbeit, Universität Erlangen-Nürnberg 1991.
83. P.H. Damgaard, H.B. Nielsen, and R. Sollacher, *Nucl. Phys. B* **385**, 227 (1992).
84. T.H.R. Skyrme, *Proc. Roy. Soc. Lond. A* **260**, 127 (1961).
85. M. Gell-Mann, R.J. Oakes, and B. Renner, *Phys. Rev.* **175**, 2195 (1968).
86. F. Lenz and M. Thies, *Ann. Phys. (N.Y.)* **268**, 308 (1998).
87. D.J. Toms, *Phys. Rev. D* **21**, 928 (1980).
88. V. Koch, E.V. Shuryak, G.E. Brown, and A.D. Jackson, *Phys. Rev. D* **46**, 3169 (1992).
89. A.P. Young, *Nucl. Phys. B* **42** (Proc. Suppl.), **201** (1995).
90. S.L. Sondhi, S.M. Girvin, J.P. Carini, and D. Shahar, *Rev. Mod. Phys.* **69**, 317 (1997).
91. J.I. Kapusta, *Finite-temperature field theory*, Cambridge University Press 1989.
92. A. Barducci, R. Casalbuoni, M. Modugno, G. Pettini, and R. Gatto, *Phys. Rev. D* **51**, 3042 (1995).
93. R.F. Dashen, S.K. Ma, and R. Rajaraman, *Phys. Rev. D* **11**, 1499 (1975).
94. F. Karsch, J. Kogut, and H.W. Wyld, *Nucl. Phys. B* **280**, 289 (1987).
95. U. Wolff, *Phys. Lett. B* **157**, 303 (1985).
96. T. Eguchi and H. Kawai, *Phys. Rev. Lett.* **48**, 1063 (1982).
97. B.J. Harrington and A. Yildiz, *Phys. Rev. D* **11**, 779 (1975).
98. L.D. McLerran and A. Sen, *Phys. Rev. D* **32**, 2794 (1985).

99. T.H. Hansson and I. Zahed, *Phys. Lett. B* **309**, 385 (1993).
100. M. Engelhardt, *Phys. Lett. B* **355**, 507 (1995).
101. M. Thies, *Nucl. Phys. A* **546**, 233c (1992).
102. V. Schön and M. Thies, *Phys. Lett. B* **481**, 299 (2000).
103. J. Gasser and H. Leutwyler, *Phys. Lett. B* **184**, 83 (1987).
104. P. Gerber and H. Leutwyler, *Nucl. Phys. B* **321**, 387 (1989).
105. P. Zhuang, J. Hüfner, and S.P. Klevansky, *Nucl. Phys. A* **576**, 525 (1994).
106. S.P. Klevansky, *Rev. Mod. Phys.* **64**, 649 (1992).
107. A. Barducci, R. Casalbuoni, M. Modugno, G. Pettini, and R. Gatto, *Mod. Phys. Lett. A* **11**, 1579 (1996).
108. A. Barducci, M. Modugno, G. Pettini, R. Casalbuoni, and R. Gatto, *Phys. Rev. D* **59**, 114024 (1999).
109. A. Barducci, R. Casalbuoni, M. Modugno, G. Pettini, and R. Gatto, *Phys. Rev. D* **55**, 2247 (1997).
110. T.F. Trembl, *Phys. Rev. D* **39**, 679 (1989).
111. A. Chodos, R.L. Jaffe, K. Johnson, C.B. Thorn, and V.F. Weisskopf, *Phys. Rev. D* **9**, 3471 (1974).
112. M. Alford, K. Rajagopal, and F. Wilczek, *Phys. Lett. B* **422**, 247 (1998).
113. I. Klebanov, *Nucl. Phys. B* **262**, 133 (1985).
114. W.L. McMillan, *Phys. Rev. B* **16**, 4655 (1977).
115. G. Theodorou and T.M. Rice, *Phys. Rev. B* **18**, 2840 (1978).
116. K. Takayama and M. Oka, *Nucl. Phys. A* **551**, 637 (1993).
117. *Handbook of Mathematical Functions*, M. Abramowitz and I.A. Stegun, eds., Dover, New York 1970.
118. W. Fischler, J. Kogut, and L. Susskind, *Phys. Rev. D* **19**, 1188 (1979).
119. E. Wigner, *Phys. Rev.* **46**, 1002 (1934).
120. H.J. Schulz, *Phys. Rev. Lett.* **71**, 1864 (1993).
121. Y.-C. Kao and Y.-W. Lee, *Phys. Rev. D* **50**, 1165 (1994).
122. H.R. Christiansen and F.A. Schaposnik, *Phys. Rev. D* **53**, 3260 (1996).
123. H.R. Christiansen and F.A. Schaposnik, *Phys. Rev. D* **55**, 4920 (1997).
124. M. Kutschera, W. Broniowski, and A. Kotlorz, *Nucl. Phys. A* **516**, 566 (1990).
125. D.V. Deryagin, D.Yu. Grigoriev, and V.A. Rubakov, *Int. J. Mod. Phys. A* **7**, 659 (1992).
126. A.W. Overhauser, *Adv. in Phys.* **27**, 343 (1978).
127. E. Shuster and D.T. Son, *Nucl. Phys. B* **573**, 434 (2000).
128. B.-Y. Park, M. Rho, A. Wirzba, and I. Zahed, *Phys. Rev. D* **62**, 034015 (2000).

- 129. A. Chodos and H. Minakata, *Phys. Lett. A* **191**, 39 (1994).
- 130. M. Sadzikowski and W. Broniowski, hep-ph/0003282.